Separation of Volatile Organic Compounds from Nitrogen by Hollow Fiber Composite Membranes

by

Yujing Liu

A thesis

presented to the University of Waterloo

in fulfillment of the

thesis requirement for the degree of

Master of Applied Science

in

Chemical Engineering

Waterloo, Ontario, Canada, 2003

I hereby declare that I am the sole author of this thesis. This is a true copy of the thesis, including any required final revisions, as accepted by my examiners.

I understand that my thesis may be made electronically available to the public.

Abstract

Many industrial processes handling organic solvents produce volatile organic compounds (VOCs). These VOCs not only cause environmental pollution, but also represent an economic loss. VOC removal and recovery have become a big issue that needs to be addressed.

Traditional techniques for VOCs removal include carbon adsorption, condensation, and absorption, and none is efficient enough to meet every need. Membrane separation has emerged as an excellent alternative or complementary technology for VOC separation.

Separation of VOCs from nitrogen by composite hollow fiber membranes is studied in this thesis. Microporous hollow fiber membranes were spun from polyvinylidene fluoride (PVDF) using the phase inversion method, and the hollow fibers were coated with a thin layer of poly(ether block amide) (PEBA), thereby forming composite membranes. PVDF was chosen as the substrate material because of its excellent thermal and chemical stabilities and good mechanical strength, and PEBA was selected as the active separating layer because of its good permselectivity and film forming properties. In PEBA polymer, the hard polyamide blocks provide high mechanical strength, and the soft polyether blocks provide flexibility and elasticity.

This study is focused on the preparation and characterization of PEBA/PVDF composite hollow fiber membranes. The membranes were tested for the removal of representative VOCs including hexane, heptane and cyclohexane, which are the main components of gasoline, and dimethyl carbonate (DMC), ethanol, methanol, and methyl t-butyl ether (MTBE) that are the oxygenates and octane number enhancers of gasoline. The separation of gasoline vapor from

nitrogen was also investigated. It was found that the PEBA/PVDF composite hollow fiber membranes are effective for the separation of hydrocarbon vapors from nitrogen. The effects of hollow fiber membrane preparation conditions on the membrane performance were studied, and the separation performance of the composite hollow fiber membranes at various operating conditions (e.g. feed concentration, operating temperature) was evaluated.

Acknowledgement

I would like to thank very much my supervisor, Professor Xianshe Feng for his invaluable guidance, encouragement, constructive criticism and support throughout the courses of this study and in the preparation of the thesis.

I would also like to thank Dr. Li Liu and Dr. Pinghai Shao for their valuable advice and discussion, thank John (Jun) Long for his nice help with contact angle and surface tension measurement, and thank Wooyoung Won for his help on Total Organic Compounds Analyzer trouble shooting. I also would like to thank Nan Chen and Krista Rennick for their proofreading the thesis and the whole membrane research group for their support.

More importantly, I am grateful for endless support from my parents, my husband, my sister, brother and lovely daughter. I could not complete this study without their support.

Finally, the financial support provided by the Natural Sciences and Engineering Research Council of Canada and the Fielding Chemical Technologies Inc. (Mississauga, Ontario) is gratefully acknowledged.

Table of Contents

List of Tables

List of Figures

Chapter 1 Introduction

1.1 Background and objectives

Volatile organic compounds (VOCs) are common pollutants emitted from chemical processes. Each year, chemical manufacturers alone must remove some 500 million lbs of organic pollutants from 50 million ft^3 of air (Simmons et al. 1994). There are many sources of VOC emissions. The synthetic organic chemicals manufacturing industry is the most significant contributor to air pollution. Petroleum industries and petroleum storage/transfer units with a total storage capacity exceeding 30,000 lb are two major sources that have the potential to emit hazardous pollutants at a rate of more than 100 tons/year. Emissions of gasoline and other light hydrocarbons are of considerable importance. Gasoline is mainly a mixture of C_6 to C_8 components. The emission of evaporated gasoline from loading, unloading and other handling operations has been under scrutiny. Dimethyl carbonate (DMC), ethanol, methanol, and methyl t-butyl ether (MTBE) are present and future octane value enhancers of gasoline and their emissions should also be considered in VOCs emission control.

Meeting regulations for VOC emission control will require a range of solutions, from complete elimination of the pollution source to more conventional end-of-pipe treatments. An increasingly common solution is to install equipment that recovers and recycles raw materials and by-products within the process. For many years, the technologies available for in-process recovery and end-of-pipe control of organic vapor emissions have been limited to incineration, adsorption, absorption and condensation. Novel innovative alternatives have been slow to

demonstrate commercial viability and to gain industrial acceptance. One of these new technologies is based on membranes that selectively permeate organic compounds over air. Membrane systems are effective, and they can be combined with other VOC emission control technologies to form hybrid processes.

Most of the experimental work on membrane vapor recovery is concentrated on composite silicone rubber membranes. There are several polymeric materials that can be used as the substrate layer, including polysulfone (Behling, 1986), poly(ether imide) (Behling et al., 1989), and polyvinylidene fluoride (Yeow et al., 2002). However, the resistance of silicone rubber to gasoline is poor (Billmeyer, 1984). Some efforts have been devoted to finding alternative polymeric materials appropriate for membranes. Poly(ether block amide) (PEBA) is considered to be one of such materials that can be used to make semipermeable membranes.

The main objective of this study is to develop a PEBA/PVDF composite hollow fiber membrane for the separation of gasoline vapor from nitrogen. For this purpose, microporous PVDF hollow fiber membranes were prepared by the phase inversion method and the hollow fibers were coated with PEBA by the dip-coating method. The hollow fiber PEBA/PVDF composite membranes were tested for separation of hexane, cyclohexane, heptane, DMC, MTBE, methanol and ethanol from nitrogen. The effects of feed concentration and operating temperature on the separation performance of the membranes were studied. In addition, the actual separation of gasoline vapor from nitrogen was demonstrated experimentally using commercial gasoline, with and without gasoline additives, in the experiments.

1.2 Scope of the thesis

This thesis covers the following aspects to provide a systematic study for recovery of VOCs using PEBA/PVDF hollow fiber composite membranes:

Chapter 1 gives an introduction to the research. Sources of VOC and their main contribution to VOC pollution are briefly reviewed. The objective of the study is also described. More detailed background and review of literature on the subject are discussed in Chapter 2, which also gives an overview of membrane material selection, membrane fabrication and mass transport through membranes. Some of the literature work is further reviewed in relevant chapters.

Chapter 3 is concerned with the thermodynamics and kinetics of PVDF membrane formation. The effects of temperature, concentration and additive on the formation of microporous PVDF membranes are studied from a thermodynamic point of view. The effects of additives and the membrane casting thickness on the kinetics of membrane formation are also investigated.

The fabrication and evaluation of microporous PVDF hollow fiber membranes are studied in Chapter 4. The effects of fiber spinning conditions (e.g., dope extrusion rate, inner coagulant speed and take-up speed) are studied. The mean pore size and effective porosity of the hollow fiber membranes are evaluated by the gas permeation method. The pore size distribution of the membranes is determined by the liquid displacement method.

The experimental work on organic vapor separation from nitrogen is provided in Chapter 5. In this chapter, the gasoline vapor recovery using the PEBA/PVDF hollow fiber membranes is investigated, and the effects of feed concentration and operating temperature on VOC separation are studied.

Finally, the general conclusions drawn from this study are summarized in Chapter 6, and recommendations for future work are provided in Chapter 7. The raw experimental data and sample calculations are presented in the Appendices.

Chapter 2 Literature review

2.1 Introduction

Volatile organic compounds (VOCs) are a class of substances in which organic carbon is bonded to hydrogen or to other elements. As an approximate rule, VOCs may be defined as organic compounds whose vapor pressures at room temperature are greater than 70 Pa and whose normal boiling points are up to about 533K but they evaporate quite slowly into the atmosphere unless they are heated (de Nevers, 1995). Most organic compounds with less than 12 carbon atoms are VOCs.

VOC emission into the atmosphere not only pollutes air, but also causes economic loss. Many efforts have been devoted to recovering VOCs from the waste gas streams. The sources of VOCs emissions are very fragmented. The synthetic organic chemicals manufacturing industry is the first on the list as the single most significant contributor to air pollution, and the petroleum refineries and related storage/transfer systems with a total storage capacity of 30,000 lb are two of the major sources that have potential to emit to the air at a rate of over 100 tons/year. When considering hydrocarbon solvent emissions, gasoline and other light oil cannot be neglected. Gasoline is a mixture of hydrocarbons with the main components being C_6-C_8. The composition depends on the gasoline specifications such as regular or premium, summer or winter quality. Methanol, ethanol and methyl t-butyl ether may also be present as oxygenates and/or octane number enhancers. The recovery of evaporated gasoline from loading, unloading and other handling processes has

been under scrutiny from an environmental point of view (e.g. smog and climate disturbance). The emitted gasoline also represents a significant economic loss.

The release of airborne contaminants into the environment continues to be one of the major problems. As the demand for reduced emissions increases, the market for innovative VOC emission control technologies also improves. A number of options are available for the reduction or elimination of VOCs (Prokop, 1992; Ruddy and Leigh, 1993). The conventional technologies for organic vapor emission control fall into two types: (1) processes to recover organic vapors, including condensation, adsorption and absorption, and (2) processes to destruct organic vapors, including thermal and catalytic incineration. Membrane technology is expected to provide an alternative to the conventional methods for organic vapor recovery. Some previous work on organic vapor emission control is listed in Table 2.1. Other methods, such as ambient oxidation and biodegradation are described in detail in the book of Hunter and Oyama (2000).

Condensation is the liquefaction of condensable contaminants at low temperatures. Specifically, the compounds are removed from the gaseous phase by lowering the temperature and/or increasing the pressure of the gas stream so that the partial pressure of the organic compounds in the gas stream exceeds their dew points, thereby achieving condensation to liquid. It is effective for removing compounds with high boiling points and at relatively high VOC concentrations, but is not suited for gas streams with large quantities of inert or non-condensable gases (i.e. air, nitrogen or methane). To remove low boiling-point organic compounds by condensation, the energy cost will be significant. Normally, condensers are used in combination with other control technologies (Gupta and Verma, 2002), and they can be used as a pretreatment of the gas stream.

Table 2.1 VOCs emission control technologies

Methods	References
Condensation	Gupta and Verma, 2002
Adsorption	Hines et al., 1993; Stenzel, 1993; Ruhl, 1993; Ruddy and Leigh, 1993
Absorption/scrubbing	Hines et al., 1993; MacDonald, 1977
Thermal incineration	Ross, 1977; Garg, 1994; Heck and Farrauto, 1995
Membrane separation	Christian, 1995; Baker, 2002; Wang et al., 2000; Feng et al., 1993; Deng et al., 1998; Yeow et al., 2002

Adsorption refers to the trapping of pollutants on a high-surface area material. The pollutants are adsorbed onto the surface or interstitial areas of an adsorbent material (such as activated carbon or molecular sieves) by physical or chemical attraction. Once the adsorbent material is saturated by the adsorbate, it can no longer adsorb any more pollutant, and the adsorbent will need to be regenerated. Usually, steam is used to drive off the pollutant to regenerate the adsorbent material. In some cases, further treatment may be needed. Adsorption is effective for removing a wide range of VOCs over concentrations from low ppb levels to about 1000 ppm. However, it is not particularly suitable to streams with very high concentrations of VOCs, nor does it work effectively on streams containing VOCs that are difficult to desorb. If the adsorbent is non-regenerable, adsorption may cause other environmental problems associated with solid waste disposal.

Absorption is a process consisting of the dissolution of a pollutant in a liquid. In absorbers (or scrubbers), the vapor stream is introduced into an absorption chamber where it is mixed with the liquid. Similar to adsorption, which involves adsorbent regeneration, the VOCs are transferred from a gas stream to liquid absorbent, and the liquid must be treated to recover the pollutant and reuse the liquid or to dispose of the spent solvent if the absorbent cannot be regenerated.

Incineration is simply the burning of combustible wastes. For many years thermal incinerators have been considered to be one of the most effective means for VOCs emission control. Incinerators are ideal for gas streams that contain a variety of organic pollutants not viable for reuse if recovered. The cost of thermal incineration is generally higher than absorption and adsorption. One potential problem associated with incineration is that new hazardous substances may be produced in the vent-off gas.

All of the forgoing technologies have advantages and disadvantages in terms of safety, performance, operating cost and facility space. A membrane process is expected to provide an alternative to the conventional processes for VOCs emission control. While the best choice depends on site conditions, the approximate best stream profiles for VOC recovery by membrane, carbon adsorption and condensation are mapped in Figure 2.1.

Membrane separation technology involves the use of semipermeable membranes to separate VOCs from a process stream. Basically, the separation is based on preferential dissolution and diffusion of VOCs across the membrane. The driving force is the difference of the chemical potential between the feed and permeate sides, which is usually achieved by maintaining a permeate pressure much lower than the feed pressure. Compared with other VOCs removal processes, membrane separation requires no regeneration. In addition,

membrane devices are easy to set up due to their modular design and can be operated continuously. Membrane processes are considered to be more economical than other processes (Baker, 2002) for many gas separation applications.

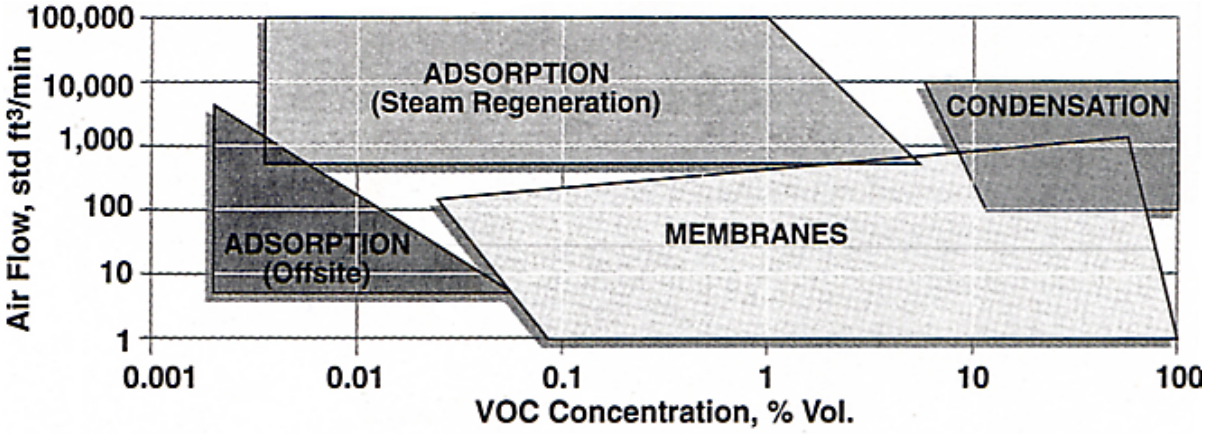

Figure 2.1 Various techniques for recovering VOCs (Simmons et al., 1994).

2.2 Membrane separation

Membrane separation technology is still growing rapidly. Many different membrane separation processes have been developed during the past two decades and new processes are constantly emerging. Microfitration is probably the oldest and still being widely used, and ultrafiltration and reverse osmosis were developed in the 1960-1970. Gas separation by membranes started to be used on an industrial scale in the 1980's. Pervaporation and vapor permeation are the latest membrane separation processes, which are economically competitive for certain industrial applications. There has been some work on VOCs removal from wastewater by pervaporation. However, studies on membrane separation of

VOCs from gas streams, which is relevant to VOCs emission control, are still very limited, and more studies are required to develop suitable membranes for practical applications in VOCs emissions control. In general, membrane systems are most suitable for treating concentrated streams, especially when the VOC concentration is higher than 1,000 ppm.

2.2.1 Mass transport through membranes

The separation of a gas mixture by nonporous membranes is due to differences in the solubility and diffusivity of the components in the membrane. The solution-diffusion model, schematically illustrated in Figure 2.2, is widely used to describe the mass transport through a membrane (Favre et al., 1994).

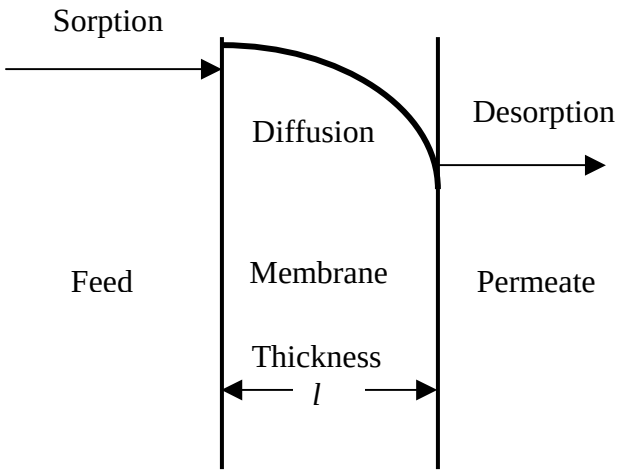

Figure 2.2 Schematic diagram of the solution diffusion model of VOC permeation.

According to the solution-diffusion model, the mass transport takes place in three consecutive steps:

(1) Sorption of components from the feed mixture onto the membrane at the upstream side,

(2) Diffusion of the sorbed components through the membrane, and

(3) Desorption of the permeant from the membrane at the permeate side.

The basic assumptions of this model are the existence of thermodynamic phase equilibria at both surfaces of the membrane that are in contact with the feed and the permeate. The sorption step is normally considered to be a fast step, and the feed gas sorption on the membrane surface is at equilibrium. The diffusion step is the rate-controlling step that determines the permeation rate. The difference in the diffusion rates of different molecules forms the basis of separation. The desorption step is normally a fast step that does not significantly affect the permeation. Therefore, the first two steps, sorption and diffusion, primarily determine the permselectivity of the membrane.

The diffusion process in the membrane can be described, as a first approximation, by the Fick's law, which is mathematically expressed as:

$$Q_i = -D_i \frac{dC_i}{dx} \tag{2.1}$$

where Q_i is the flux, D_i is the diffusivity coefficient of component i in the membrane, x is the perpendicular distance from the surface of membrane contacting with feed, and C_i denotes the concentration of component i in the membrane at a given position. Assume (1) the diffusivity coefficient is constant, and (2) the gas sorption obeys the Henry's law, that is

$$C_i = S_i p_i \tag{2.2}$$

where S_i is the solubility coefficient and p_i is the partial pressure. Then Equation (2.1) can be integrated to give

$$Q_i = D_i \frac{\Delta C_i}{l} = \frac{D_i S_i \Delta p_i}{l} = \frac{P_i \Delta p_i}{l} \tag{2.3}$$

where Δp_i is the partial pressure difference across the membrane, l is the membrane thickness and P_i is the permeability coefficient of component *i*, which is equal to the product of diffusivity coefficient D_i and solubility coefficient S_i.

The diffusivity coefficient tends to decrease with increasing permeant diameter, since large molecules interact with more segments of the polymer chain and are thus less mobile. The diffusivity is generally dependent on operating temperature and feed concentration. The solubility of vapor in a membrane can be obtained from vapor-sorption experiments. The sorption uptake in the membrane can be determined with a microbalance at a given temperature as a function of the pressure of solvent vapor to obtain the sorption isotherms (Blume et al., 1991; Heintz et al., 1991).

According to the solution-diffusion model, both sorption and diffusion affect the permeation through the membrane. A substantial amount of work has been done from the membrane materials science perspective to develop polymers with good solubility and diffusivity characteristics. For a given membrane material and gases to be separated, the diffusivity and solubility coefficients are fixed, and engineering approaches to minimize the membrane thickness has contributed significantly to the successful development of industrially important membranes.

2.2.2 Characterization of membrane performance

The separation performance of a membrane, which largely depends on the selective permeability of the membrane, is normally characterized by permeance (J) and separation factor (α). They are defined as:

$$J = Q / \Delta p \tag{2.4}$$

$$\alpha_{i/j} = \frac{Y_i / Y_j}{X_i / X_j} \tag{2.5}$$

where Y_i is the mole fraction of component i in the permeate, and X_i is the mole fraction of component i in the feed, and Y_j and X_j are the mole fractions of component j in the permeate and the feed, respectively. These quantities are usually determined experimentally. Another parameter that will be employed in this study to characterize membrane permselectivity is permeance ratio (β). The relationship between the permeance ratio and separation factor can be derived from the following permeate concentration and permeation rate equations.

$$Y_i = \frac{Q_i}{Q_i + Q_j} \tag{2.6}$$

$$Q_i = J_i (p^f X_i - p^p Y_i) \tag{2.7}$$

where p^f and p^p are the feed side and permeate side pressure respectively. When the permeate side is connected to vacuum, which is the case for VOCs removal, the permeate side pressure is much lower than the feed pressure. Therefore, Equation (2.7) can be rewritten as

$$Q_i \approx J_i p^f X_i \tag{2.8}$$

Combining Equation (2.8) with Equation (2.6), the following equation can be obtained,

$$Y_i = \frac{J_i X_i}{J_i X_i + J_j X_j} = \frac{\beta X_i}{\beta X_i + X_j} \tag{2.9}$$

where β ($=J_i/J_j$) is the permeance ratio of the two components *i* and *j*. Comparing Equation (2.5) and (2.9), it can be seen that the separation factor equals to the permeance ratio when the permeate pressure is negligibly small.

The permeance (*J*), which is the permeation flux normalized by the transmembrane pressure differential, describes the productivity of the membrane. As shown before, the permeability coefficient is a quantity determined primarily by the solubility coefficient (*S*) and the diffusivity coefficient (*D*). To achieve a good productivity, the only thing that can be done effectively for a given membrane material is to reduce the thickness of the membrane.

The separation factor defined in Equation (2.5) is independent of concentration units used as it is a ratio of concentration ratios. When the separation factor is equal to unity, there is no separation. The higher the separation factor is than unity, the better the separation will be achieved. An ideal membrane would be one that can perfectly permeate one component while retain other component, in which case the separation factor is infinitely large.

The stability of the membrane is also an important factor. The stability is not quantitatively defined, but generally it is said to be instable when (1) there is a change or loss in the separation properties, and (2) decomposition or degradation of the membrane occurs. The membrane can lose its stability by thermal, chemical or mechanical causes

(Mulder, 1996). To obtain a stable membrane is as important as achieving a good permeance and selectivity.

All of these characteristics of membranes largely depend on the materials from which the membranes are made. Chemical modifications of existing materials are often attempted to improve these properties, and they generally include crosslinking, blending, grafting, co-polymerization and other modifications such as substitution or subtraction of certain functional groups in the polymer chains. Poly(ether block amide) (PEBA), which will be discussed later, is a relatively new polymer produced by co-polymerization, having properties that are not available in either polyamide or polyether polymer alone.

2.3 Thin film composite membranes

Dense membranes generally have low fluxes but high selectivity, whereas porous membranes have low selectivity but high permeability. To increase the flux through a dense membrane while retaining its high selectivity, the thickness of the membrane must be reduced as much as practically feasible. In the meanwhile, the membrane should be defect-free and have sufficient mechanical strength. This can be achieved by the use of thin film composite membranes. Such composite membranes often consist of two layers, with a thin dense selective skin layer supported by a porous substrate. The substrate is commonly prepared from high strength engineering plastics. A schematic diagram of the thin film composite membrane is shown in Figure 2.3. The thin barrier layer can be formulated to achieve the desirable permselectivity, while the porous support can be optimized for the maximum strength and compression resistance combined with minimal resistance to the

permeate flow. Moreover, a variety of polymers can be used to form a thin barrier layer of the composite membrane, depending on specific applications.

A composite membrane is usually formed by a two-step process (Lonsdale, 1987). A thick, porous and nonselective substrate is formed first and then coated or laminated with an ultrathin barrier layer on its surface. The porous substrate provides the mechanical strength while offering little resistance to the transport of the permeant, and the skin layer is responsible for the permselectivity. The skin layer may be formed by dip-coating, plasma polymerization, radiation grafting, or in situ polymerization (Lonsdale, 1987; Bartels, 1989). The dip-coating method is easy to handle and cost effective, and it is most widely used for making composite membranes for various applications.

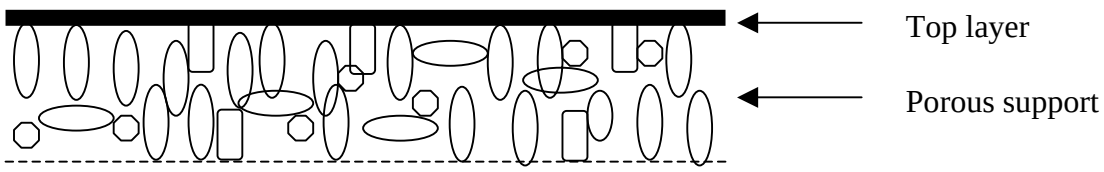

Figure 2.3 Schematic diagram of a composite membrane

As mentioned before, the skin layer should have high selectivity and permeability. Unfortunately, most polymeric membrane materials have either a high permeability or a high selectivity, but seldom both. Normally, rubbery polymer materials have high permeabilities, while glassy polymer materials have high selectivities. The permeability-selectivity trade-off is illustrated in Figure 2.4 (Feng, 2001), which shows the permselectivity of different kinds of glassy and rubbery materials to CO_2/CH_4. Glassy polymers such as polysulfone and polyimides preferentially permeate small non-

condensable gases over larger condensable gases, whereas the opposite is true with rubbery polymers such as silicone rubber (polydimethylsiloxane). For organic vapor permeation, the sorption aspect is more important to permeation than for permeation of non-condensable gases, and rubbery membranes have been primarily used, which will be discussed further in the following sections.

In order to support the selective layer in the form of a composite membrane, the substrate layer should have a high permeance to minimize the mass transfer resistance of the substrate, and the substrate with microporous structure is often used. Ideally, the substrate should have high porosity with reasonably small and even pore size to retain its good stability.

Membranes may be formed in several forms: tubular, flat sheet or hollow fiber. Table 2.2 summarizes the main features of these three types of membrane modules. Hollow fiber modules' self-supporting and low cost make them very attractive. In this study, hollow fiber membranes were used as the substrate in making composite membranes for VOC separation.

Recently, many studies have been done on VOCs removal by polydimethylsiloxane (PDMS) membranes. Baker et al. (1987) studied the permeability of four organic vapors (octane, toluene, trichloroethane and acetone) and nitrogen in several polymeric materials, which were listed in Table 2.3. It was found that when the VOC concentration in feed increased, the permeability of the organic vapor increased, while the permeability of nitrogen was only affected by the feed composition slightly. Although the permeability for each organic vapor varied by 10- to 100-fold for different membranes, the pattern of the permeability was similar, i.e., octane > toluene > trichloroethane > acetone >> nitrogen.

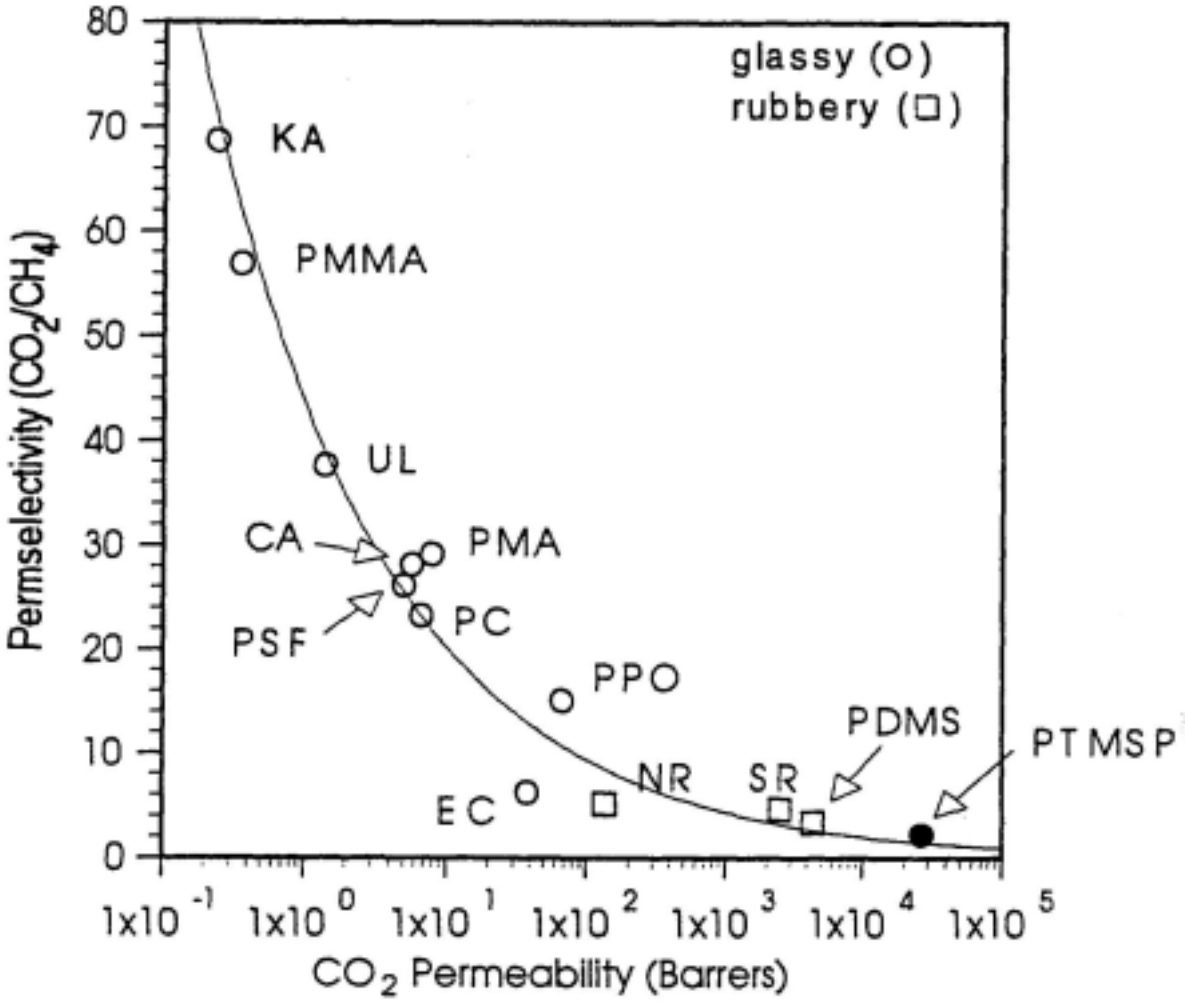

Figure 2.4 Selectivity- permeability relation for commercial glassy and rubbery polymeric membrane materials (Feng, 2001). KA = "Kapton" poly(imide); PMMA = poly(methyl methacrylate); UL = "Ultem" poly(ether imide); PMA = poly(methyl acrylate); CA = cellulose acetate; PSf = polysulfone; PC = polycarbonate; PPO = poly(phenylene oxide); EC = ethyl cellulose; NR = natural rubber; PDMS = poly(dimethyl siloxane); PTMSP = poly(trimethylsilyl propyne)

Table 2.2 Qualitative comparisons of various membrane configurations

	Tubular	Plate-and frame	Hollow fiber
Packing density (m^2/m^3)	20-30[a]	400-600[a]	30,000[b]
Estimated manufacturing cost ($/$m^2$)	Very high[c]	1,000-3,000[a]	50-200[a]
Operating cost	Very high	High	Low
Self -supporting	No	No	Yes

[a] Feng (2002); [b] Mulder (1991); [c] no exact number was found, but its cost is believed to be the highest (Mulder, 1991)

Blume et al. (1991) studied vapor sorption and diffusion of methylene chloride, chloroform and carbon tetrachloride in flat polydimethylsiloxane films and found that both the solubility and diffusivity depended on the feed concentration. The flat sheet membranes were prepared by the solvent casting technique followed by cross-linking at 80^{o}C for 15 hr. The permeability of methylene chloride achieved was as high as 1.87×10^{-14} mol.m/s.m^2.Pa.

Cha et al. (1997) and Bhaumik et al. (2000) employed microporous polypropylene hollow fibers having a plasma polymerized coating of silicone rubber to remove methanol and toluene from nitrogen. Bore-side feed was employed in both studies. As high as 98% of the VOC in feed can be removed from nitrogen, indicating that hollow fiber modules are suitable to remove VOCs from nitrogen and the silicone rubber membrane has excellent selectivity for preferential permeation of organic vapors.

Table 2.3 Polymers used by Baker et al. (1987) for vapor permeation membranes

Polymer	Chemical Formula	Remarks
Neoprene®, chloroprene	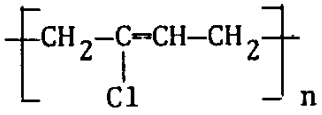	
Hypalon® Chlorosulfineated polyethylene	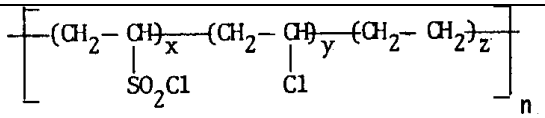	Soluble in toluene; several grades available
Fluorel® fluoroelastomer	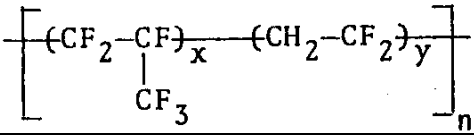	Available in a number of grades
Polydimethyl siloxane	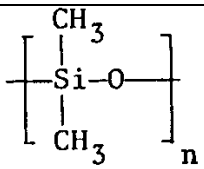	Available as polymerizable oligomers or linear polymers;
Polyvinyl chloride (PVC) [a]	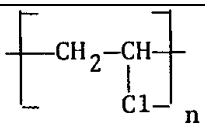	Can be easily plasticized
Nitrile rubber, polyacrylonitrile-butadiene [b]	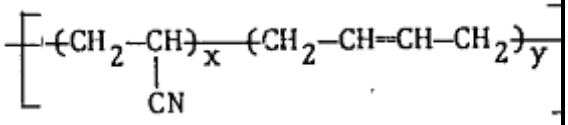	Available in a number of grades
Silicone-polycarbonate	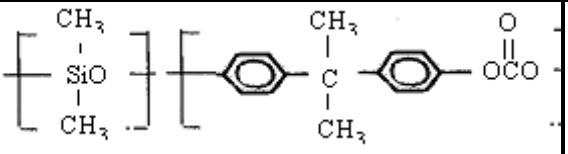	Used by GE to develop MEM-213 flat membrane

[a] Three kinds of PVC with different dioctyl phthalate (DOP) 25%, 40%, and 50% were used

[b] Two kinds of nitrile rubber with 21% PAN and 33% PAN were used

Gales et al. (2002) removed acetone, ethyl acetate and ethanol vapors from air by using composite hollow fiber membranes comprising of a polyetherimide substrate and a polydimethylsiloxane top selective layer. It was found that the permeation flux of the organic vapor increased with an increase in its concentration in feed. They also studied the effects of permeate pressure and feed pressure on the membrane performance. A mathematical model was presented, which could represent the experimental results fairly well. Although the hollow fiber module had a reasonably high permeation flux and VOCs removal rate, the polyetherimide substrate represented a significant mass transport resistance, which compromised the overall separation efficiency. There are also some studies using PDMS flat sheet membranes. Yeom et al. (2002a, b) discussed the effects of feed concentration, operating temperature and feed flow rate on the permeability and selectivity of the membranes and investigated the concentration polarization in the boundary layer. Kimmerle et al. (1988) tested the separation of acetone vapor from air using polydimethylsilicone/polysulfone composite hollow fiber membranes in a pilot plant.

Based on the work done on PDMS, it can be concluded that PDMS membranes can separate VOCs from waste gas streams effectively, and composite hollow fiber PDMS membranes have been shown to be efficient for VOC separation in terms of permeation rate and VOC recovery rate. However, one of the disadvantages associated with PDMS material is that it is not very stable in gasoline (Billmeyer, 1984), and thus the membrane stability will be a primary concern when PDMS membranes are to be used for gasoline vapor separation. There have been efforts to modify PDMS (Guizard et al. 2001; Mishima and Nakagawa, 1998) to make it more stable or develop alternative membrane materials that are more suitable for VOCs removal.

Aromatic polyimide and polyetherimide membranes have also been used for VOC separations (Feng et al., 1991, 1993; Deng et al., 1995). The membranes were prepared by the phase inversion method. Table 2.4 lists the representative permeability and selectivity of

Table 2.4 Separation of organic vapors from air using polyimide and polyetherimide membranes

Material	VOCs	Permeance $\times 10^8$ (mol/s.m^2.Pa)	Separation factor	Reference
Polyimide[a]	Methanol	5.02	221.2	Feng et al. (1991)
	Ethanol	6.73	296.9	
	Acetone	1.07	41.7	
	Benzene	1.15	50.5	
	Toluene	4.09	179.9	
	p-Xylene	10.4	460.2	
	m-Xylene	11.6	513.3	
	1,2-Dichloroethane	1.18	52.1	
	1,2-Dichloropropane	1.3	57.2	
	Chloroform	0.479	21.1	
	Carbon tetrachloride	0.556	24.4	
	Hexane	0.733	32.4	
Polyetherimide[b]	Pentane	0.248	72.9	Deng et al. (1995)
	Pentanol	6.2	1820	

Temperature: [a] 23~24 ^{o}C, [b] 48 ^{o}C.

two different kinds of imide polymer membrane materials. The separation factor of methanol/air and ethanol/air can be as high as over 200 by using aromatic polyimide flat sheet membrane, and the permeability is about $5\sim7\times10^{-8}$ mol/m^2.s.Pa. Interestingly, the membranes do not exhibit a high permselectivity to non-condensable gases such as H_2/N_2 and O_2/N_2. Presumably, the high VOC/N_2 selectivity is due to surface diffusion of VOC through the very fine pores of the membranes.

In this study we have attempted to use poly(ether block amide) membranes for VOC separation because of its good chemical resistance and mechanical strength, as discussed below. To the best of our knowledge, this material has not been used to make membranes For VOC separation.

2.4 Poly(ether block amide) (PEBA)

PEBA resin was developed in 1972, but only in 1981 did it begin to be used commercially under the trade name PEBAX®. PEBA is a new member of the thermoplastic elastomer family having the following general chemical structure (Deleens, 1987):

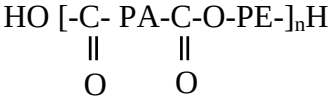

where PA is an aliphatic polyamide “hard” block (e.g., nylon-6, nylon-12) and PE is a polyether “soft” block (e.g. poly(ethylene oxide)[PEO], poly(tetramethylene oxide)[PTMEO]. The hard polyamide blocks provide the mechanical strength, whereas the polyether “soft” blocks provide elastic properties. The copolymer has a regular linear chain where the rigid PA segments are trespassed with the flexible PE segments. This two-phase

crystalline and amorphous structure creates a blend of properties bridging the gap between thermoplastics and rubbers. Table 2.5 lists the physical properties of PEBA material (Kim et al., 2001; Bondar et al., 2000). As one may expect, with the content of PA in the polymer increases, the elongation of polymer decreases, while the hardness and tensile strength increase.

PEBA has excellent chemical resistance. As shown in Table 2.6 (Bondar et al., 1999) most of the solvents cannot dissolve it. This is another good feature to a membrane material which will be used to remove VOCs.

PEBA has been employed in sporting goods (shoe soles), industrial equipment (conveyor belts), as well as functional films (breathable clothing, drying films). Only in recent years have PEBA polymers been used to make membranes. Pervaporation of aqueous ester solutions through a series of PEBA membranes was carried out by Djbbar et al. (1998). The membrane was prepared by dissolving PEBA in DMAc solution at 100 ^{o}C and the polymer solution containing up to 2% PEBA was cast on a glass plate to form a flat sheet membrane. It was found that the higher the polyether portion is in the PEBA polymer, the higher the flux can be achieved. A comparison with PDMS membrane showed that the PEBA membrane was slightly less permselective than the PDMS membrane in that particular case of ester extraction. However, in other cases involving various volatile organic compounds, the performance of PEBA membranes was usually better than PDMS membranes.

Table 2.5 Physical properties of PEBAX® series[a] (Bondar et al. 1999; Dennis and O'Brien, 2000)

Polymer	Commercial name	PE content (wt%)	Density[b] (g/cm^3)	T_g (^oC)	T_m (PE) (^oC)	T_m (PA) (^oC)	Crystallinity in PA block (wt%)	Hardness	Elongation (%)	Tensile strength, ultimate (psi)
80PTMEO/PA12	PEBAX® 2533	80	1.01	-77	9	126	14	25D	640	4950
53PTMEO/PA12	PEBAX® 4033	53	1.01	-78	-1	159	32	40D	390	5700
30PTMEO/PA12	PEBAX® 5533	30	1.01	-	20	160	30	55D	430	7300
55PEO/PA12	PEBAX® 1074	55	1.09	-55	11	156	40	-	-	-
57PEO/PA6	PEBAX® 4011	57	1.14	-53	13	201	51	-	-	-

[a] PE: PTMEO=poly(tetramethylene oxide), PEO=poly (ethylene oxide). PA: PA12=polyamide 12 (Nylon 12), PA6=poly amide 6 (Nylon 6)

[b] Density values reported by manufacturer

- No data found in references

Table 2.6 Solubility of poly(ether block amide) (Bondar et al., 1999)

Solvent	Solubility
Methanol	Non-soluble
Ethanol	Non-soluble
Chloroform	Non-soluble
γ-Butylolactone	Non-soluble
N, N-Dimethyl formamide (NMF)	Partially soluble
N, N-Dimehtyl acetamide (DMAc)	Partially soluble
N-methyl-2 pyrrolidone (NMP)	Partially soluble
Trichloroethane	Soluble
Formic acid/sulfuric acid	Soluble
Mixture (3:1) of 1-propanol /1-butanol (80 ^{o}C)	Soluble

PEBA membranes have also been used in gas separation and good separation has been reported. Bondar et al. (2000) studied CO_2/N_2 and CO_2/H_2 separation by using different kind of PEBA membranes. In their experiment, the solvent-cast films of PEBA1074 were prepared by casting 2 wt% polymer solution in n-butanol on a Teflon-coated glass plate, followed by air drying at ambient conditions for one week and then drying in vacuum at 80^{o}C for three days. The membrane thickness was 95 μm. Melt extruded films of PEBA 2533, 4033, and 4011 were supplied by Schoeller Technical Paper, Inc. and the thickness of these films ranged from 25 to 36 μm. It was also found that as the content of the polyether block increased, the permeability of the membrane would increase. Kim et al. (2001)

reported that PEBA membranes had very high permeability and selectivity for polar/nonpolar gas pairs. The selectivity of CO_2/N_2 was 61 and SO_2/N_2 was as high as 500. They also observed that with an increase in the PA content in the PEBA material, the permeability would decrease. The membranes used in the study were formed by the solvent casting technique using 3 wt% PEBA in the mixture propanol/butanol (weight ratio 3:1) that was poured into a Petri dish and dried at 40 ^{o}C for 24 hr.

Rezac et al. (1997) evaluated the sorption and diffusion characteristics of water and methanol vapors in a series of PEBA copolymers. Their results indicated that PEBA membranes could be used to selectively permeate methanol from air, but not methanol from water. There are other studies on the solubility and diffusivity of organic compounds in the PEBA material. Groβ and Heintz (2000) have reported the diffusion coefficients of aromatic compounds in non-porous PEBA membranes. However, very little work has been done in the literature on VOC separation by using PEBA membranes.

In this study, PEBA 2533 will be selected as the top layer material to prepare composite membranes for gasoline vapor separation from air because of its good permeaselectivity and chemical stability, and polyvinylidene fluoride will be used to prepare the microporous substrate to support the top PEBA layer.

2.5 Polyvinylidene fluoride (PVDF)

PVDF is a semicrystalline polymer containing a crystalline phase and an amorphous or rubbery phase. Its general structure is shown below:

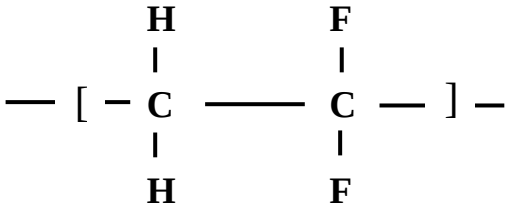

Table 2.7 lists some of the physical properties of PVDF. PVDF has high mechanical strength and excellent chemical and thermal stabilities. These properties make PVDF an attractive polymer for various industrial applications, including electrical and electronic manufacturing, chemical processing, pulp and paper, and transportation (Dohany and Robby, 1994).

PVDF combines the properties of rubber and plastic materials. It is a promising material for membranes because of its excellent chemical resistance. Li et al. (1999) tried to use asymmetric PVDF hollow fibers to remove H_2S from waste gas streams. Dimethyl acetamide (DMAc) and poly(1-vinyl- 2-pyrrolidone) (PVP) were employed as the solvent and additive, respectively, in the membrane manufacturing by the phase inversion technique.

Table 2.7 Physical properties of PVDF (Kroschwitz and Howe-Grant, 1991)

Density (g/cm^3)	1.75~1.80
Water absorption (24 hr, 23 ^oC), %	0.04
Tg (^oC)	-40
Tm (^oC)	156~180
Impact strength at 25 ^oC, J/m^2 (unnotched)	800-4270

The hydrophobic property of PVDF makes it a potential material in membrane distillation. Tomaszewska (1996) also prepared PVDF membranes by the phase inversion technique using dimethyl formamide (DMF) or DMAc with LiCl as an additive. The polymer solution was cast on a glass plate to form flat-sheet membranes. The hydrophobicity of the membrane was maintained during membrane distillation tests, and the PVDF membrane was found to be suitable for membrane distillation. It was also shown that with an increase in the amount of LiCl in the membrane casting solution, the mechanical properties of the resulting membrane would decrease, while the permeation flux would increase. Due to its strong chemical stability and hydrophobicity, PVDF has been used to make porous membranes for membrane-based gas absorption, and oil/water emulsion separation (Yeow et al., 2002).

Deshmukh and Li (1998) described the dry-wet spinning method to manufacture PVDF hollow fiber membranes. They discussed the effects of coagulant and additive (polyvinyl pyrrolidine) on the morphology of the hollow fiber membranes. Wang et al. (1999) did a more detailed study on the effects of the concentration and molecular weight of PVDF, concentration of additive (PVP), the inner coagulant and other processing conditions on the morphology of the hollow fiber membranes. Comparing with previous work, Wang et al. (2000) found that using small molecular additives (LiCl/water or LiCl/1-propanol) membranes with high porosity, good mechanical strength and excellent hydrophobicity could be prepared. Increasing in temperature of coagulant could slightly decrease the membrane permeability.

As mentioned earlier, the substrate of a composite membrane should have good chemical and thermal resistance and mechanical strength. In this study microporous PVDF

hollow fiber membranes will be prepared as a substrate, which will be coated with a thin layer of PEBA, thereby forming a composite membrane.

Chapter 3 Phase separation pertinent to the formation of microporous PVDF membranes

A microporous polyvinylidene fluoride (PVDF) membrane will be used as a substrate layer for making PEBA composite membranes for VOC separation. This chapter deals with the phase separation of the PVDF/solvent/nonsolvent system pertinent to the formation of microporous PVDF membranes. Depending on the target application, the phase inversion may be accomplished by either a dry-wet or wet process. In the dry-wet process, the solvent in the polymer solution system is subject to partial evaporation prior to exchange with the nonsolvent. The membranes formed through this process generally have a dense skin layer which may function as a separation layer. Several theoretical models have been proposed to describe the solvent evaporation pertinent to the dry step during the formation of asymmetric membranes (Huang and Feng, 1995). In this study, the PVDF membrane was going to be used only as a substrate, which was highly microporous as opposed to a dense skin layer. The formation of microporous membranes by the phase inversion technique depends upon both the thermodynamics and kinetics of the phase separation process. The former is related with the phase equilibria of polymer/solvent/nonsolvent in the system, whereas the latter is dependent upon the mutual diffusivities of the solvent and nonsolvent. An insight into the thermodynamic and kinetic behavior is important to understanding the phase inversion phenomena.

In some cases, additives are used to adjust or control the properties of the resulting membranes. Additives generally increase the pore interconnectivity and the pore size of the

membrane (Di Luccio et al., 2002). Additives may also increase the viscosity of the polymer solution, which is important in the formation of hollow fiber membranes because of the minimum viscosity required in order to extrude the polymer solution through a spinneret in an integral form (Boom et al., 1992). The presence of an additive in a polymer solution system increases the complexity of the phase inversion process. Polymeric materials, such as polyvinylpyrrolidone (PVP), have been employed as an additive for making PVDF hollow fiber membranes (Han and Nam, 2002; Chen and Hong, 2002). Smaller molecular additives (such as $CaCl_2$, $LiNO_3$ and LiCl) have also been used because they are easy to leach out from a polymer solution during the phase separation process (Wang et al., 2000).

The objective of this experiment was to investigate the precipitation of PVDF during the course of phase inversion from both a thermodynamic and a kinetic point of view. The thermodynamics and kinetics of the polymer precipitation were studied by measuring (1) the cloud points of the polymer solution, and (2) the leaching rates of the additive and the solvent during the polymer precipitation respectively.

3.1 **Experimental**

3.1.1 Materials

Polyvinylidene fluoride 741 was supplied by Atochem Company (Philadelphia, PA,). It was used after thorough drying at 70 °C for 24 hours. Reagent grade N, N-dimethylacetamide (DMAc) supplied by Fluka Chemical was used as the solvent. Lithium chloride (LiCl) purchased from Sigma Aldrich Chemical was used as the additive. Deionized water was used as the nonsolvent.

3.1.2 Turbidimetric titration

The equilibrium phase separation data on polymer precipitation was determined by the turbidimetric titration technique. The PVDF powder was dissolved in DMAc solvent at a predetermined concentration and a given temperature. When LiCl was used as an additive, it was dissolved in DMAc first during preparation of the polymer solutions. The polymer solution was titrated with deionized water drop wise, using a 0.5-mL syringe, until the polymer solution became turbid. The turbidity was easily recognized because of the clarity of the polymer solutions involved. During titration, the polymer solution was agitated by a Teflon-coated stirrer bar as shown in Figure 3.1. For polymer solutions below 10 wt%, the solution viscosity was low and the cloud point for titration was easy to detect. For higher concentrations of polymer solutions, titration was enhanced by heating the sample at 70 ^{o}C to facilitate water dispersion. If turbidity of the polymer solution did not appear after being cooled down to the temperature of interest, more water was added. Since water was added drop wise, with one drop of water amounting to approximately 7 mg, the titration process was tedious, but this method allowed for systematic treatment of many samples without significant overshooting of the end points. An analytical balance was used to weigh the amount of water that was put into the solution. To minimize the solution evaporation, small mouth glasswares and caps were utilized during the titration process. In this study, the effect of temperature and LiCl additive on the polymer precipitation were studied.

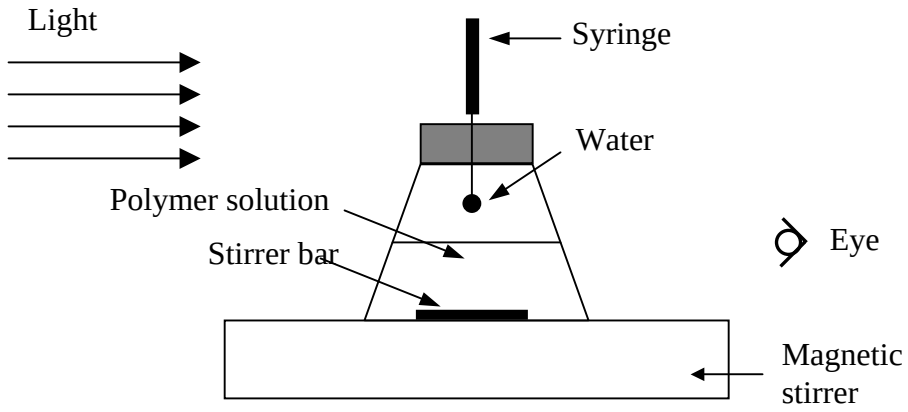

Figure 3.1 Schematic diagram of turbidimetric titration setup for polymer precipitation experiments

3.1.3 Kinetics of polymer precipitation

The kinetics of polymer precipitation was studied by measuring the solvent (DMAc)-nonsolvent (water) exchange rate. In addition, when the additive LiCl was present in the polymer system, the kinetics of the LiCl leaching rate was also measured.

The homogeneous polymer solution, DMAc/LiCl/PVDF (75/5/20 wt%), was cast onto a smooth glass plate at room temperature (22 °C). The membrane together with the glass plate was then placed into a water bath immediately. A Teflon-coated stirrer bar was used to keep the LiCl concentration uniform in the water bath. As soon as the polymer solution film along with glass plate was placed into the water bath, the conductance of the gelation bath was monitored using a YSI Conductance Meter (Model 35) in order to measure the variation of LiCl concentration in the gelation bath during LiCl leaching from the polymer solution. In this study, the organic solvent (DMAc) was found to have essentially no effect on the conductance of the solution in the bath under the experimental conditions tested.

Therefore, conductance readings could be converted to the concentration of LiCl in the water bath directly. To determine the solvent (DMAc)-nonsolvent (water) exchange rate during the phase inversion, a Total Organic Carbon Analyzer (TOC) (Model 915, Shimadzu) was employed to measure the concentration of DMAc in the gelation bath. A microsyringe was used for the sample injection during TOC analysis. Since the TOC only detects the concentration of organic carbon, the presence of LiCl had little effect on the TOC reading of gelation bath. In addition, since PVDF is a hydrophobic polymer and will coagulate easily when contacted with water, the concentration dissolved in water was negligibly small. Therefore, the TOC readings could be converted to the DMAc concentration in the gelation bath. As such, the polymer precipitation kinetics can be represented by the solvent-nonsolvent exchange and the additive leaching rates. Since both solvent-nonsolvent exchange and additive leaching involve diffusive transport through the polymer film, the effect of membrane thickness on the kinetics of polymer precipitation was also investigated.

3.2 Results and discussion

3.2.1 Thermodynamics of PVDF precipitation

Phase inversion for membrane formation is based on solvent-nonsolvent exchange, which makes the polymer solution system unstable until the solution starts to demix into a polymer-rich phase and a solvent-rich phase. The polymer-rich phase forms the matrix of the membrane upon precipitation by gelation, while the solvent-rich phase is primarily responsible for the microporous structure of the membrane. The equilibrium phase separation characteristics can be represented by a ternary phase diagram. The polymer solution systems studied here were comprised of DMAc/PVDF/H_2O with and without LiCl

additive. Their equilibrium phase separation data are shown in Figure 3.2. The phase diagram consists of a boundary curve, i.e. PVDF precipitation curve, distinguishing the homogeneous and the heterogeneous regions. The homogeneous liquid region lies mainly in the space between the PVDF and solvent axes and the precipitation curve. The size of this region is an indication of the amount of water required for the PVDF precipitation to take place. From Figure 3.2, one can see that the amount of water required for precipitation of PVDF decreases with an increase in the concentration of PVDF in the polymer solution. The phase separation data at 40 ^{o}C shows that the polymer solution initially containing 5 wt% LiCl required a smaller amount of water to precipitate than did the polymer solution without LiCl. The presence of LiCl facilitates liquid-liquid demixing of the solution during phase inversion. As an inorganic salt, LiCl dissociated in the aqueous solution, which would enhance the formation of polymer aggregates due to the existence of a charge transfer complex between the monomeric units of PVDF. This results in a reduction in the polymer solubility (Huang and Feng, 1995). Luccio et al. (2002) also noticed that the addition of LiCl to a polycarbonate/NMF system would significantly decrease the miscibility gap of the system. While the presence of LiCl additive reduces the amount of water imbibed in the polymer system, which tends to decrease the porosity of the membrane, the additive also contributes to the formation of pores in the membrane after it leaches out of the polymer during polymer precipitation. Hence, the additive has two opposite effects on the membrane structure from a thermodynamic point of view. Subsequently, the resulting membrane morphology will be influenced by the two opposing effects simultaneously.

In the absence of LiCl additive, the polymer solution at 40 ^{o}C needed more water to precipitate than the polymer at 25 ^{o}C. This observation can be explained by the change in

the solubility. As a higher temperature, the solubility of PVDF in DMAc is greater, and consequently the polymer solution can tolerate the presence of a larger amount of water without causing phase separation.

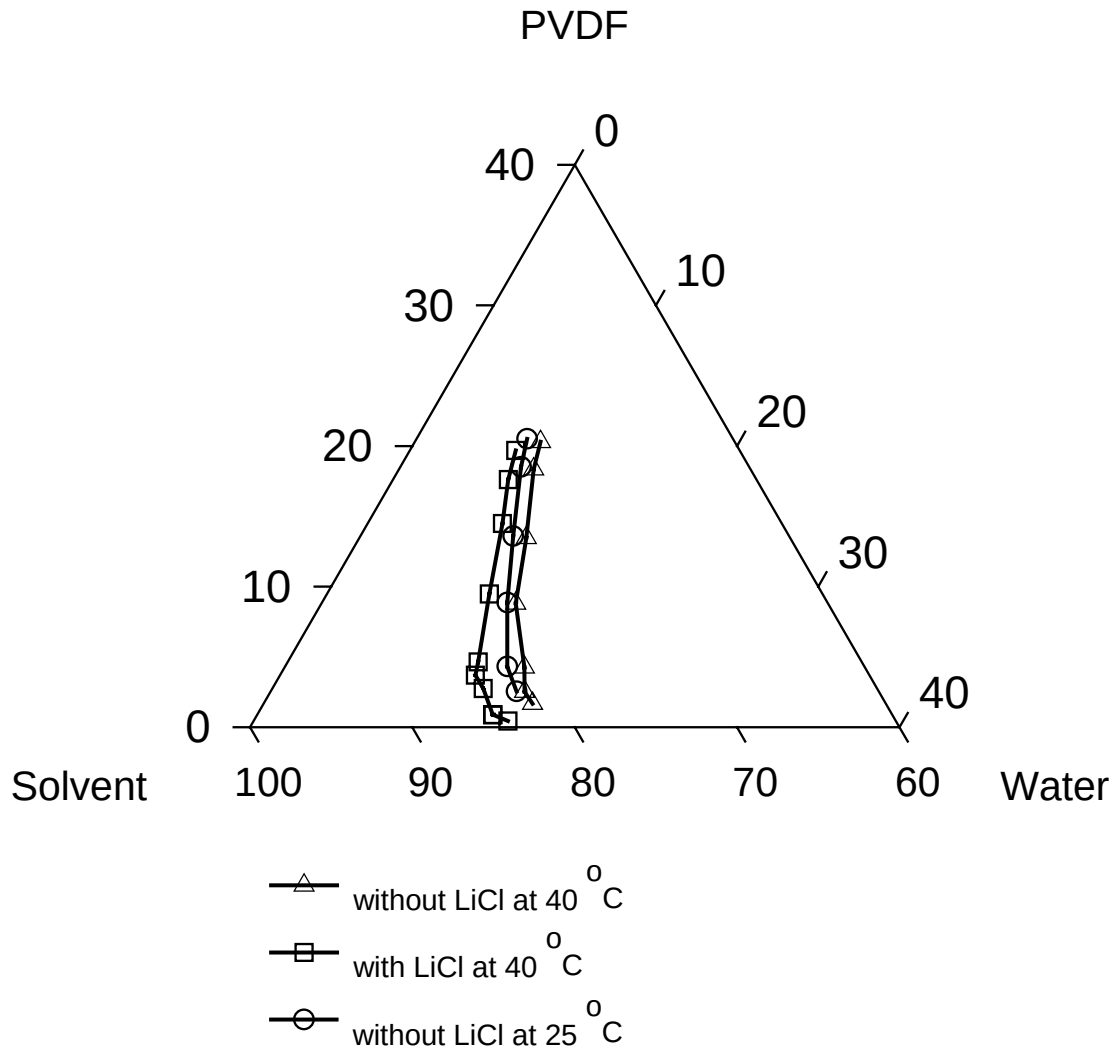

Figure 3.2 Phase separation data for PVDF/solvent/water systems

The above discussion is based only on the equilibrium phase separation data, i.e. the thermodynamic aspect of polymer precipitation. The first appearance of turbidity indicates

that some polymer aggregates have began to come out of the solution due to phase separation. In hollow fiber membrane formation processes, the bore side of the fiber came into contact with water, first, and at the same time, the outside of the fiber was exposed to air before being immersed in a water bath. Therefore, the above thermodynamic data cannot be taken for granted and care should be exercised in applying the thermodynamic information in the formation of hollow fiber membranes.

3.2.2 Kinetics of PVDF precipitation

The kinetics of polymer precipitation is characterized by the additive leaching rate and the solvent-nonsolvent exchange rate, which can be obtained experimentally by following the composition change in the gelation bath. To determine the leaching rate of LiCl from polymer solution, the relative concentration (C_t/C_∞) was used in Figure 3.3 with C_t and C_∞ denoting the concentration at time t and at infinite time when the concentration reached a constant respectively. Similarly, the relative concentration of DMAc was used to determine the DMAc/water exchange rate during the phase inversion process.

After being immersed in the gelation bath, the cast film soon peeled off from the glass plate, and the solvent-nonsolvent exchange and additive leaching began to occur on both sides of the film. It is shown that the LiCl leaching rate was very fast in the early stage of phase separation, and then began to slow down. It may be explained as follows: (1) as LiCl leached from the polymer solution, the difference between LiCl concentration in polymer solution and that in the gelation bath became small, and thus the leaching rate decreased due to the reduced driving force for LiCl leaching out of the membrane; (2) precipitation at the bath/solution interface would develop a greater resistance or barrier to mass transfer at the

interface between the bath and the polymer film. This resistance layer increases as the precipitation proceeded. This is in agreement with the observation that the thicker the membrane, the slower the LiCl leaching rate, as shown in Figure 3.3. It is interesting to note that even for a cast film thickness of 0.185 mm, more that 90% of LiCl leached out of the polymer system within 2 mins. This indicates that the phase separation is fairly quick, a feature that is favorable for hollow fiber membrane formation.

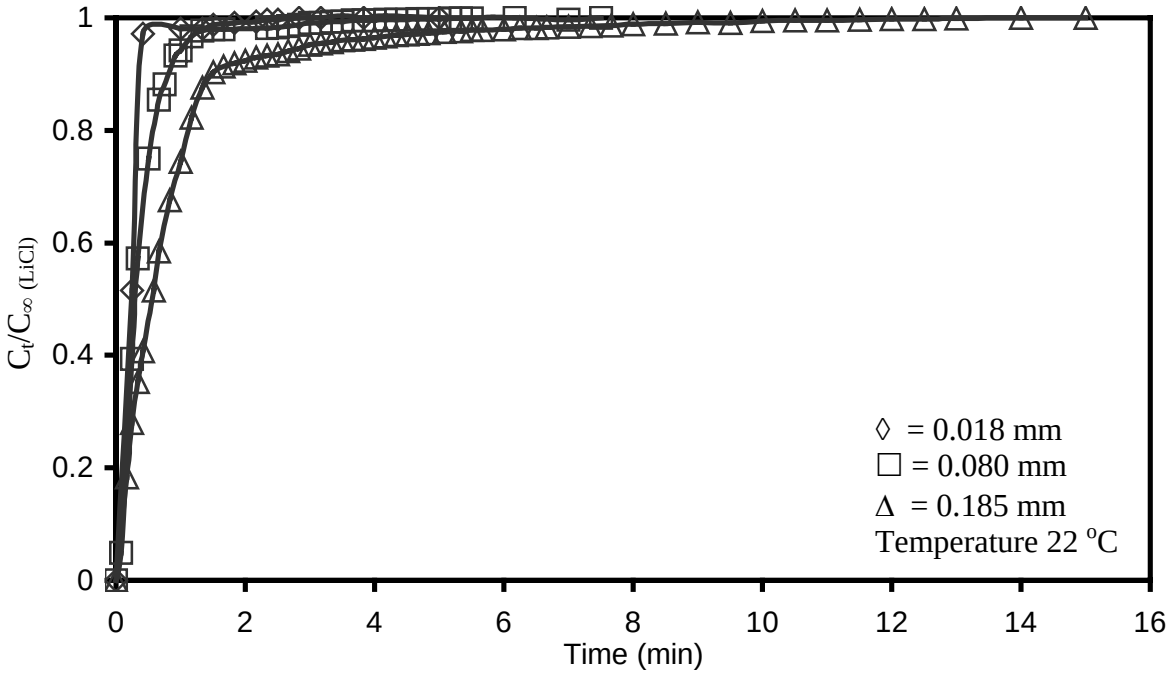

Figure 3.3 Leaching curves of LiCl during polymer precipitation for membrane of different thicknesses (dry).

Two polymer solution formulations were used in the experiments to determine the DMAc solvent-nonsolvent exchange rate: (1) PVDF/DMAC/LiCl (25/70/5 wt%), and (2) PVDF/DMAC (26/74 wt%). The experimental results are shown in Figure 3.4, which shows the trends was similar to that of additive leaching. Note that it took DMAc a longer time to

leach out from the polymer solution than LiCl did. One reason may be that not only were LiCl molecules smaller than DMAc, LiCl was present in the solution in ionic form. As a result, LiCl molecules could move among the polymer chains. The other reason may be the concentration of LiCl (5 wt%) is much smaller than that of DMAc (75 wt%).

It was also found that the solvent-nonsolvent exchange rate in the absence of LiCl additive was faster than the case where LiCl additive was present. This is illustrated more clearly in Figure 3.5, which represents a magnification of the data in Figure 3.4 over the first eight minutes for the two membranes with similar thickness. Because of the relatively fast leaching rate of LiCl, gelation will take place on the membrane surface quickly. The gelation layer will thus slow down the movement of DMAc from the membrane to the water bath, resulting in a slower solvent-nonsolvent exchange.

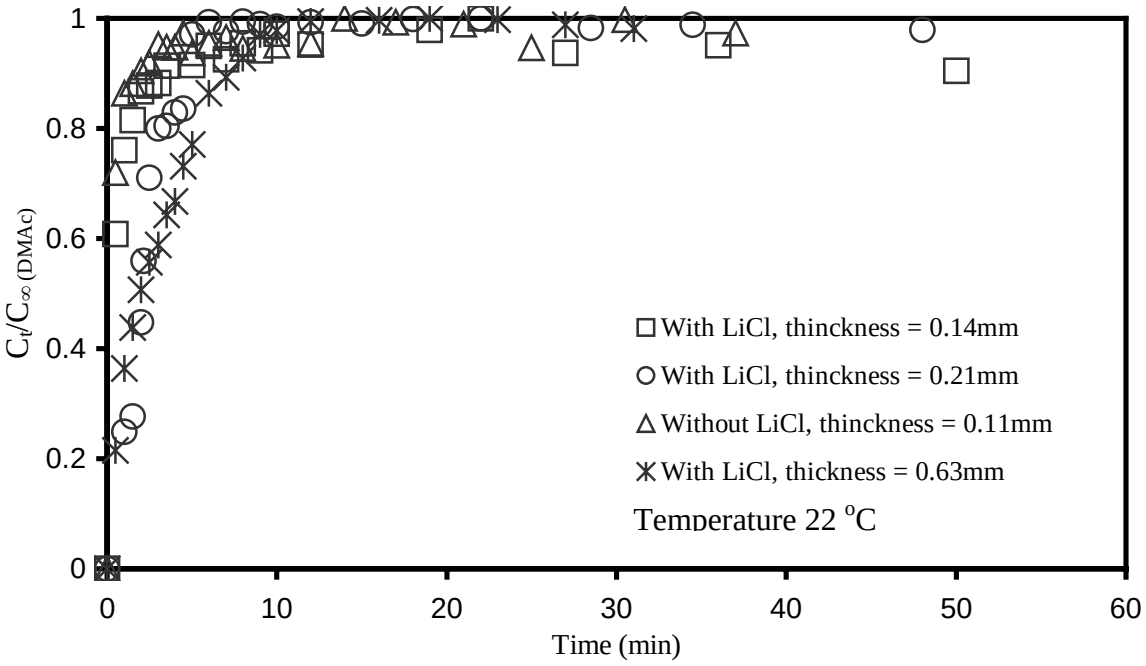

Figure 3.4 Solvent-nonsolvent exchange curves during polymer precipitation for membranes of different thicknesses (dry) and compositions

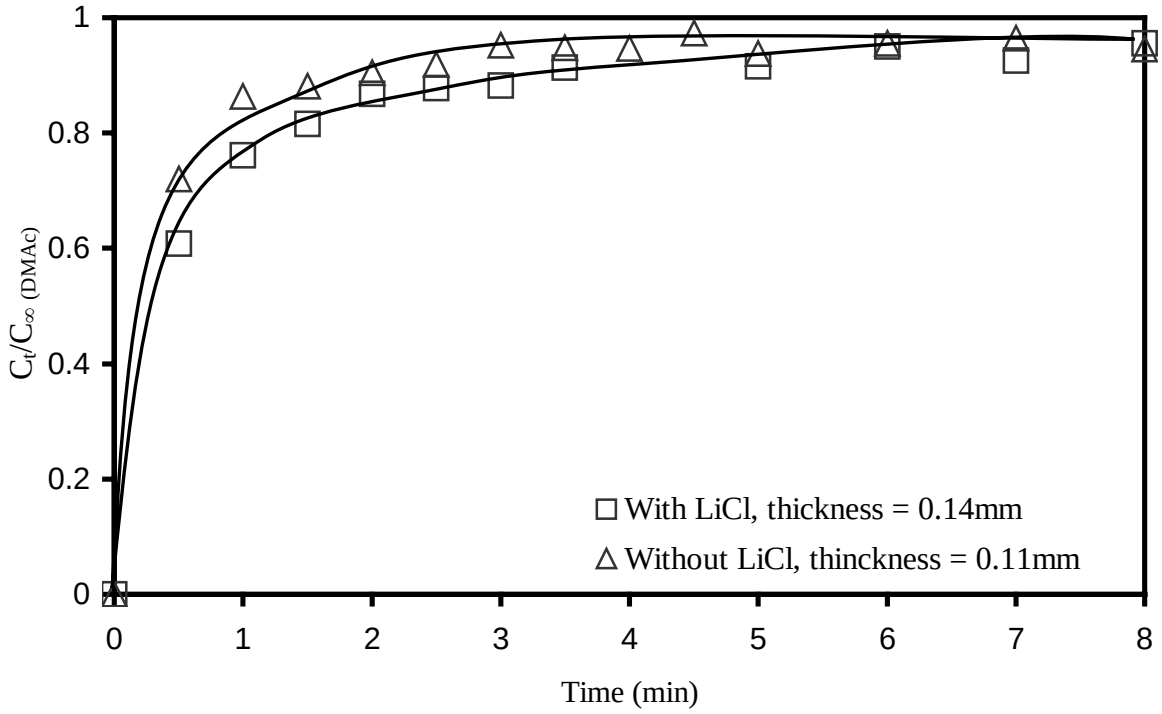

Figure 3.5 Solvent-nonsolvent exchange curves during polymer precipitation for membranes of different compositions over the first eight minutes

3.3 Conclusions

The equilibrium phase separation for PVDF/DMAc/H_2O systems with and without LiCl additive was studied. The solvent (DMAc)-nonsolvent (H_2O) exchange rate and the additive leaching rate during polymer precipitation in nonsolvent water were measured. The following conclusions can be drawn:

1) The presence of LiCl additive in the polymer solution influenced not only the thermodynamics but also the kinetic aspects of polymer precipitation.

2) The thermodynamic stability of the polymer solution was influenced by temperature.

3) When LiCl additive was used, the LiCl leaching rate was faster than the DMAc/water exchange rate.

4) Both LiCl leaching rate and DMAc/water exchange rate decreased during the course of the phase inversion process.

5) The thicker the membrane was, the slower the LiCl leaching and solvent-nonsolvent exchange were.

Chapter 4 Preparation and characterization of PVDF hollow fiber membranes

4.1 Introduction

Hollow fibers are commonly prepared using the dry-wet phase inversion technique. A problem encountered during the preparation is related to the viscosity of the spinning solution. Polymeric solutions can be cast on a support surface to form a film from very dilute solution as long as some minimum surface tension is maintained to keep the mechanic integrity of the layer. However, during the spinning process of hollow fiber preparation, the nascent fiber is retained as a result of the solution viscosity. A relatively high viscosity is often required in order to eliminate the formation of unstructured macrovoids in the fiber walls (Cabasso et al., 1976). There are three methods that may be employed in order to achieve a high viscosity of a polymer solution: (1) increase polymer concentration or molecular weight of the polymer, (2) choose suitable solvents near the solubility area boundary (i.e. poor solvent), and (3) incorporate a third additive component into the spinning solution to increase the viscosity of the casting solution. The last method was effective when LiCl was used as a third component.

There are several factors that determine the functionality and the efficiency of porous membranes, including the mean pore size, effective porosity and pore size distribution. The effective porosity is defined as the fractional volume of open pores which extend from one side of the fiber wall to the other side. This definition specifically excludes consideration of

closed cell 'dead' pores. The effective porosity determines the mechanical strength and permeation resistance of the membrane. Additionally, the pore size distribution is a very important parameter to the substrate of composite membranes. Careful consideration with respect to such parameters is essential in predicating the membrane structure and the ultimate performance of the membrane.

This study aims to develop the appropriate substrate PVDF hollow fiber membranes for the preparation of composite PEBA membranes. The effects of spinning conditions (i.e., dope extrusion rate, take-up speed, and inner coagulant speed) on the mean pore size, effective porosity and the morphology of fibers were analyzed using the gas permeation method. The porometric method based on liquid displacement by gas was employed to determine the relative distribution of pore sizes in the fiber wall.

4.2 Theoretical

The gas permeation method is one of the most frequently used methods to determine the mean pore size of porous membranes. Different mechanisms may be involved in the transport of a gas across a porous membrane (Koros and Fleming 1993; Pandey and Chauhan 2001).

The mechanism of gas permeation through a porous membrane is dependent on the ratio of the pore radius (r) and the mean free path (λ). The mean free path (λ), which is the average distance that the gas molecule travels between collisions, is given by

$$\lambda = \frac{kT}{\sqrt{2}\pi Dp} \tag{4.1}$$

where k is the Boltzmann constant, T is the temperature, D is the diameter of the gas molecule, and p is the pressure.

If $r/\lambda >> 1$, viscous or Poiseuille flow predominates and the gas flux (Q_{vis}) through one pore with radius r is described by the Hagen-Poiseuille equation:

$$Q_{vis} = \frac{r^2(p_1^2 - p_2^2)}{16l\eta RT} \tag{4.2}$$

where l is the effective pore length, p_1 is the pressure of the gas on the feed side, and p_2 is the pressure on the permeate side.

When $r/\lambda << 1$, there are more collisions between a gas molecule with the pore walls than with other gas molecules. Upon collision with the pore walls, the gas molecules are momentarily absorbed and then reflected in a random direction. Due to the fact that there are fewer collisions among molecules than with the pore walls, each molecule will move independent of others. Hence, the separation of a gas mixture is achieved if different gas species move at different velocities. This is called Kundsen flow. In this case, the flux of gas permeating through one pore with radius r can be described by

$$Q_{knu} = \frac{8r\ (p_1 - p_2)}{3l(2\pi MRT)^{1/2}} \tag{4.3}$$

where M is the molecular weight of the gas.

Gas permeating through a nonporous membrane can be described by the solution-diffusion mechanism. Normally, the permeability of a gas through a nonporous membrane is much lower than that through a porous membrane. Subsequently, the solution-diffusion flow through nonporous part of the membrane is neglected during the calculation for determination of porous structure of a porous membrane, and only viscous flow and

Knudsen flow may be considered under these circumstances. Then, the permeance of a gas through the membrane with a model pore radius *r* and porosity ε can be obtained (Wang et al., 1999):

$$J_{total} = \frac{F_{total}}{A\Delta p} = \varepsilon \frac{1}{lRT}[\frac{r^2}{8\eta}\bar{p} + \frac{2r}{3}(\frac{8RT}{\pi M})^{1/2}] \tag{4.4}$$

or

$$J_{total} = a\bar{p} + b \tag{4.5}$$

where $a = \frac{r^2\varepsilon}{8\eta RTl}$, $b = \frac{2}{3}(\frac{8RT}{\pi M})^{1/2}\frac{1}{RT}\frac{r\varepsilon}{l}$ and $\bar{p} = (p_1 + p_2)/2$. The permeance J_{total} can be determined by measuring the gas permeation rate under a certain pressure difference across the membrane. The values of *a* and *b* can be determined from the intercept and slope respectively in the J_{total} versus $\bar{p}$ plot. The mean modal pore radius is calculated by

$$r = \frac{16}{3}(\frac{a}{b})(\frac{8RT}{\pi M})^{1/2}\eta \tag{4.6}$$

The effective surface porosity over effective pore length $\frac{\varepsilon}{l}$ can thus be calculated as follows:

$$\frac{\varepsilon}{l} = \frac{8\eta RT}{r^2}a \tag{4.7}$$

Note that the effective pore length (*l*) is difficult to measure in practice and it is, in fact, not necessary to measure it. Instead, it is convenient to use a combined parameter ε/l to represent the porous structure of the membrane.

The pore size distribution is another important parameter to consider for both manufacturing and application purposes. Many techniques are available for the

measurement of porosity, such as mercury penetration, liquid-gas displacement, liquid-liquid displacement, and dynamic flow-weighed thermoporometry (Nakao, 1994). When using the mercury penetration technique, mercury is used to fill the pores of a membrane. This technique is useful for membranes with large pores (such as microfiltration membranes), but is not suitable for membranes with relatively small pores due to the fact that an extremely high pressure may be needed, which could eventually destroy the membrane network. The liquid-gas displacement method, also called the bubble pressure method, can be used to evaluate pore size by measuring the pressure needed in order to force a gas through the membrane so as to displace the liquid initially filling in the pores (Shao et al., 2003). This method was used in the present work and will be discussed later.

The bubble pressure methods are based on the consideration that the large pores will be opened first by the gas, and that the first bubble corresponds to the largest pore. In addition, as the pressure of the gas increases, the pores of smaller sizes will gradually open. Figure 4.1 illustrates the liquid-gas displacement method for determination of the porous structure of the membrane.

Assuming cylindrical pores, according to the Laplace equation,

$$\Delta p = \frac{2\gamma \cos\theta}{r} \tag{4.8}$$

where γ is the surface tension of the liquid, θ is the contact angle of the liquid with the pore surface, and Δp is the pressure difference across the membrane can be rearranged to give

$$r = \frac{2\gamma \cos\theta}{\Delta p} \tag{4.9}$$

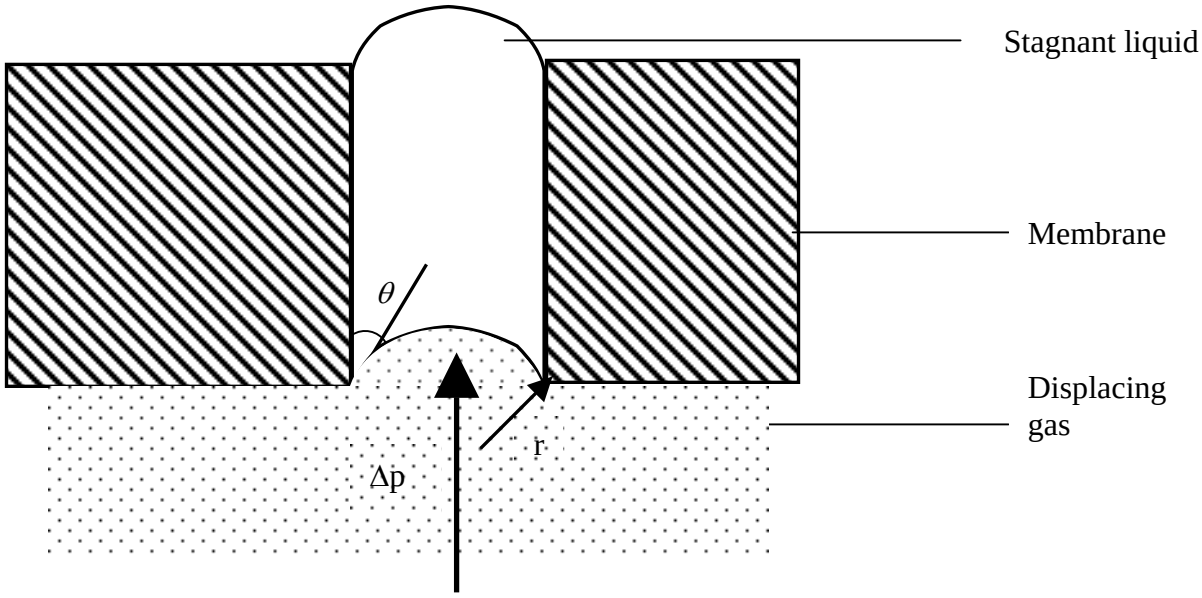

Figure 4.1 Schematic representation of liquid-gas displacement for determining the porous structure of membranes

This equation relates pressure and pore radius. The pressure required to open a pore increases as the pore size decreases. When the membrane pores are partially opened (i.e. larger pores are open and smaller pores are still filled with liquid), the gas may pass through the opened pores by viscous or Knudsen flow, depending on the magnitude of the pore size relative to the mean free path of the gas molecules at the operating conditions. Normally, when a gas is used as the displacing fluid, the size of the open pores is always larger than the mean free path of the gas at the operating conditions, and viscous flow predominates. According to the Hagen-Poiseuille equation, the gas permeation rate through a group of pores of nominal radius r_i and porosity of ε_i can be written as:

$$J_i = \frac{\varepsilon_i r_i^2}{8\eta Tl} \overline{p}_i \tag{4.10}$$

If there are *N* groups of pores of different pore sizes that have been opened by the gas, then the total permeation rate of the gas permeating through the (*N+1*) groups of pores can be written as:

$$J_{total} = \sum_{1}^{N} J_{N+1} = \frac{\sum_{1}^{N} \varepsilon_i r_i^2}{8\eta T l} \overline{p_{N+1}} + \frac{\varepsilon_{N+1} r_{N+1}^2}{8\eta T l} \overline{p_{N+1}} \tag{4.11}$$

The pore size distribution function $f(r)$ can be defined as,

$$f(r) = \frac{1}{\varepsilon_t} \frac{d\varepsilon}{dr} = \frac{1}{\varepsilon_t / l} \frac{\varepsilon_i / l}{(r_{i-1} - r_i)} \tag{4.12}$$

where ε_i is the porosity of a group of pores with radius r_i, and ε_t is the total porosity of the membrane. Detailed treatments of applying this method can be found in Shao et al. (2003).

Through this method, the pore size distribution can be determined. A narrow pore size distribution indicates that the membrane has an even pore size, which is desired. If the pore size distribution is wide or has more than one 'peaks', it is likely that the membrane would be hard to coat in order to form a defect free composite membrane.

4.3 **Experimental**

4.3.1 Materials

Unless specified otherwise, all materials used were the same as those described in Chapter 3. Nitrogen gas (research grade, >99.5%) was supplied by Praxair Company, and 2-Ton epoxy was supplied by ITW Devcon. Deionized water was used as the inner coagulant during hollow fiber spinning.

4.3.2 Preparation of PVDF hollow fiber membranes

PVDF and LiCl were dried in an oven at 70 °C for 24 h before use. First, LiCl was dissolved in DMAc. Then, a predetermined amount of PVDF was added to the solution. After stirring, the solution was heated at 60 °C for 0.5 h to facilitate the dissolution of PVDF. The solution bottle was sealed tightly throughout the process in order to eliminate any solvent loss due to evaporation. The PVDF homogenous solution was transferred into a stainless steel dope tank at a given temperature. Before spinning, the solution was kept in the solution tank for at least 8 hours to ensure the removal of fine air bubbles entrapped in the polymer solution.

All PVDF hollow fiber membranes were spun via the dry-wet phase inversion method. The equipment used to spin hollow fibers, illustrated in Figure 4.2, consists of a solution dope tank (made of stainless steel), a dope solution filter, a tube-in-orifice spinneret (shown in Figure 4.3), a coagulant bath, a washing bath, and a fiber collecting device. Helium gas was used to control the extrusion rate of the dope solution through the orifice of the spinneret. The internal coagulant was pumped to the tube side of the spinneret using a high pressure precision metering pump. The nascent fiber emerging from the spinneret was partially solidified by the internal coagulation fluid. The spinneret was positioned above the coagulation bath so that the outer surface of the fiber was exposed to air for partial evaporation of solvent before being immersed in the coagulation bath, where coagulation occurred on the outer surface of the membrane due to solvent-nonsolvent exchange. As a result, asymmetric hollow fibers could be obtained. The fibers remained in the water bath to complete coagulation before being taken out. During the coagulation period, most of the LiCl additive leached out from the membrane. Finally, the membranes were rinsed in

deionized water for at least 7 days before use. The hollow fiber preparation conditions are listed in Table 4.1.

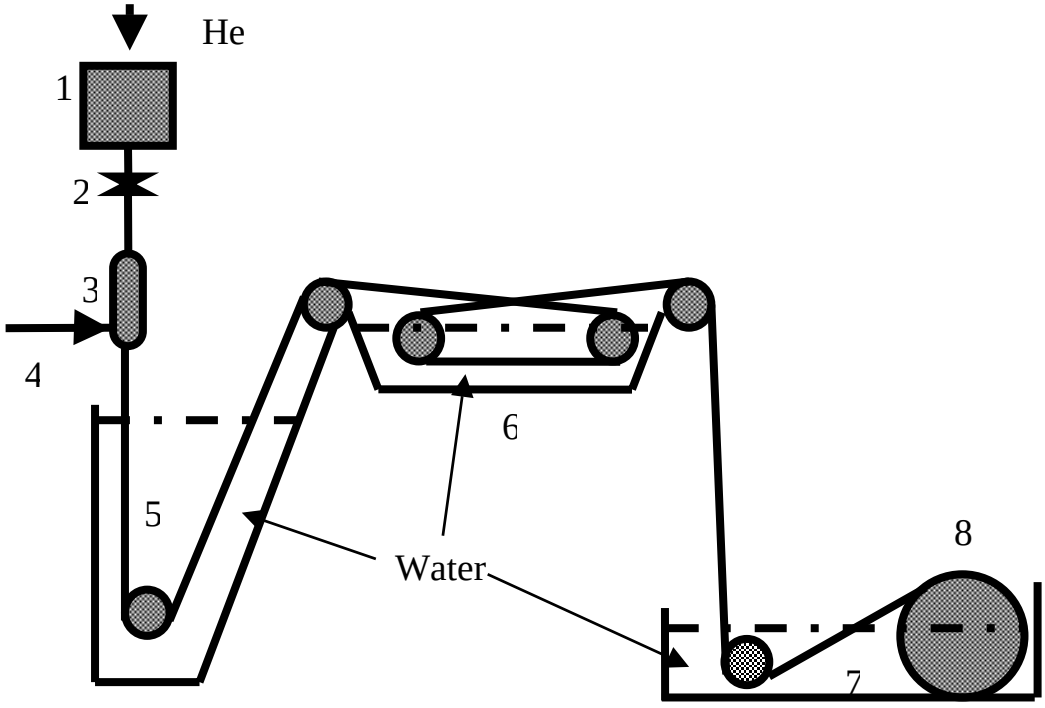

Figure 4.2 Schematic diagram of a hollow fiber spinning process. (1) solution dope tank, (2) dope solution filter, (3) spinneret, (4) internal coagulant, (5) external bath, (6) washing bath, (7) fiber collecting bath, (8) fiber windup drum

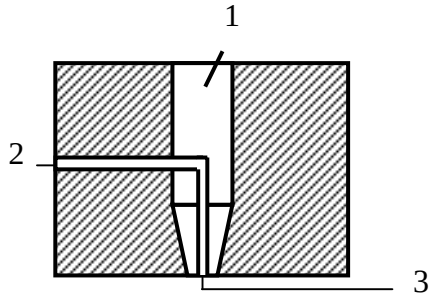

Figure 4.3 Schematic structure of the tube-in-orifice spinneret. (1) Spinning solution entry port, (2) coagulating fluid entry, (3) extrusion orifice.

Table 4.1 Spinning conditions of hollow fiber membranes

Spinning Conditions	
Dope composition (DMAc/PVDF/LiCl) (wt%)	80/15/5 or 75/20/5
Internal coagulant speed	10~40 m/min
Spinneret orifice size (OD/ID)	1.0/0.5 mm
Fiber take-up speed	7~14 m/min
Air gap between spinneret and coagulant bath	10 cm
Dope Extrusion rate	2.9~5.7 ml/min
Dope solution temperature	22 °C or 50 °C
Room temperature	22 °C
Relative humidity	40~50%
Temperature of inner coagulant	22 °C
Temperature of external coagulant bath	35 ° C

4.3.3 Membrane morphology

The membrane morphology was examined by using a JSM-840 (JSL) scanning electron microscope (SEM). To prepared the specimen, the hollow fiber membranes were immersed in liquid nitrogen for 3 minutes, and then the membrane samples were carefully fractured. After being coated with gold using an ion sputter device, the morphology of the samples was examined under a SEM.

4.3.4 Gas permeation

The hollow fiber membranes were dried at ambient conditions. The hollow fibers were assembled to form a test module, as shown in Figure 4.4. One end of the hollow fiber was kept open, and the other end sealed with epoxy. The gas permeation experiments were performed at ambient temperature (22 °C). The test gas, nitrogen, was fed to the shell side of the membrane module at a given pressure. Figure 4.5 illustrates a schematic diagram of the gas permeation setup. The downstream pressure was 1 atm, and the nitrogen flux was measured using a bubble flow meter. The permeance data at different feed pressures were used to determine the mean pore radius and ε/l based on the gas permeation method.

4.3.5 Pore size distribution

Test modules containing five or six fibers (with each fiber being 26 cm long) were used in the determination of the pore size distribution by the liquid-gas displacement method. The experimental setup was essentially the same as that shown in Figure 4.5. Nitrogen gas was used as the test gas, and ethanol was used as the liquid to be displaced. The test module was initially filled with ethanol liquid so that the pores of the membrane were filled with the liquid due to the capillary force. Nitrogen was then fed on the bore side while the pressure was increased stepwise. The interval of the pressure change was about 2 psi. The gas follow rate through the open pores was measured at different pressures. All of the membrane pores were considered to be opened when the gas permeance began to follow a linear relationship with the pressure. Each run was completed within 30 minutes to minimize the swelling of the membrane by ethanol, which could affect the true pore size distribution of the dry membrane.

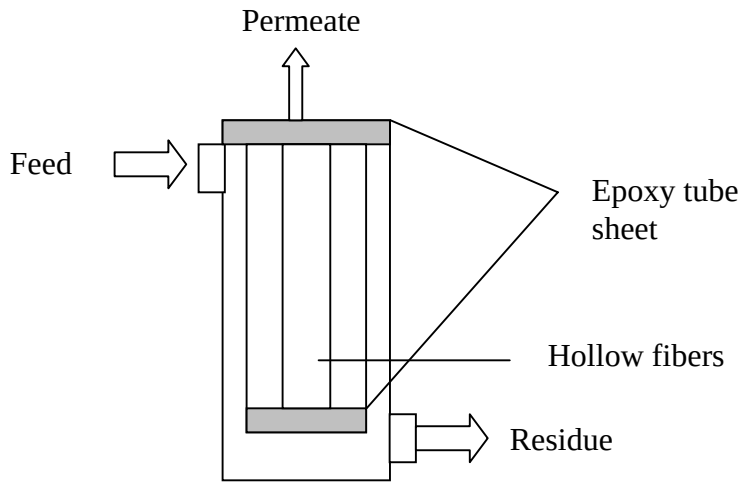

Figure 4.4 Schematic of a hollow fiber module

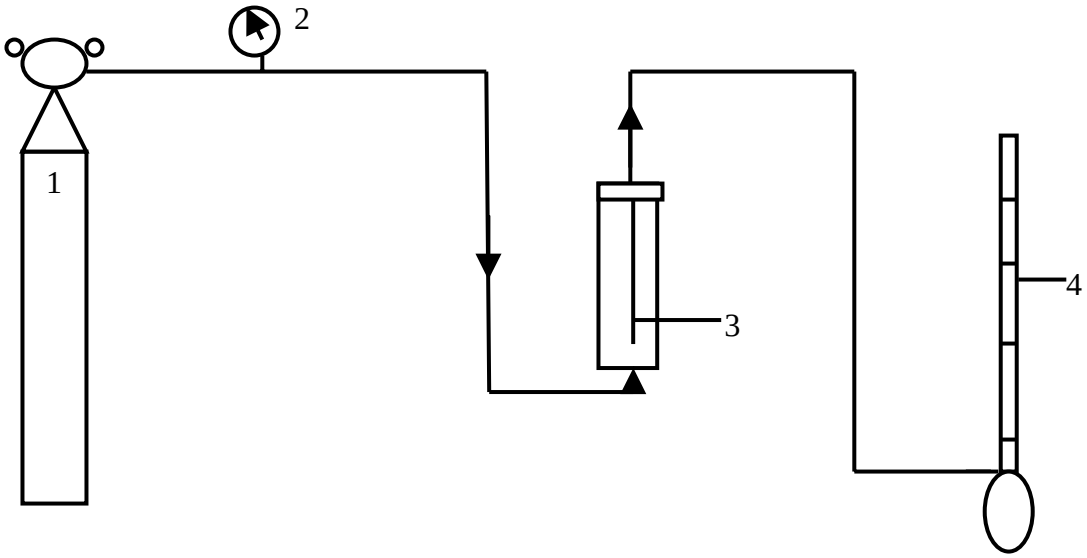

Figure 4.5 Schematic diagram of the gas permeation setup

(1) Nitrogen cylinder, (2) Pressure gauge, (3) Hollow fiber membrane,

(4) Bubble flow meter

4.4 **Results and discussion**

4.4.1 Effects of dope extrusion rate

The effect of dope extrusion rate on the fiber outside diameter (OD) and thickness (TH) are summarized in Figure 4.6; other conditions involved in fiber preparation are shown in Table 4.2. The mean pore radius of the membranes determined from the gas permeation experiment are presented in Figure 4.7, and the experimental data of gas permeation rate at different pressures are summarized in Appendix A. As the dope extrusion rate increased, both the outside radius and thickness increased, whereas the mean pore radius did not change substantially except at a very low extrusion rate of the dope solution. This may be explained from a shear rate point of view. When the dope extrusion rate increases, the extrusion shear rate will also increase. The rheology of most polymer solutions at high viscosity follows the non-Newtonian power-law relation, and the PVDF solution is a shear-thinning solution.

$$\eta = K\dot{\gamma}^{n-1} \tag{4.13}$$

where n is smaller than 1, K is a constant, and $\dot{\gamma}$ is the shear rate. When $\dot{\gamma}$ increases, the viscosity will decrease, which is referred to as a shear dilute solution. However, when the shear rate is high enough, the viscosity will tend to be constant. It is noted that one of the experimental data point in Figure 4.7 is much higher than that would be expected. There are two possible reasons: i) experimental error in the measurement; ii) the fiber may have a defect. A low viscosity of the polymer solution tends to result in a loose structure of the membrane, and thus the mean pore radius, outside diameter and thickness will increases as the shear rate is increased (Aptel et al. 1985). However, when the extrusion rate is very

high, both the viscosity and mean pore radius will be constant. This is in agreement with the experimental results reported in literature (Aptel et al., 1985; Fischer et al., 1988; Sharp et al., 1999; Chung et al., 2000).

Hagler (1981) developed a simple model, based on an average elongational rate, to predict qualitatively the effects of spinning parameters on the orientation of fibers spun from viscoelastic melts. He used a simple expression for the ultimate orientation factor, f_L, at the take-up point:

$$f_L = Const(Fext/W)\{V_L - V_0 \exp[(1-L)W/\rho bFextV_L]\} \quad (4.14)$$

where *Fext* is the force at take-up position, W is the mass flow rate, V_L is the take-up velocity, V_0 is the extrusion velocity, L is the spin draw ratio (V_L/V_0), ρ is the density, and b is τ/η^*, where η^* is the extrusion viscosity, and τ *is* relaxation time. From this equation it can be deduced that when V_L and other parameters are fixed, increasing V_0 will lead to a

Table 4.2 Fiber spinning conditions

Spinning condition	
Temperature of dope (^{o}C)	50
Temperature of inner coagulant (^{o}C)	22
Temperature of outer coagulant T (^{o}C)	33
Dope extrusion rate (ml/min)	2.89~5.70
Air gap (cm)	10
Fiber take up speed (m/min)	8.3
Inner coagulant speed (m/min)	23.58

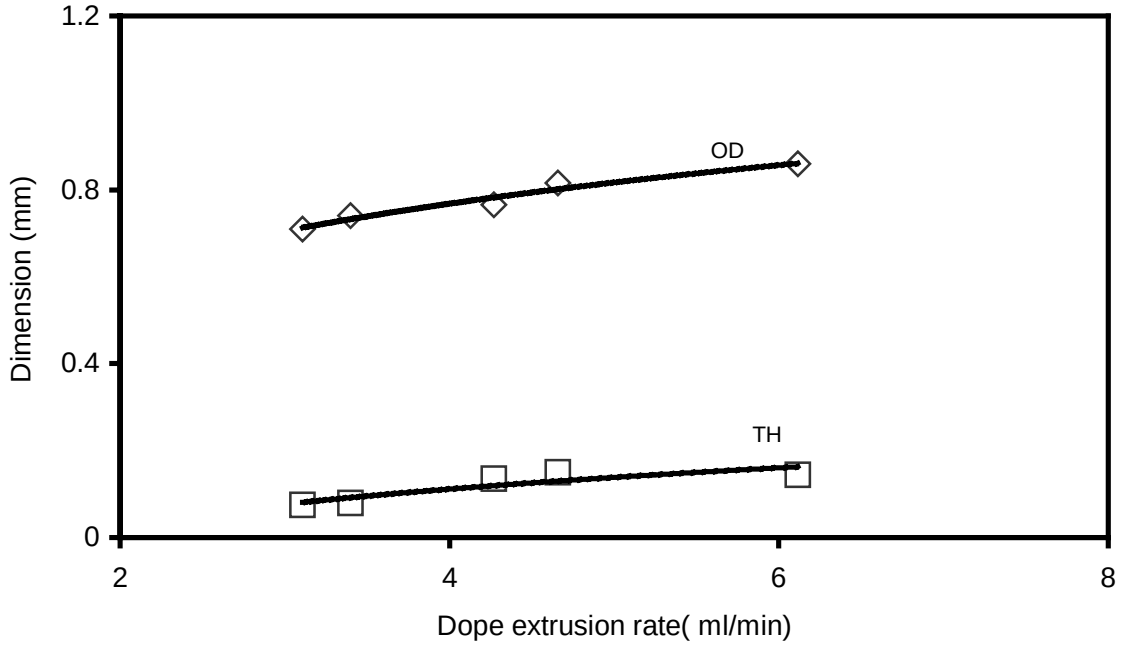

Figure 4.6 Effects of dope extrusion rate on fiber dimensions (OD: outside diameter, ID: inside diameter)

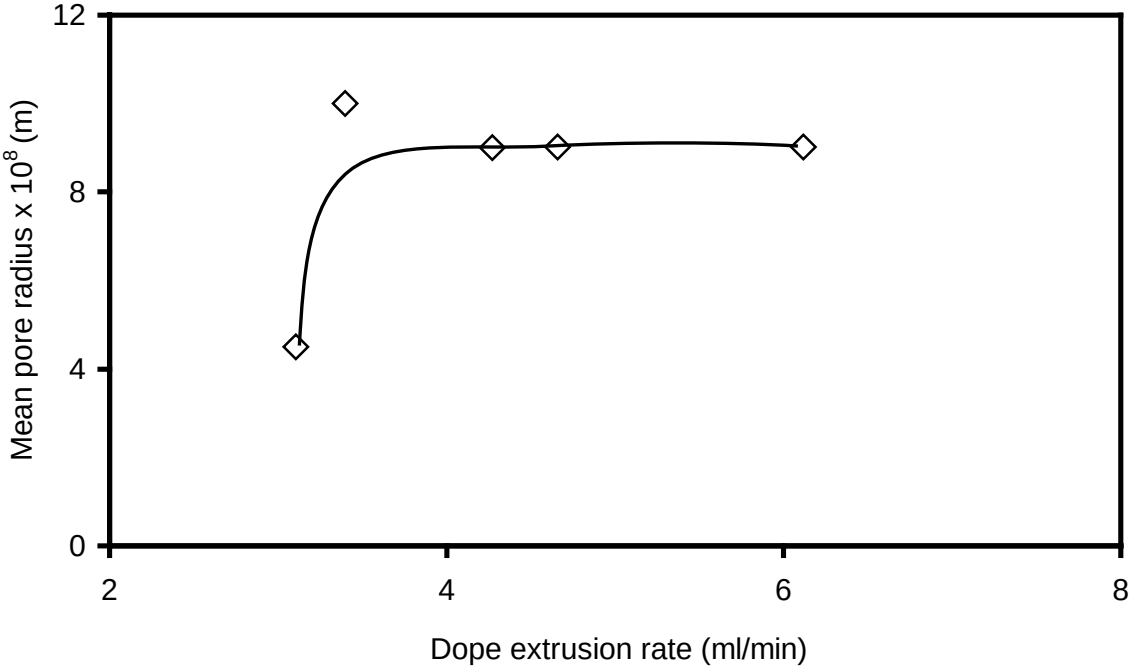

Figure 4.7 Effects of dope extrusion rate on the fiber mean pore radius determined from gas permeation experiments

decrease in f_L, which means that an increase in extrusion rate decreases the molecular chain orientation. Less orientated molecular chains lead to the formation of loose fiber structures, as reflected by the increase in OD and TH. In addition, the values of ε/l in this experiment were found to vary from 43 to 174 m^{-1}, and there is no clear definite relation between the porosity of the membrane with the dope extrusion rate during fiber spinning.

4.4.2 Effects of inner coagulant speed

As soon as the nascent fiber leaves the spinneret, the inner coagulant contacts with the bore side of the fiber immediately, and the solvent-nonsolvent exchange begins. The inner coagulant speed affects both the solvent-nonsolvent exchange rate and the fiber morphology. The effect of the inner coagulant speed on the physical characteristics of the fibers is shown in Figure 4.8. Other conditions of fiber spinning were the same as those shown in Table 4.2 except the dope extrusion rate, which was 1.42 m/min. When the inner coagulant speed increased, the outside as well as inside diameters (ID) increased and the thickness decreased slightly. This is understable since the high pressure required to increase the inner coagulant speed will cause an expansion of the hollow fiber. Consequently, the fiber diameter increases, and the wall thickness decreases. When the inner coagulant speed varied from 9.8 to 39.8 m/min, the mean pore radius and ε/l were varied in the range $(6.4\sim1.6) \times 10^{-8}$ m and 58~232 m^{-1}, respectively and no simple relations between these membrane structural parameters and the inner coagulant speed during fiber spinning can be observed.

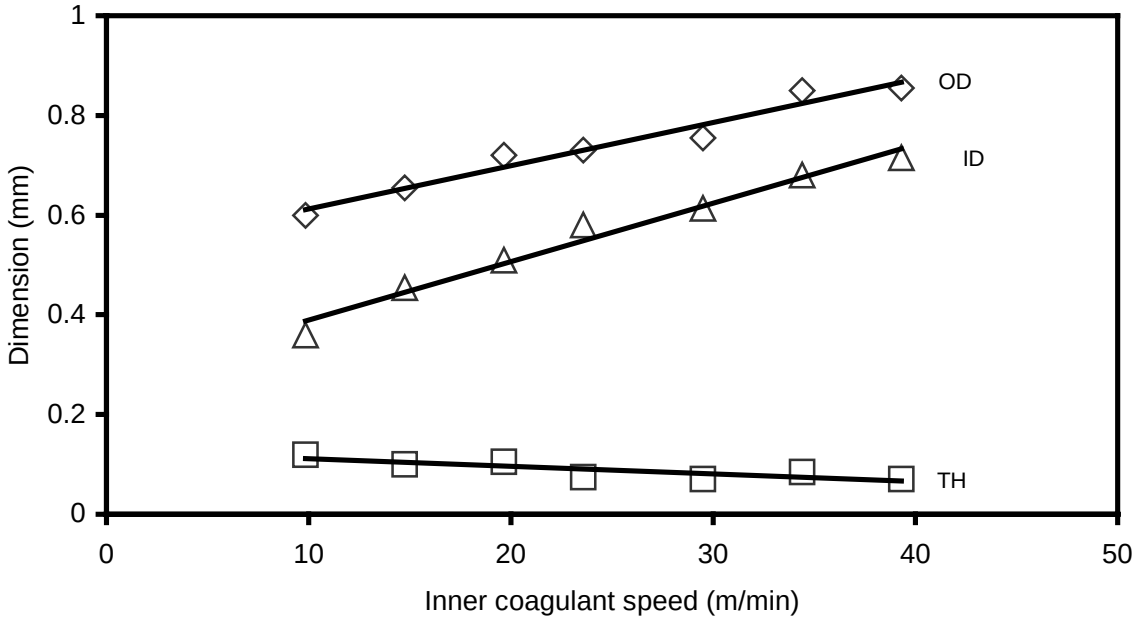

Figure 4.8 Effects of inner coagulant speed on the fiber dimensions (OD: outside diameter, ID: inside diameter and TH: thickness)

4.4.3 Effect of fiber take-up speed

Figure 4.9 shows the effect of the fiber take-up speed on the outside diameter, inside diameter and wall thickness of the hollow fibers. Other conditions for fiber spinning are the same as shown in Table 4.2 except for the dope temperature (22 ^{o}C) and the dope extrusion rate (1.15 m/min). An increase in take-up speed leads to better molecular orientation of the polymer. This means the polymer molecular chains stay closer, which results in smaller hollow fibers. Interestingly, the thickness of the hollow fiber wall did not change significantly. According to Equation (4.14), an increase in V_L increases the polymer orientation. When the fiber take-up speed increases, there will be a force along the extrusion direction. Consequently, because the membrane matrix is very weak, the pores in the membrane will tend to be enlarged by this force. This is shown by the data presented in Figure 4.10. Interestingly, the ratio ε/l decreases with an increase in the take-up speed. While

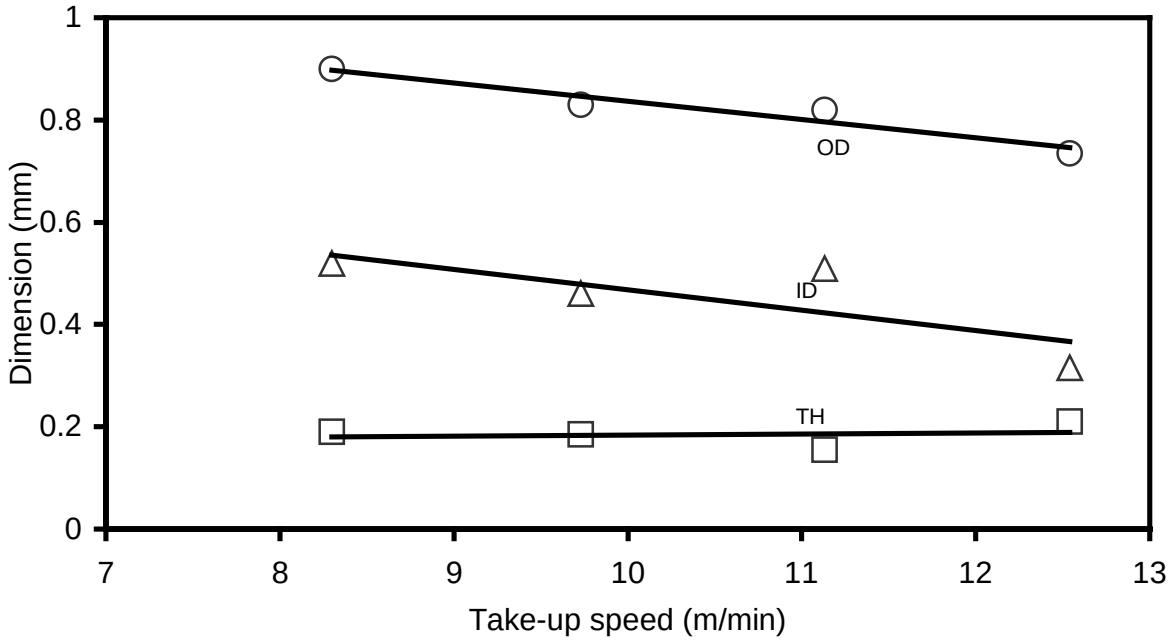

Figure 4.9 Effects of take-up speed on hollow fiber dimensions

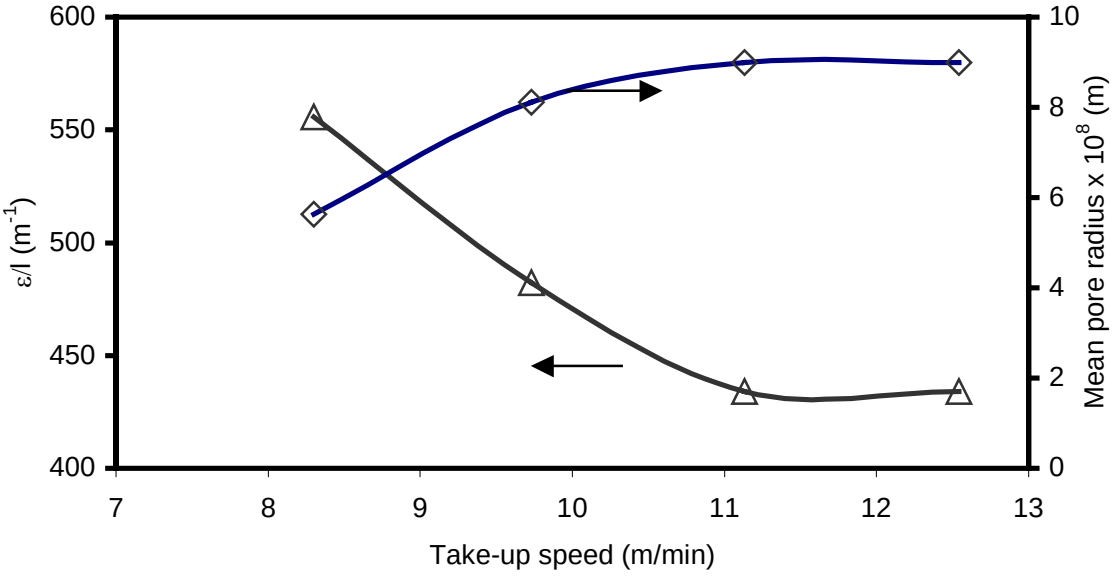

Figure 4.10 Effects of take-up speed on ε/l and mean pore radius of the hollow fiber

the stretching of the membrane caused by an increase in the fiber take-up speed tends to result in larger pore sizes and hence a larger porosity, the pores in the membrane will be more tortuous as the membrane is gradually solidified during the take-up. Obviously, when the increase in the pore length outweighs the increase in the porosity, ε/l will decrease as the take-up speed increases.

4.4.4 Membrane morphology

The spinning process is accomplished in two steps: (1) exposure of the external surface of the extruded dope solution to a gas phase (i.e. air) while the inner surface is coagulated by the inner coagulant, followed by (2) immersion in an external coagulating liquid (i.e. water). The dry-wet spinning procedure is accompanied by the formation of cavities, and/or 'finger-like' intrusion cells within a hollow fiber wall (Cabasso et al., 1977a). In order to illustrate that the membrane preparation conditions are critical to the structure of resulting membrane, the macrostructures of PVDF hollow fibers were examined under electron scanning microscope. Figure 4.11 and 4.12 show the SEM pictures of the cross sections of two hollow fibers prepared under the same conditions except for the internal coagulant speed (see Table 4.3 Fiber #16 and 17). Both fibers exhibit a sponge like structure in the region near the outer surface, a finger-like structure near the inner surface, and a thin skin layer on the outer surface. The cross section of #16 fiber appeared to have more finger pores than #17 fiber. It is also noted that the lumen of #16 fiber was not perfectly round, compared to that of #17 fiber. The sponge structure is attributed to the slow solvent-nonsolvent exchange caused by partial evaporation of solvent when the fibers pass the air gap, during which period the local polymer concentration on the external surface

increases. As a result, the subsequent solvent-nonsolvent exchange slows down. Fast solvent-nonsolvent exchange generally results in finger-like structures. This is the case for the finger pores near the inner surface of the fiber. When comparing the two membranes, it is found that both the size and the number of the finger pores are different. In addition, due to the relatively low pressure used in delivering a low inner coagulant flow rate in preparing #16 fiber, the fiber lumen was not fully bolstered up (see Figure 4.11).

Macrovoids, such as finger pores, offer little resistance to permeation and lead to a low mechanical membrane strength. On the other hand, the sponge structure is mechanically strong, but it will increase the permeation resistance. Therefore, in selecting and formulating membrane preparation conditions the balance between these two aspects should be considered.

Table 4.3 Spinning conditions of # 2, #13, #16 and #17 fibers

Spinning condition	#2	#13	#16	#17
Temperature of dope (^{o}C)	50	22	50	50
Temperature of inner coagulant (^{o}C)	22	22	22	22
Temperature of outer coagulant (^{o}C)	34	34	33	33
Dope extrusion rate (m/min)	1.42	1.13	2.72	2.72
Air gap (cm)	10	10	10	10
Take up speed (m/min)	8.3	9.7	8.3	8.3
Inner coagulant speed (m/min)	9.8	23.6	4.91	39.32

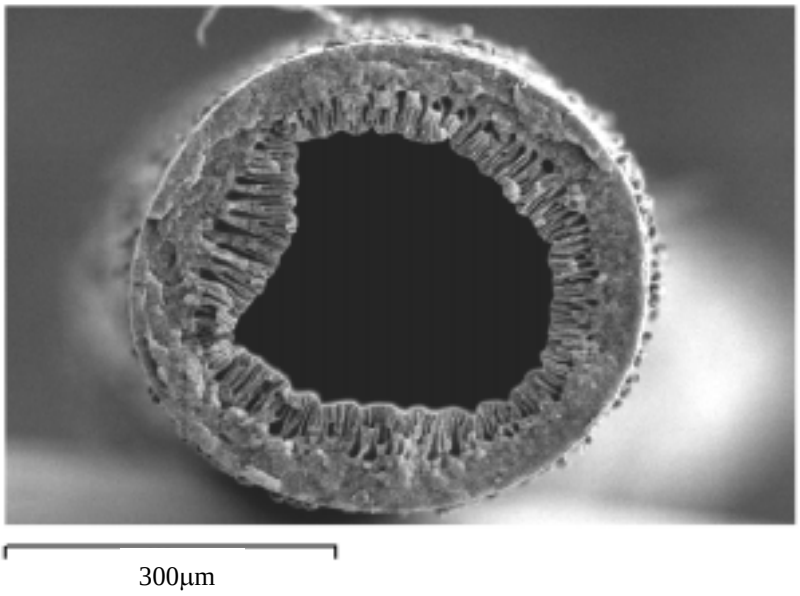

Figure 4.11 SEM of the cross-section of #16 PVDF hollow fiber

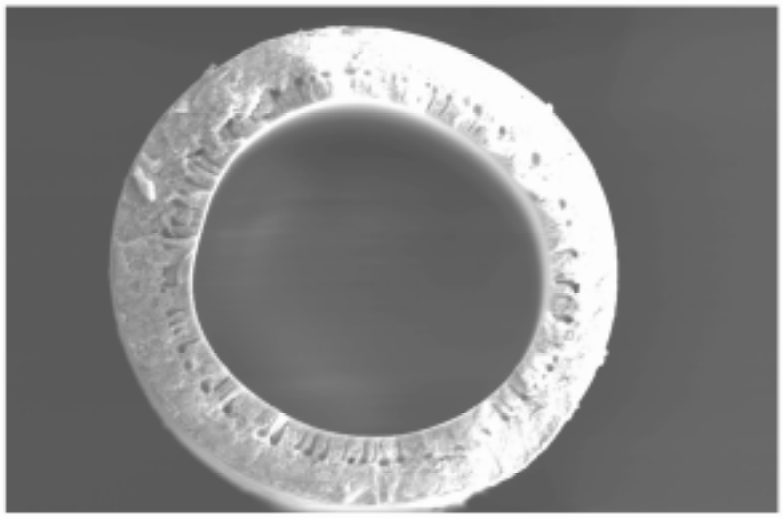

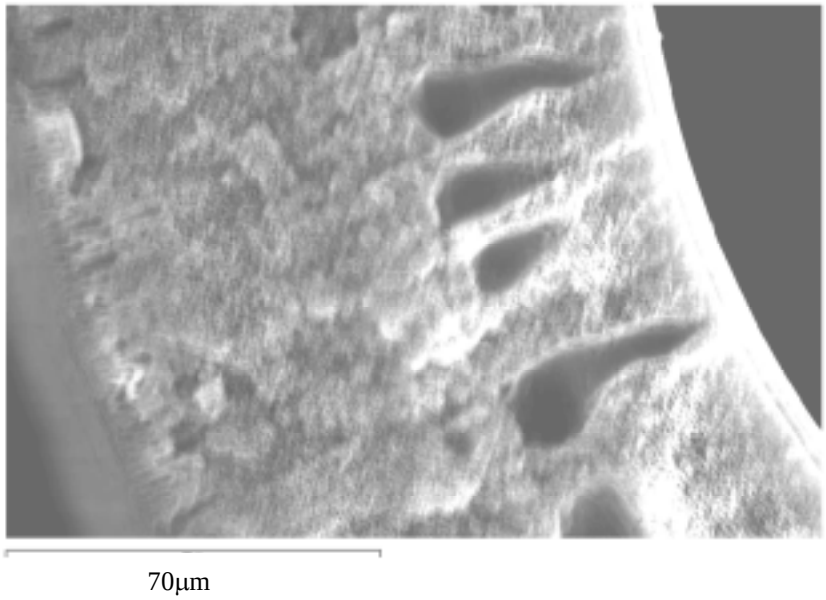

Figure 4.12 SEM of the cross-section of #17 PVDF hollow fiber

4.4.5 Pore size distribution

In screening suitable PVDF hollow fibers as a substrate membrane for preparation of PEBA/PVDF composite membrane, the hollow fibers were subject to a mechanical stability test. Three hollow fibers were found to the stable at an elevated pressure of over 110 psig. These membranes were further investigated in terms of their pore size distributions. Refer to Table 4.3 for the spinning conditions. The contact angle between the ethanol and PVDF membrane was zero and the ethanol surface tension was 23.5 dyn/cm, which were measured by the Axisymmetric Drop Shape Analysis – Profile (ADSA-P) method. Their dimensions are listed in Table 4.4. The mean pore radius and ε/l of the fibers, measured by the gas permeation method, are also presented in the table.

Table 4.4 Dimension and structure of the fibers

Fiber number	OD (mm)	TH (mm)	Mean pore radius (m)[a]	ε/l^a
#2	0.83	0.19	8×10^{-8}	482.36
#13	0.60	0.12	4×10^{-8}	85.09
#16	0.49	0.22	9×10^{-8}	86.82

[a] determined by the gas permeation method

To determine the pore size distribution of the membrane, the liquid-gas displacement experiments were carried out. The relationship between the nitrogen flux and pressure for the three fibers is shown in Figure 4.13. The corresponding pore size distribution of these fibers are shown in Figure 4.14. It is found that the pore size of fibers #2, #13 and #16 were mainly distributed at approximately 3.70×10^{-8}, 3.55×10^{-8} and 3.55×10^{-8} m, respectively. It is

interesting to note that the pore size distribution of fiber #13 matched its mean modal pore radius determined by gas permeation method, while the pore size distribution of other two fibers indicated an underestimation of the mean pore sizes. The discrepancy is mainly due to the measurement methods. In gas permeation, the mean modal pore size measured is really the equivalent of cylindrical pores. In using the fluid displacement method, the actual geometry of the pores will significantly influence the capillary force that is required in order for the gas to displace the liquid imbibed in the pore. The values of ε_t/l determined by this method are summarized in Table 4.5. It can be seen that the values of ε_t/l are much smaller than the values obtained by the gas permeation method. The reasons are (1) the pore size measured by this method have been underestimated compared to that determined by gas permeation, and (2) some small pores were not open at the end of the experiment since a very high pressure would be required to open small pores as suggested by Equation (4.8). Nevertheless, these results are still valuable in screening hollow fibers on a relative basis. It is clear that the pore size is fairly evenly distributed with quite a narrow range of pore sizes. This is desired if the hollow fiber is to be used as a substrate to prepare composite membranes by dip coating technique.

Table 4.5 ε_t/l of the fibers determined by the liquid-gas displacement method

Fiber number	ε_t/l
#2	0.64
#13	0.25
#16	12.4

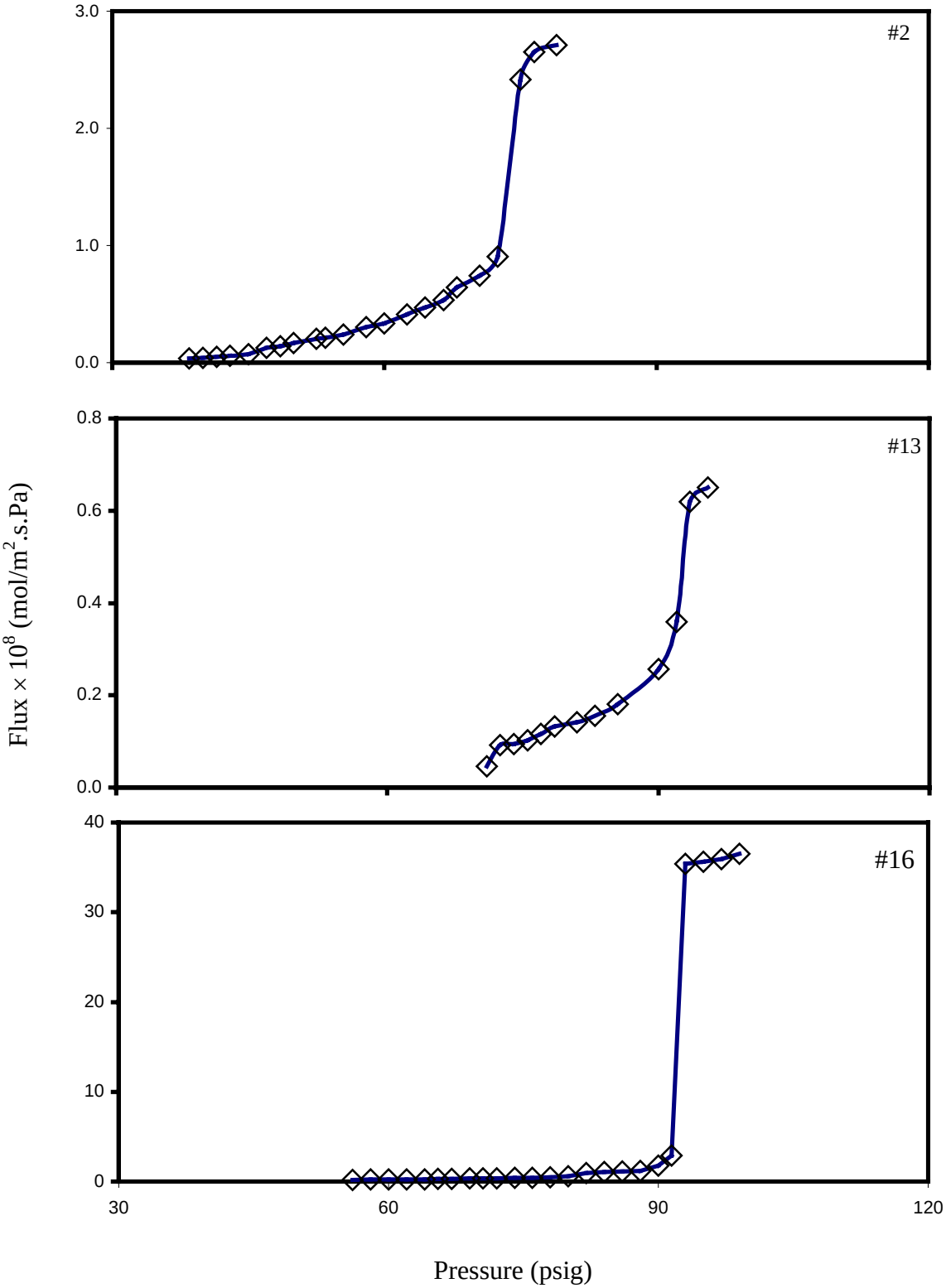

Figure 4.13 Relationship between nitrogen flux and pressure in liquid-gas displacement experiment

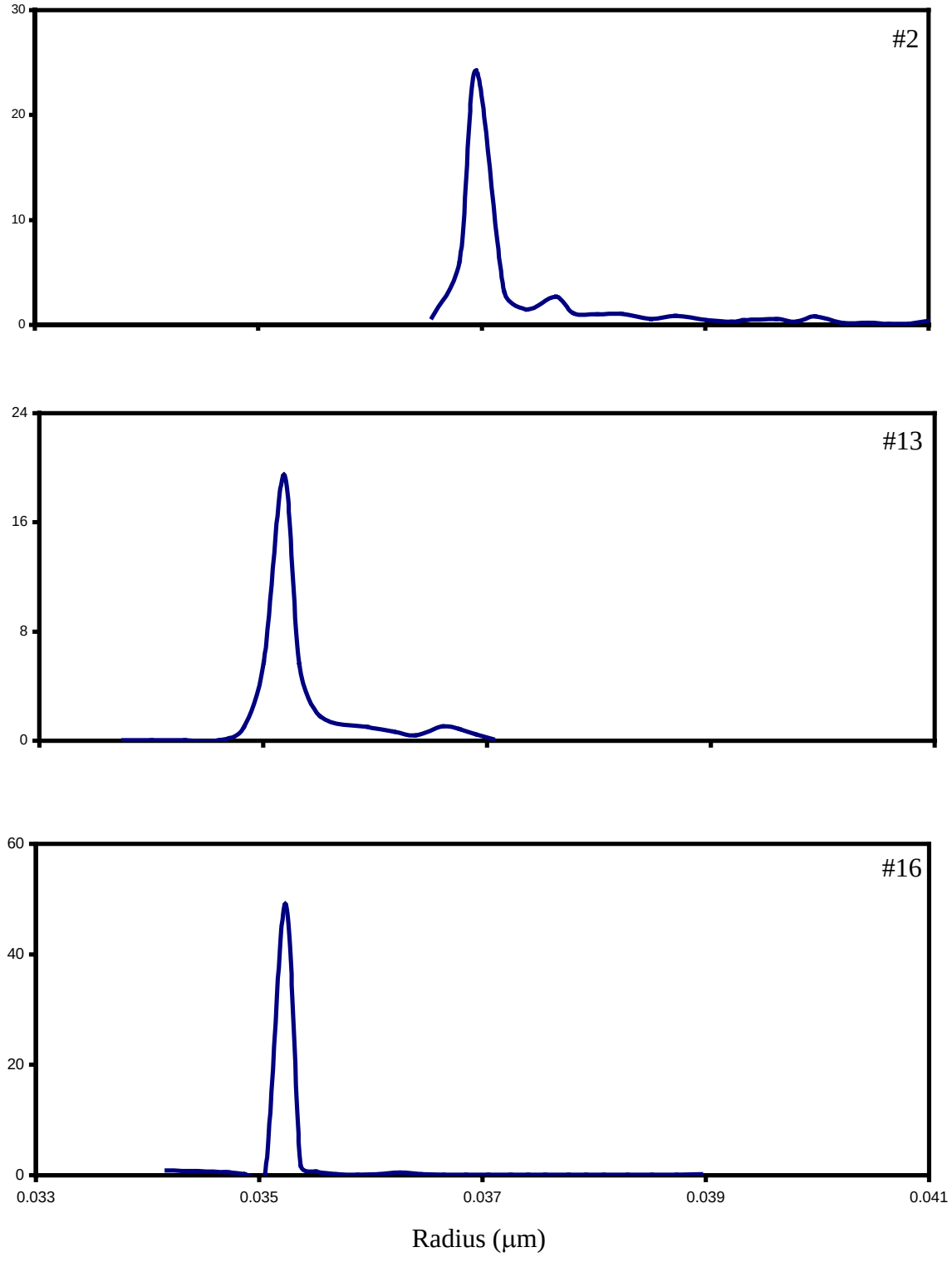

Figure 4.14 Pore size distribution determined by the liquid-gas displacement experiment

4.5 **Conclusions**

PVDF hollow fiber membranes were successfully prepared by the dry-wet spinning technique. The effects of parameters involved in the membrane preparation procedure were investigated. The porous structure of the membranes was characterized experimentally by the gas permeation, gas-liquid displacement and electron scanning microscopy. The following conclusions can be drawn:

1) The geometric dimensions and morphological structure of the fibers are affected by the dope extrusion rate, inner coagulant speed and fiber take-up speed.

2) The hollow fibers have finger-like and a sponge-like substructures with a thin skin layer that are suitable for use as a substrate.

3) Fiber #16 has a sharp pore size distribution and is mechanically stable at a transmembrane pressure of over 110 psi, in spite of its non-circular lumen.

Chapter 5 VOC/N_2 separation by PEBA/PVDF composite membranes

In this study, composite membranes consisting of a PEBA skin layer and a PVDF substrate were prepared for organic vapor separation, having the ultimate objective of recovering gasoline vapors for emission control. The main components of the gasoline (i.e. hexane, cyclohexane and heptane) as well as the common gasoline additives (i.e. dimethyl carbonate (DMC), ethanol (EtOH), methanol (MeOH), and methyl t-butyl ether (MTBE)) were used in the experiments as the model VOCs to be separated from nitrogen using the PEBA/PVDF composite membranes. The effects of feed VOC concentration and operating temperature on the membrane performance were evaluated in terms of permeance and permeate concentration. Finally, the membranes were tested for separation of gasoline vapors from nitrogen. The membranes were tested for 10 months under varying conditions (high or low feed concentration and operating temperature) and were found stable.

5.1 Experimental

5.1.1 Materials and equipments

For this study, #16 hollow fiber membrane, whose dimensions were listed in Table 4.4, were employed as the substrate. Butanol and heptane were purchased from BDH Inc. Methanol was purchased from Fisher Scientific. Hexane and ethanol were purchased from MERCK, KGaA (Germany). Cyclohexane was provided by Matheson Colemane & Bell Manufacturing Chemists. MTBE was purchased from Aldrich Chemical. Gasoline with an

octane number of 87 was purchased from a local gas station. 2-Ton epoxy was supplied by ITW Devcon.

5.1.2 Preparation of PEBA/PVDF composite membrane

Seven PVDF hollow fiber membranes with a each fiber length of 25 cm were assembled into a bundle. One end of the bundle was potted into a rigid PVC tube (2" length and ½" nominal diameter) with epoxy to form a gas tight tube sheet. To coat a layer of PEBA on the external surface of the fiber, the fiber bundle was immersed in 1 wt% PEBA/butanol homogeneous solution for 10 minutes, and then dried in a fumehood at room temperature for about 30 minutes. Caution was exercised to make sure that the fibers did not stick with each other and were dust free. The coating step was repeated three times. After the membrane bundle was completely dry, the fibers at the tube sheet were cut open and the other end was sealed with epoxy. A ½" diameter copper tubing was used as the shell containment of the fiber module whose structure was similar to that shown in Figure 4.4. The effective fiber length was 16.5 cm and the effective membrane area based on the outer diameter was 17.7 cm^2.

5.1.3 VOC separation experiment

The experimental setup is shown in Figure 5.1. A mixture of organic vapor(s) and nitrogen was prepared by bubbling nitrogen through a sintered porous stainless steel ball immersed in a selected organic liquid, which was placed in a thermostated bath at a given temperature. The gas stream comprised of VOC and nitrogen were fed into the shell side of the hollow fiber membrane module at atmospheric pressure. The membrane module was placed in a water bath at a given temperature that was controlled to be within ±0.5 ^oC. The

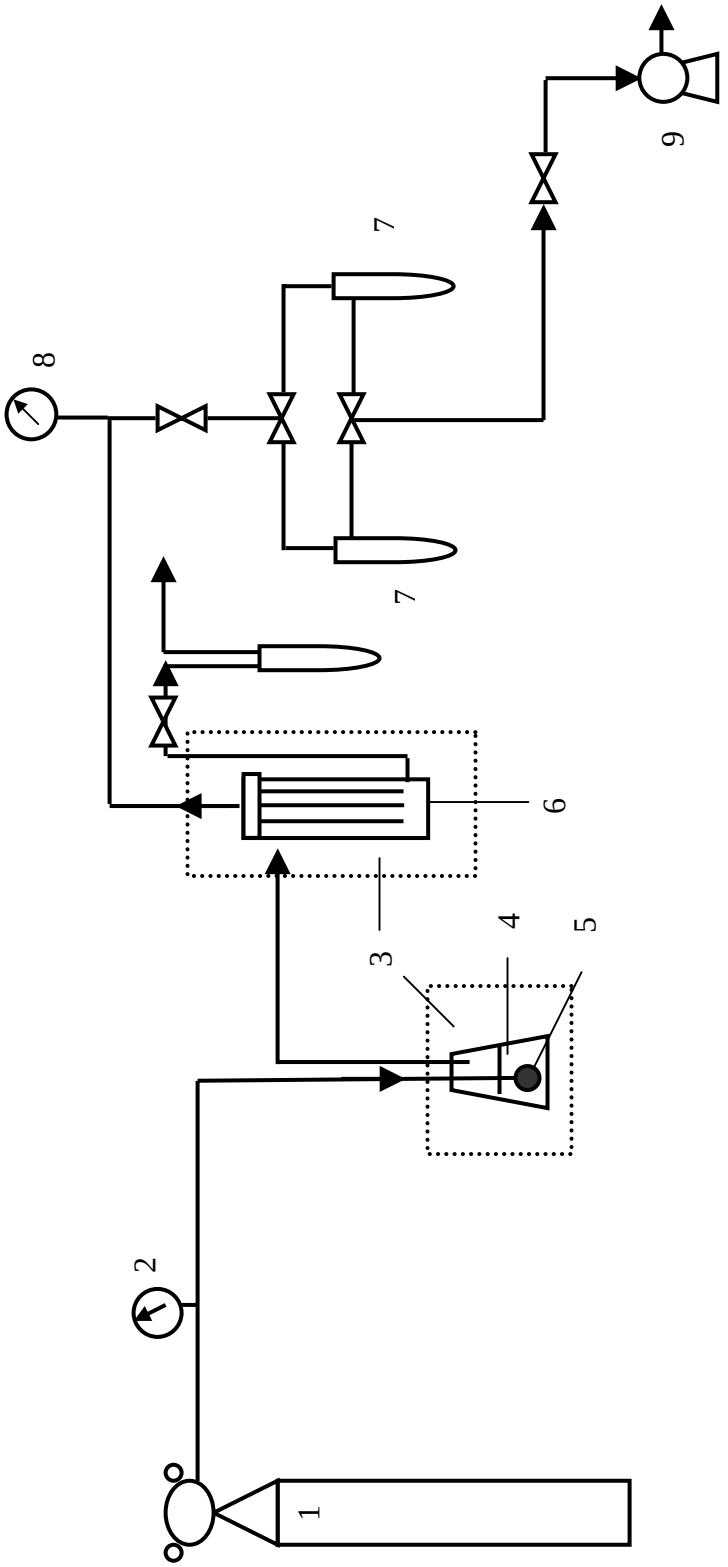

Figure 5.1 Schematic diagram of VOC recovery experiment. (1) nitrogen cylinder, (2) pressure gauge, (3) thermostated bath, (4) organic liquid reservoir, (5) gas bubbler, (6) membrane module, (7) cold trap, (8) vacuum gauge, (9) vacuum pump

temperature of the module was kept at least 2 ^{o}C higher than the temperature of the organic liquid reservoir to prevent VOC condensing in the membrane module. The permeate side (i.e. the bore side) of the membrane was connected to two cold traps that were immersed in liquid nitrogen. A vacuum pump was used to keep the permeate pressure at 10 mbar, which was measured by a Pirani vacuum gauge (MKS Instruments). The permeated organic vapors were condensed and collected initially in one of the cold traps, and switched to the other cold trap after 0.5~1 hour for the membrane to reach the steady permeation state. The permeation rate of VOC was determined gravimetrically by weighing the condensed VOC sample collected in a predetermined period of time. The concentrations of VOC in feed and residue streams were measured by a Varian CP 3800 gas chromatograph equipped with a thermal conductivity detector and a 60 m long capillary column. The feed flow rate was controlled to be in the range of 7.5~45 ml/s, which was high enough to neglect the effect of boundary layer (Yeom et al., 2002b). Because of the high feed flow rate, the variation in the concentration of the gas on the feed side is negligible and the feed flow rate can be approximately represented by the residue flow rate, which can be conveniently measured by a bubble flow meter. By changing the nitrogen flow rate and the temperature and the level of the organic solvent in the reservoir, different concentrations of VOC in feed can be obtained.

Before and after running each series of experiments, the nitrogen permeance was measured to check the stability of the membrane. In order to determine the pure nitrogen permeance, a bubble flow meter was connected to the residue outlet of the membrane module and the inlet valve was closed, as illustrated in Figure 5.2. As the permeate side was evacuated by a vacuum pump, the soap film in the bubble meter moved downward. The

nitrogen permeance was then calculated from the nitrogen permeance J_N (mol/m^2.s.Pa) using the following equation:

$$J_N = \frac{F_N}{22400} \times \frac{273.15}{T} \times \frac{1}{A(p^f - p^p)} \tag{5.1}$$

where F_N is the volumetric permeation rate (ml/s) of the nitrogen measured at ambient conditions, T is the room temperature (K), A is the effective membrane area (m^2), p^f is the upstream (feed) pressure (Pa), and p^p is the downstream (permeate) pressure (Pa). Generally, J_N is not affected by the presence of VOC, but is dependent upon the operating temperature, which will be discussed later.

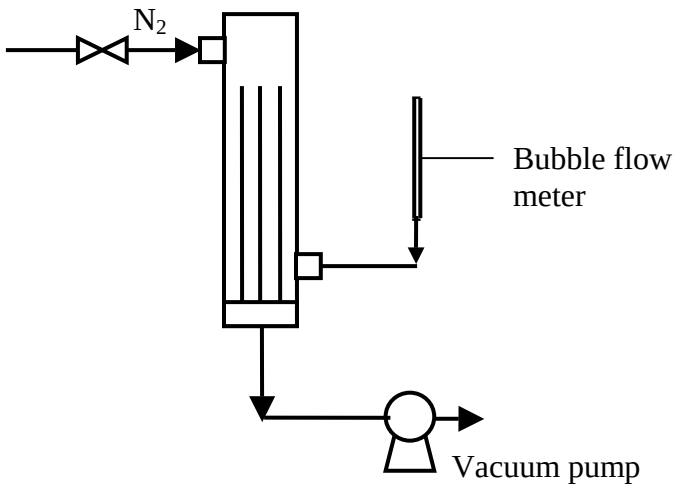

Figure 5.2 Schematic diagram of nitrogen permeation setup

5.1.4 Characterization of membrane performance for VOC separation

Considering the permeation of a binary organic vapor/nitrogen mixture, the flux of VOC component through the membrane, Q_v (mol/m^2.s), can be obtained by

$$Q_v = \frac{G_v^p}{MtA} \tag{5.2}$$

where G_v^p is the weight (g) of the organic compound permeated through the membrane in t seconds, and M is the molecular weight (g/mol) of the VOC. The permeance of VOC through the membrane, J_v (mol/m^2.s.Pa), is obtained by

$$J_v = \frac{Q_v}{(p^f X - p^p Y)} \tag{5.3}$$

The permeate concentration (in mole fraction) is related to the partial permeation fluxes by

$$Y = \frac{Q_v}{Q_v + Q_N} \tag{5.4}$$

The permeation flux of nitrogen, Q_N is given by

$$Q_N = J_N[p^f(1-X) - p^p(1-Y)] \tag{5.5}$$

Under the experimental conditions, the nitrogen permeability can be assumed to be constant, and J_N can thus be obtained from pure nitrogen permeation experiments mentioned above. Since Q_v, X, J_N, p^f and p^p are known quantities from experiments, Y and J_v can be solved from Equation 5.3 and 5.4

For the current study where the permeate pressure is much lower than the feed pressure, when the feed contains more than one organic vapor, Equations 5.3 and 5.5 can be rewritten to be

$$J_{vi} = \frac{Q_{vi}}{p^f X_i} \tag{5.6}$$

and

$$Q_N = J_N p^f (1 - \sum_i X_i) \tag{5.7}$$

where *i* represents the organic vapor component *i*. The quantities Q_{vi} and X_i are obtainable from experiments, and the concentration of VOC in permeate can be calculated by

$$Y_i = \frac{Q_{vi}}{\sum_i Q_{vi} + Q_N} \tag{5.8}$$

Since only the VOCs were condensed and collected in the cold trap, the composition of the collected organic liquid can be calculated from

$$Y_i^{'} = Q_{vi} / \sum Q_{vi} \tag{5.9}$$

5.2 **Results and discussion**

5.2.1 Separation of hexane, cyclohexane and heptane from binary VOC/N_2 mixtures

Hexane, cyclohexane and heptane are the main components of gasoline. Knowing about the separation of these three organic solutions is very important to study the gasoline removal by the composite membrane. The separation of a VOC from binary VOC/N_2 mixtures was studied, and the effects of feed VOC concentration and temperature on the membrane performance were investigated.

Figure 5.3 and 5.4 show the effects of feed VOC concentration on the VOC flux and VOC concentration in permeate for separation of binary hexane/N_2, cyclohexane/N_2 and heptane/N_2 mixtures. The experiments were conducted at 22 ^oC, at which the nitrogen permeance was determined to be 4.1×10^{-8} mol/m^2·s·Pa. When the feed VOC concentration increased, the VOC flux and VOC concentration in the permeate increased as well.

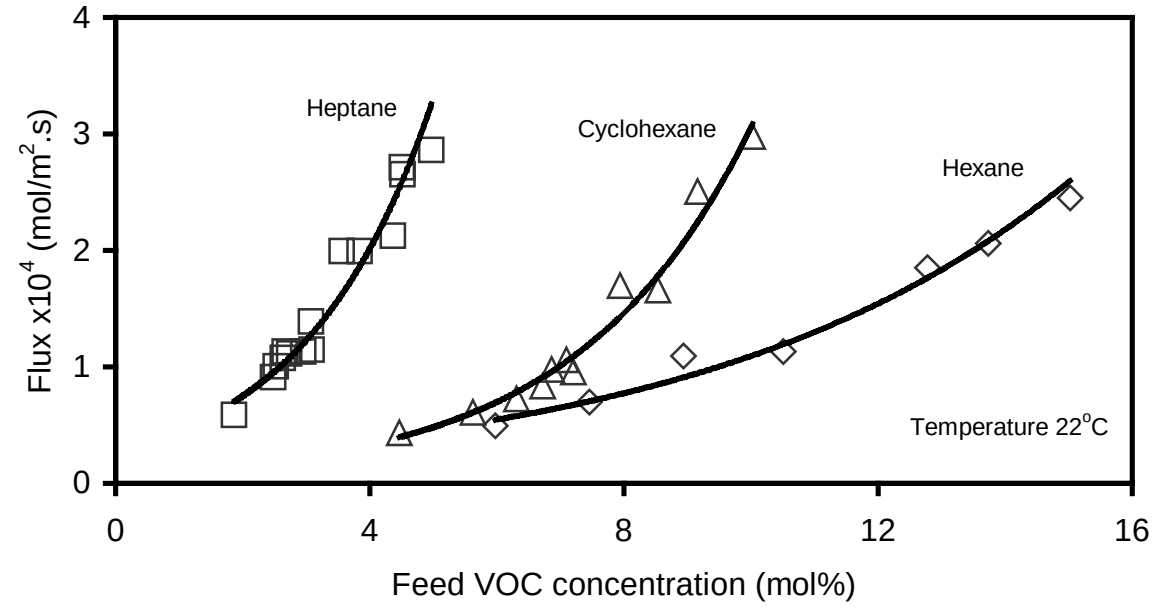

Figure 5.3 Effect of feed VOC concentration on VOC flux for permeation of binary hexane//N_2, cyclohexane/N_2 and heptane/N_2 mixtures

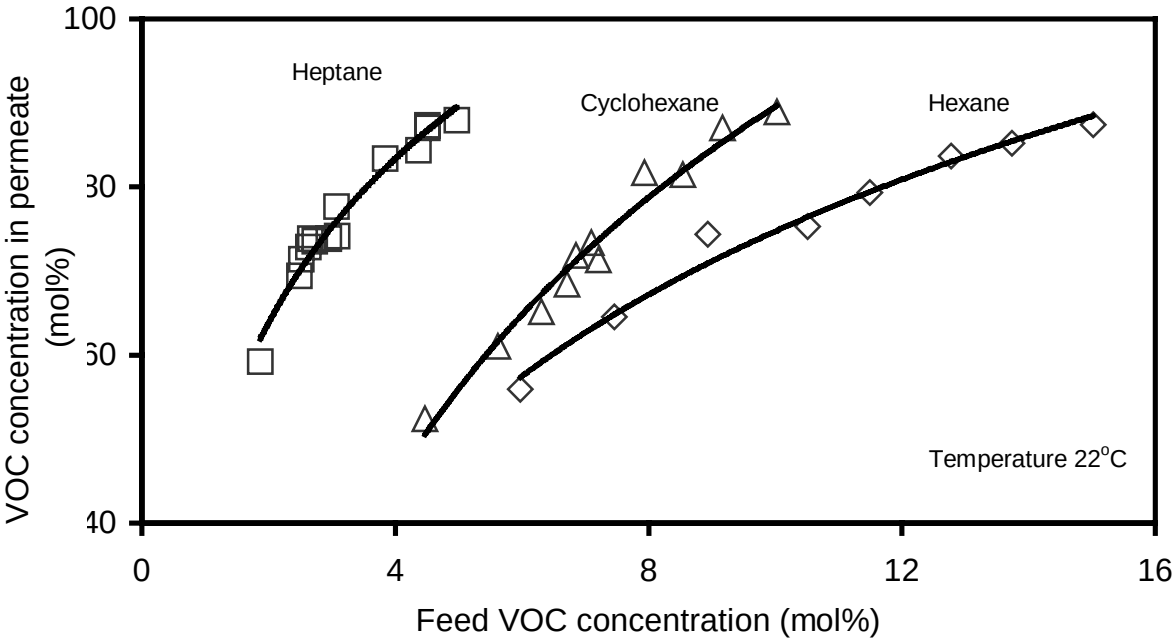

Figure 5.4 Effect of feed VOC concentration on VOC concentration in permeate for permeation of binary hexane//N_2, cyclohexane/N_2 and heptane/N_2 mixtures

According to the solution-diffusion model, there are three steps involved in the permeation through the membrane, including sorption, diffusion and then desorption. As indicated by Equation (2.1), the permeation flux is directly affected by the partial pressure difference across the membrane. Since the permeate side was connected to vacuum, the permeate side pressure was negligible when compared to the feed pressure. Therefore, the flux increase with an increased in the feed concentration.

The permeance of the organic compounds through the membrane is shown in Figure 5.5. When the feed concentration increased, the solubility of the organic vapor increased. Since permeability is the product of solubility and diffusivity, thus the permeance increased with increasing VOC concentration in feed. Nitrogen permeance was assumed not to be affected by the presence of organic vapors, which is generally true for organic vapor separation from nitrogen (Feng et al., 1993), so the permeance ratio of VOC/N_2 follows the same trend, as shown in Figure 5.6. It can be seen that when the feed VOC concentration was high enough, the permeance ratio of heptane/N_2 could reach as high as 150, while that of hexane/N_2 was only 30. It was shown that the VOC concentration in the permeate was always greater than 50 mol% and could be as high as 90 mol% for all these vapors under the experimental conditions tested.

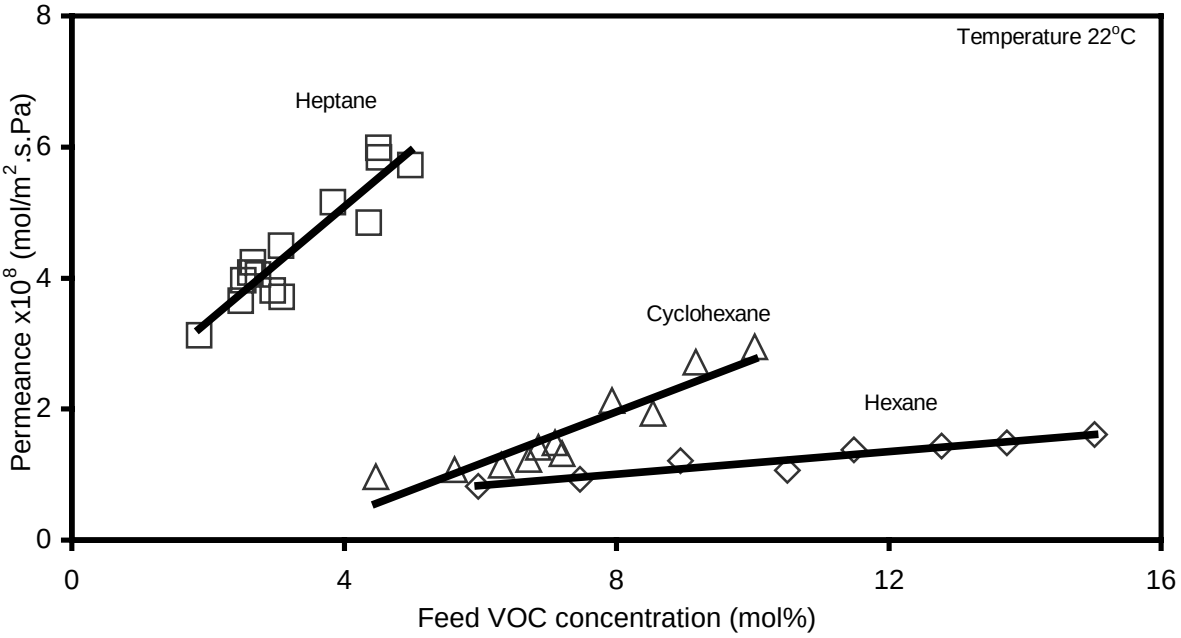

Figure 5.5 Effect of feed VOC concentration on VOC permeance for permeation of binary hexane//N_2, cyclohexane/N_2 and heptane/N_2 mixtures

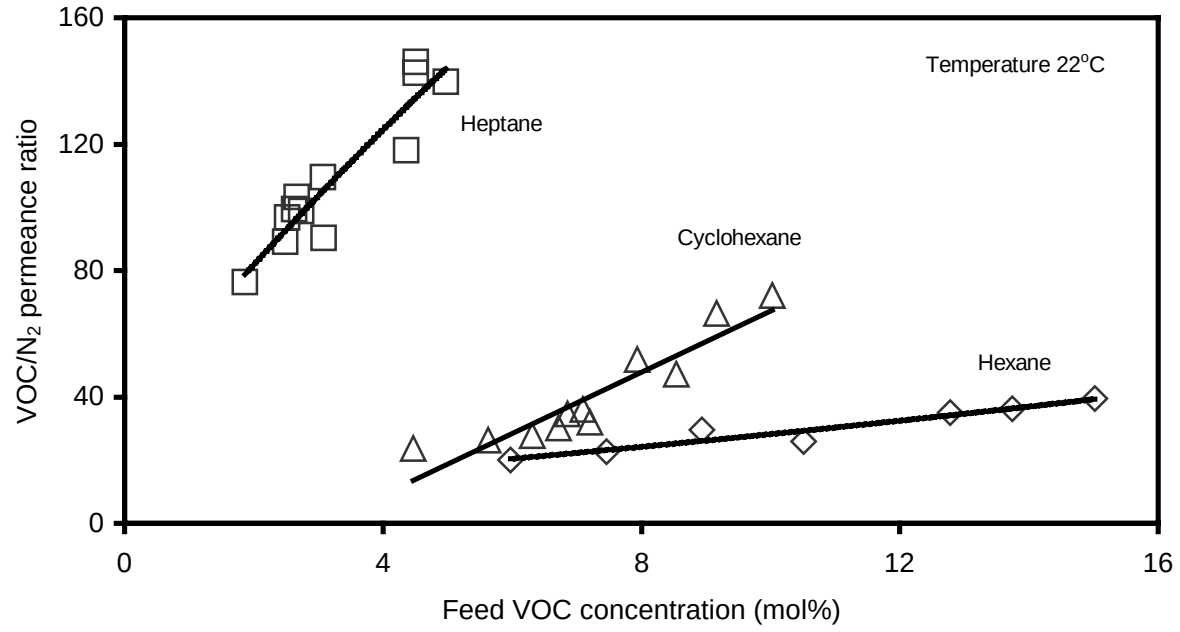

Figure 5.6 Effect of feed VOC concentration on VOC/N_2 permeance ratio for permeation of binary hexane//N_2, cyclohexane/N_2 and heptane/N_2 mixtures

In order to determine the effects of temperature on the membrane performance, the operating temperature was varied from 0 to 40 ^oC with a fixed feed VOC concentration (i.e. hexane 5.0 mol%, cyclohexane 3.3 mol% and heptane 1.1 mol%). Figure 5.7 and 5.8 show the effects of temperature on the permeation flux and concentration of VOC in permeate for the separation of binary hexane/N_2, cyclohexane/N_2 and heptane/N_2 mixtures. It was found that when the temperature increased, both VOC flux and VOC concentration in permeate tended to decrease. However, when the temperature was above 25 ^oC, the VOC flux did not change with the temperature significantly.

The permeance of nitrogen and VOC was plotted against reciprocal temperature, as showed in Figure 5.9. It is interesting to note that with an increase in temperature, the VOC permeance decreased, while the nitrogen permeance increased. The temperature dependence of nitrogen permeance followed a logarithmic relationship with *1/T*, while those of hexane, cyclohexane and heptane didn't. Figure 5.10 shows that the permeance ratio of hexane/N_2, cyclohexane/N_2 and heptane/N_2 decreased with an increase in temperature.

In general, permeation of a non-interactive gas (i.e. nitrogen) through a dense polymeric membrane is considered to be an activated process, and an Arrhenius type of equation can be used to express the temperature dependency of the permeability, solubility and diffusivity:

$$P = P_0 \exp(\frac{-E_p}{RT}) \tag{5.10}$$

$$S = S_0 \exp(\frac{-\Delta H_s}{RT}) \tag{5.11}$$

$$D = D_0 \exp(\frac{-E_d}{RT}) \tag{5.12}$$

where E_p, E_d and ΔH_s are the activation energies for permeation, diffusion and the heat of sorption, respectively; they are related by $E_p = \Delta H_s + E_d$. P_0, S_0 and D_0 are the pre-exponential factors. Since both E_d and ΔH_s are normally positive and constant values for noncondensable gas such as nitrogen (Yeom et al. 2000), the solubility and diffusivity of nitrogen increase with increasing temperature. In the case of VOC, however, ΔH_s is negative and E_d is positive. In addition, the values of E_d and ΔH_s are temperature dependent, which makes the situation more complex. The results shown in Figure 5.9 can be explained as follows. When the temperature is low, the sorption aspect dominates the permeation. In this case, the VOC permeability decreases with an increase in temperature. However, when the temperature is high enough, both the diffusion and sorption are significant for VOC permeation. While the diffusivity tends to increase with an increase in temperature, the solubility decreases. As a result, the temperature dependence of permeability is less significant.

Because the nitrogen permeance increased and VOC permeance with increasing temperature, good separation can be achieved at low operating temperatures. This is clearly shown in Figure 5.8 and 5.10. For example, when the temperature decreased from 40 ^{o}C to 0 ^{o}C, the heptane concentration in permeate increased from 60% to 80% and the permeance ratio increased from 50 to 200. Similarly, for the same temperature change, the hexane concentration in permeate increased from 40% to 70% and the permeance ratio increased from 20 to 80.

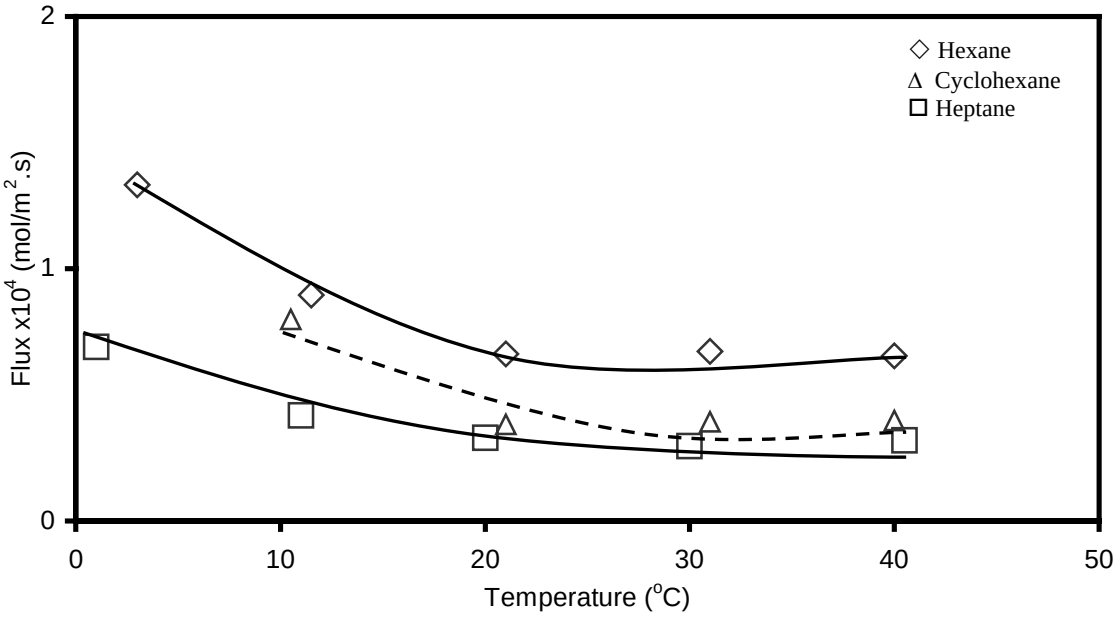

Figure 5.7 Effect of temperature on VOC flux for permeation of binary hexane/N_2, cyclohexane/N_2 and heptane/N_2 mixtures

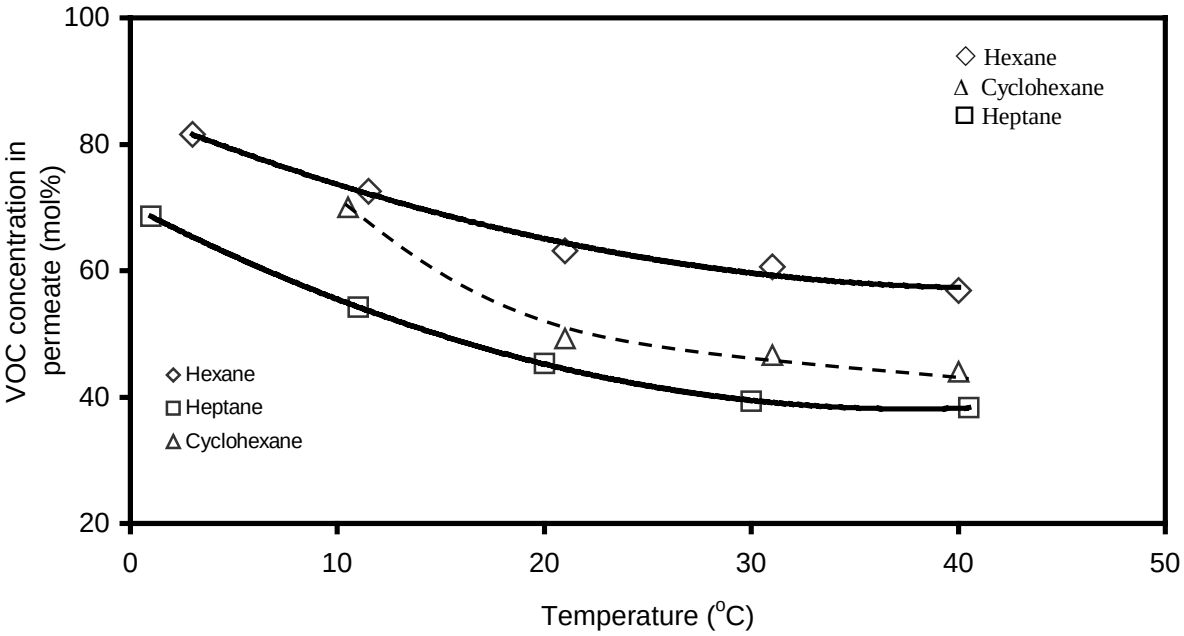

Figure 5.8 Effect of temperature on VOC concentration in permeate for permeation of binary hexane/N_2, cyclohexane/N_2 and heptane/N_2 mixtures

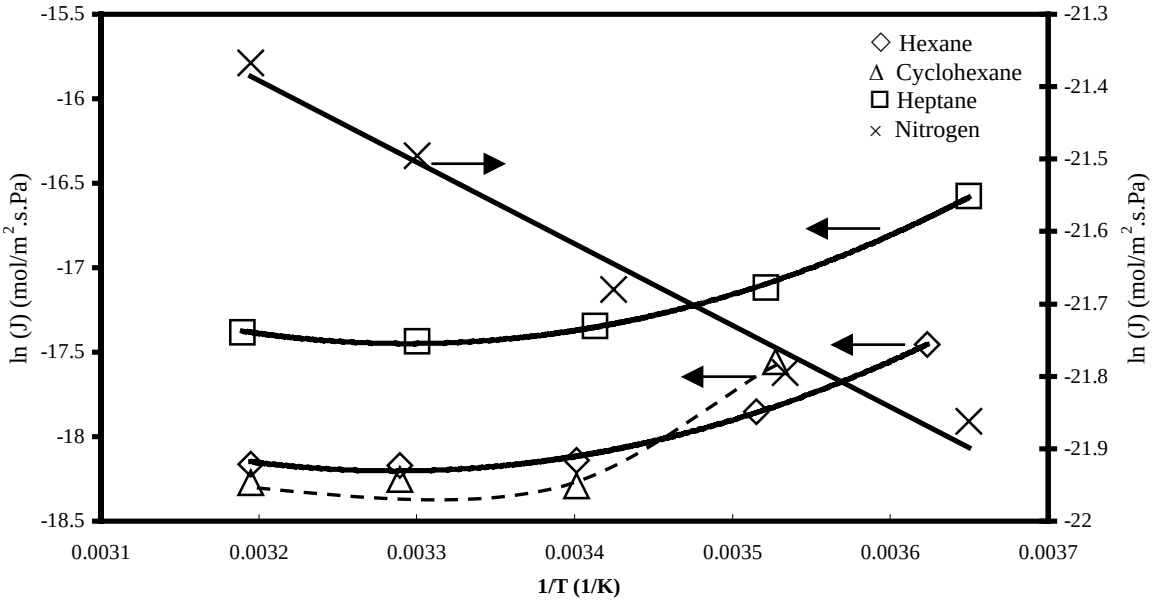

Figure 5.9 Effect of temperature on VOC and N_2 permeance for permeation of binary hexane/N_2, cyclohexane/N_2 and heptane/N_2 mixtures

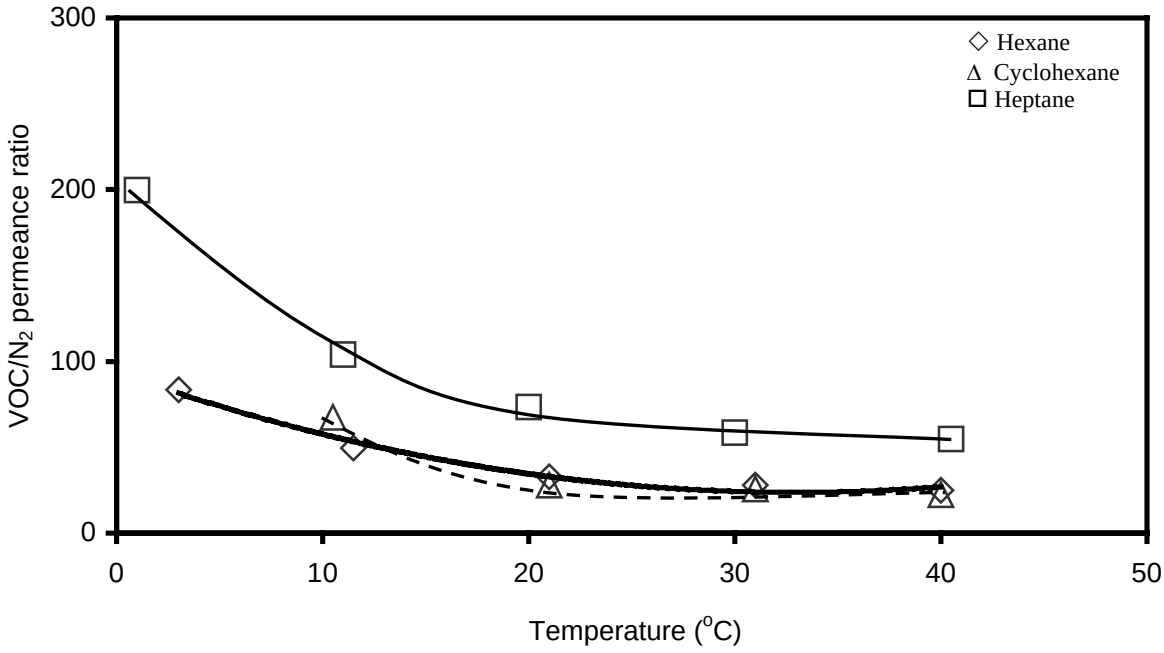

Figure 5.10 Effect of temperature on VOC/N_2 permeance ratio for permeation of binary hexane/N_2, cyclohexane/N_2 and heptane/N_2 mixtures

5.2.2 Separation of a mixture of hexane, cyclohexane and heptane vapors from nitrogen

The separation of a mixture of hydrocarbon vapors from nitrogen was studied. The feed mixture was obtained by bubbling nitrogen through a liquid mixture of hexane. cyclohexane and heptane. Because these three organic compounds have different volatilities, the feed concentration would change as the experiment proceeded. The feed concentration variation was minimized by adding about 20 ml premixed organic liquids to the liquid tank once every 20 minutes while keeping a total liquid volume of 850 ml. The flow rate of the feed gas stream varied from 7.36 to 16.36 ml/s to change the feed composition.

The experimental results are summarized in Table 5.1. It is found that when the feed VOC concentration was in the range of 4~11 mol%, the VOC concentration in permeate was 70~80 mol%, indicating that the VOCs were enriched significantly at the permeate side. Figure 5.11 shows the corresponding enrichment factors for VOC permeation, defined as the ratio of permeate to feed concentration of VOC components, of these three vapors at ten different feed concentrations. Heptane had the highest enrichment factor, which was almost twice as much as cyclohexane had, and cyclohexane was more enriched than hexane. This is in agreement with their permeance ratios shown in Figure 5.6.

Table 5.1 Permeate composition at different feed compositions for simultaneous separation of three organic vapors from nitrogen

Experiment	Feed composition (mol%)				Total VOC flux	Permeate composition (mol%)			
number	Nitrogen	Hexane	Cyclohexane	Heptane	(mol/m^2.s)	Nitrogen	Hexane	Cyclohexane	Heptane
1	89.63	5.85	2.87	1.65	1.68	19.89	36.34	20.85	22.92
2	92.50	1.96	5.20	0.34	1.73	19.47	17.68	55.19	7.65
3	93.89	3.12	1.97	1.01	1.17	26.25	26.10	22.42	25.23
4	94.14	1.22	3.21	1.44	1.51	21.64	10.64	34.92	32.80
5	93.56	3.83	1.82	0.79	0.96	30.32	28.56	20.70	20.41
6	93.91	3.41	1.68	1.00	1.45	22.42	35.65	20.24	21.69
7	93.99	0.97	4.54	0.50	1.37	23.39	9.39	55.08	12.13
8	94.75	0.98	3.44	0.83	1.16	26.56	9.48	45.16	18.80
9	93.06	1.93	4.49	0.51	1.29	24.48	18.00	47.73	9.79

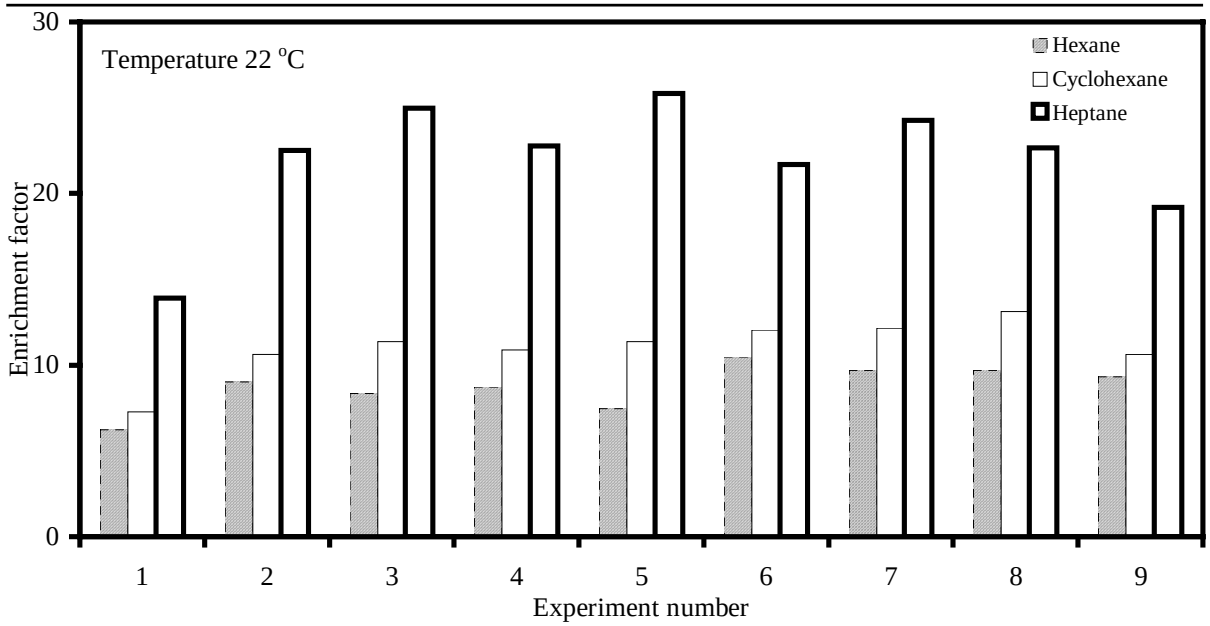

Figure 5.11 Enrichment factor for separation of mixed VOCs from nitrogen

5.2.3 Separation of DMC, EtOH, MeOH and MTBE vapors from binary VOC/N_2 mixtures

EtOH, MeOH and MTBE are commonly used as oxygenates in gasoline and DMC is considered to be a replacement for MTBE due to environmental concerns associated with the use of MTBE. The separation of these vapors from nitrogen was tested. For simplicity, the effects of feed VOC concentration and operating temperature on membrane performance were investigated using binary VOC/N_2 mixtures. Figure 5.12 and 5.13 show the VOC flux and VOC concentration in permeate as a function of feed VOC concentration at room temperature 22 ^{o}C. One may see that with an increase in feed VOC concentration, both the VOC flux and VOC concentration in permeate increased. These results agree with the those for the separation of hexane, cyclohexane and heptane from nitrogen, as discussed in the previous section.

The permeance of the organic compounds through the membrane was shown in Figure 5.14. When the feed VOC concentration increased, the VOC permeance increased. Based on a nitrogen permeance of 4.1×10^{-8} mol/m^2.s.Pa, the corresponding permeance ratio for the VOCs is shown in Figure 5.15, which shows the same trend as the VOC permeance. It is clear that the membrane showed the highest permeance ratio for DMC/N_2 (as high as 550), and the lowest permeance ratio for MTBE/ N_2, which was about 30.

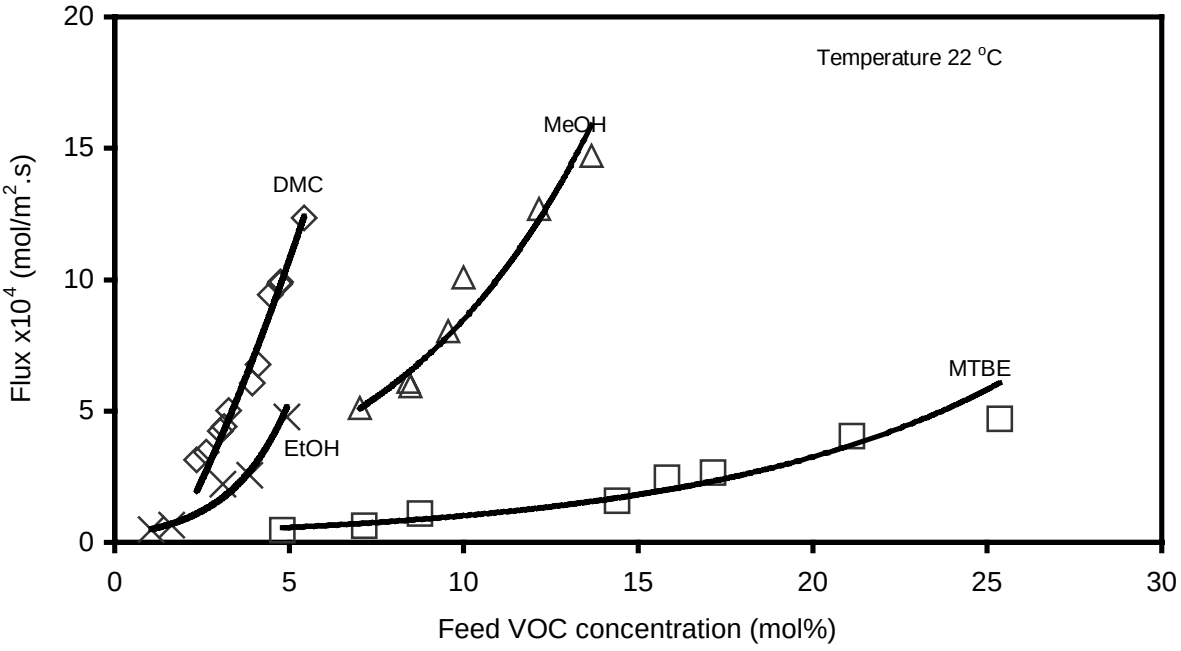

Figure 5.12 Effect of feed VOC concentration on VOC flux for permeation of binary DMC/N_2, MeOH/N_2, EtOH/N_2 and MTBE/N_2 mixtures

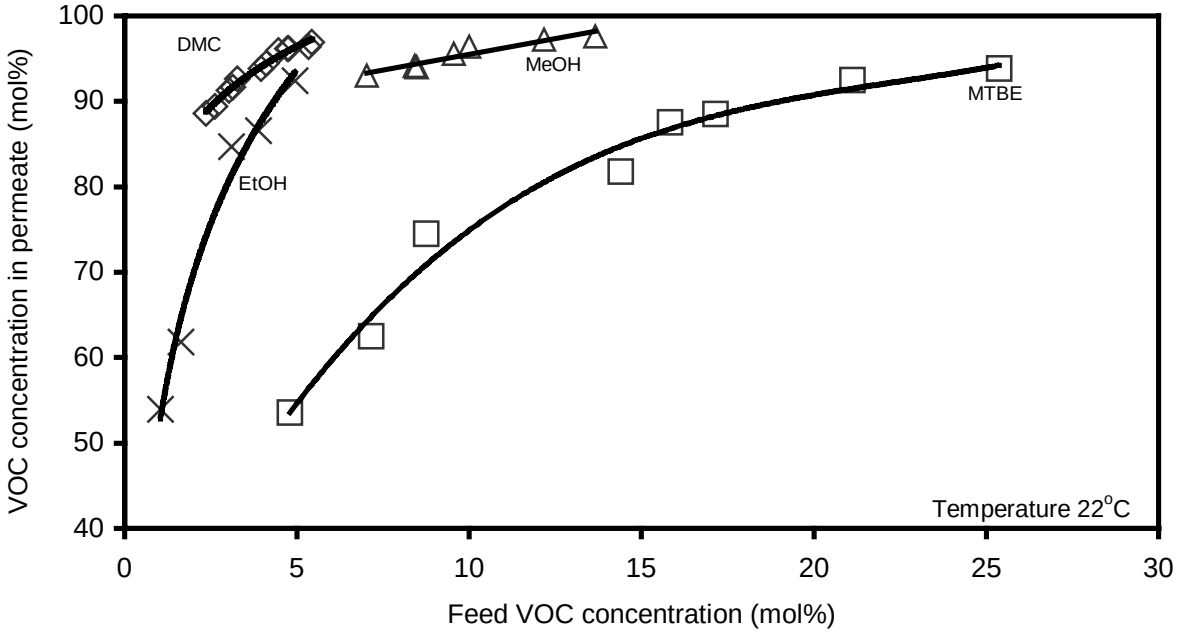

Figure 5.13 Effect of feed VOC concentration on VOC concentration in permeate for permeation of binary DMC/N_2, MeOH/N_2, EtOH/N_2 and MTBE/N_2 mixtures

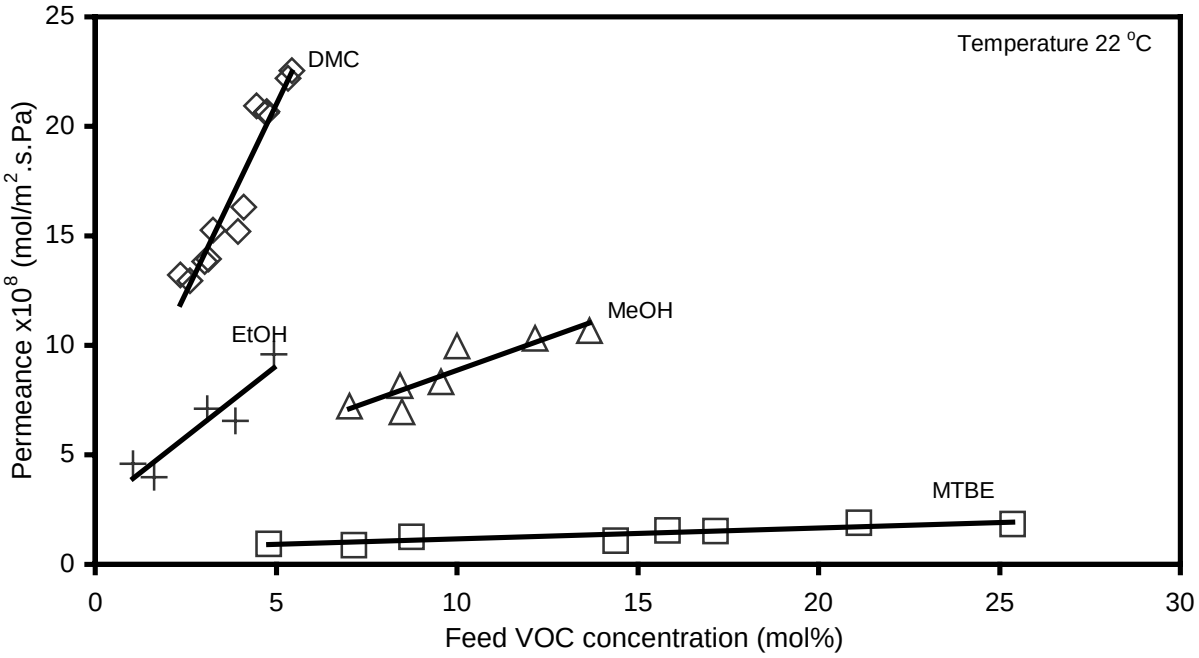

Figure 5.14 Effect of feed VOC concentration on VOC permeance for permeation of binary DMC/N_2, MeOH/N_2, EtOH/N_2 and MTBE/N_2 mixtures

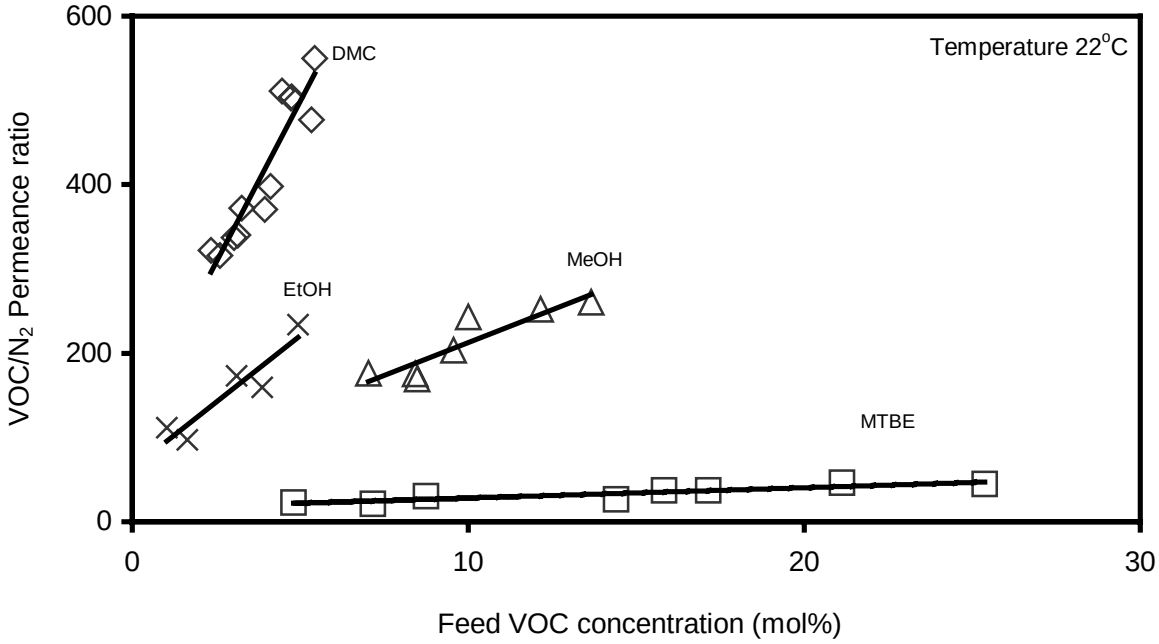

Figure 5.15 Effect of feed VOC concentration on VOC/N_2 permeance ratio for permeation of binary DMC/N_2, MeOH/N_2, EtOH/N_2 and MTBE/N_2 mixtures

To look at the relative magnitude of permeabilities of all the seven VOCs studied, the permeance was plotted vs the relative pressure (p/p^0), which is ratio of the pressure of VOC and its saturated vapor pressure p^0. this is shown in Figure 5.16. It may be seen that as the relative pressure increases, the VOC permeance also increase. At the same relative pressure, DMC has the highest permeance, while MTBE, cyclohexane and hexane are least permeable, and methanol and ethanol have almost the same permeability. The seven vapors showed a permeability in the order of DMC > MeOH ≈ EtOH > heptane > cyclohexane ≈ hexane ≈ MTBE. These results generally agreed with the study of Cen et al. (2002), except for DMC, which was not included in their study.

Baker et al. (1987) mentioned that the critical temperature of a gas was a measure of its condensability. Feng et al. (1993) observed that organic vapor permeance through polyetherimide membranes was related to the boiling point of VOC. In this study, it was interesting to notice the correlation between the saturated vapor pressure of an organic vapor and its permeance. The saturated vapor pressure was a measure of the condensability and hence sorption of the vapor. If the saturated vapor pressure of an organic compound is low, implies a good sorption on the membrane. However, this was found not to be case for the present system. Although both heptane and DMC have the lowest saturated vapor pressures (see Table 5.2), DMC showed much higher permeance than heptane. MTBE, hexane and cyclohexane showed almost the same permeance in spite of their different saturated vapor pressures.

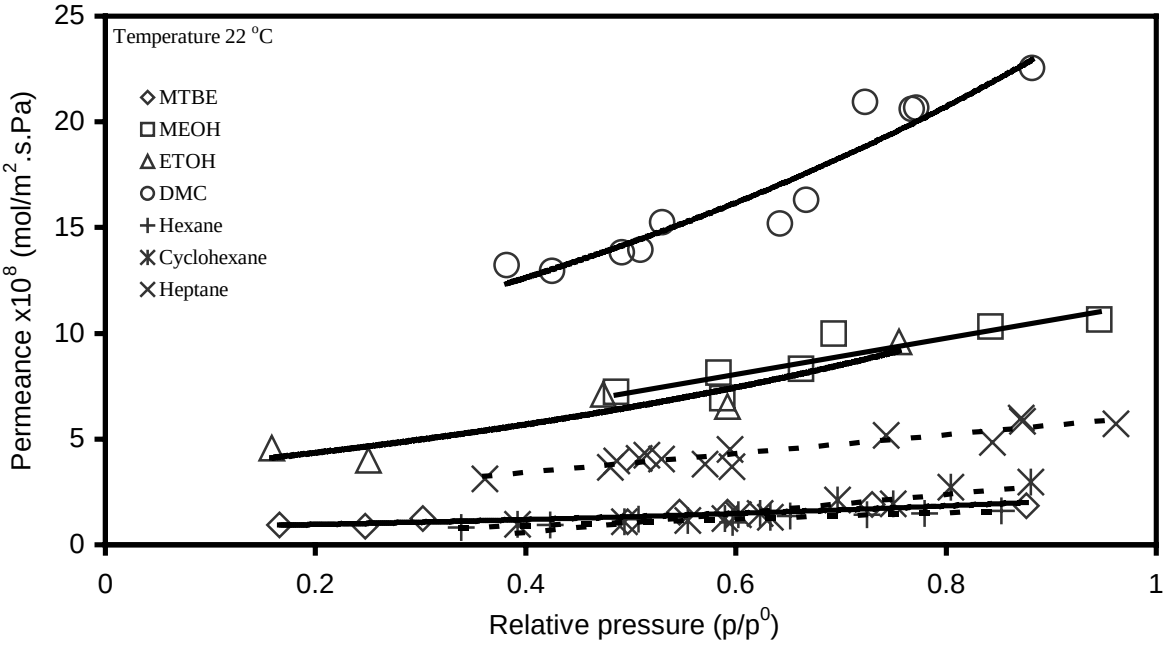

Figure 5.16 Effect of relative pressure vapor on permeance of vapors

Table 5.2 Saturated vapor pressures at 22 ^{o}C(Yaws, 1994)

VOC	Saturated vapor pressure (mmHg)
Hexane	133.8
Cyclohexane	85.9
Heptane	39.1
DMC	46.6[a]
MTBE	220.1
EtOH	49.72
MeOH	109.4

[a] Steele et al. (1997)

As the permeance is the product of solubility and diffusivity, the contribution of diffusivity on permeance is as important as that of solubility. The diffusivity of a permeant is strongly related to its molecular weight (larger molecules generally have smaller diffusivities) and molecular structure (the straight-chain molecules usually have higher diffusivities than those molecules with branched and cyclic molecular structures). The diffusivity of heptane is expected to be lower than that of DMC. Cyclohexane and hexane have very close molecular weights, but they possess totally different molecular structures. Because of the cyclic molecular structure, cyclohexane molecules would need more free volume in the membrane to diffuse through than the straight chain hexane molecules, indicating a smaller diffusivity of cyclohexane than hexane. Apparently, the VOC permeance is determined by neither the diffusivity nor the solubility alone.

To study the effects of temperature on the membrane performance for separation of binary DMC/N_2, MeOH/N_2, EtOH/N_2 and MTBE/N_2 mixtures, the operating temperature was varied from 0 to 40 ^oC. The feed concentrations of DMC, MeOH, EtOH and MTBE were maintained at 1.4, 1.4, 3.4 and 9.0 mol% , respectively. Figures 5.17 and 5.18 depict the membrane performance for the separation of VOC from binary VOC/N_2 mixtures at different temperatures. It was observed that when the temperature increased, both the VOC flux and VOC concentration in permeate decreased, and the decreases became less significant at high temperatures. These results are similar to those observed for the separation of hexane, cyclohexane and heptane from their binary VOC/N_2 mixtures.

Figures 5.19 and 5.20 show the effects of temperature on the permeance of VOC and VOC/N_2 permeance ratio. When the temperature increased, both the permeance and permeance ratio decreased.

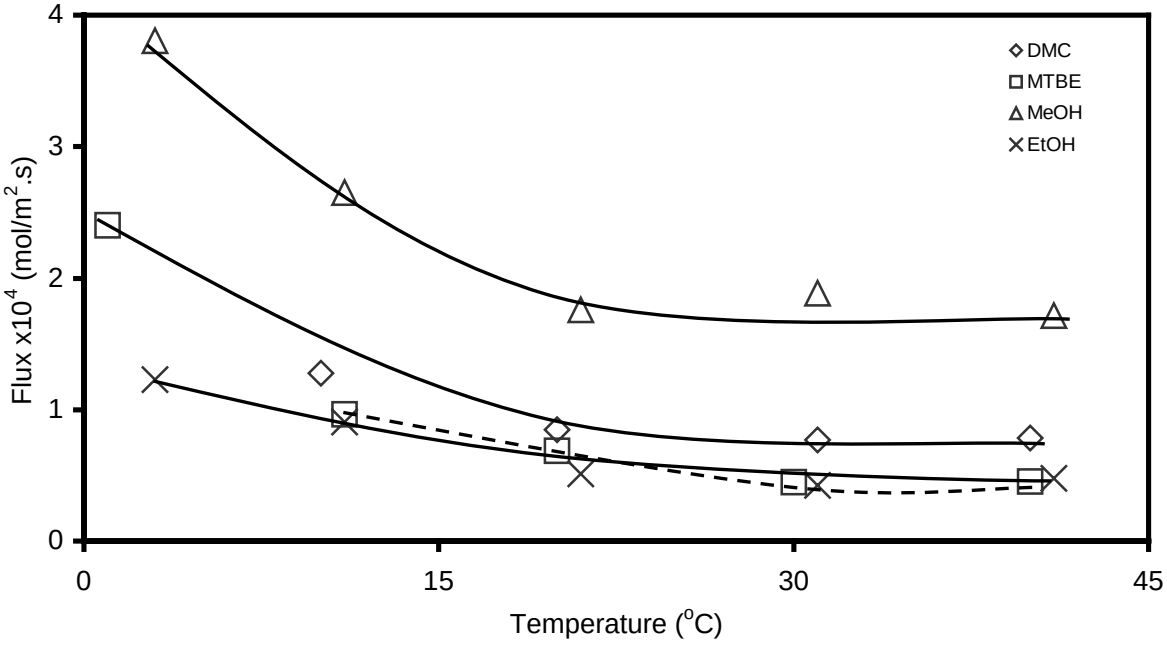

Figure 5.17 Effect of temperature on VOC flux for permeation of binary DMC/N_2, MeOH/N_2, EtOH/N_2 and MTBE/N_2 mixtures

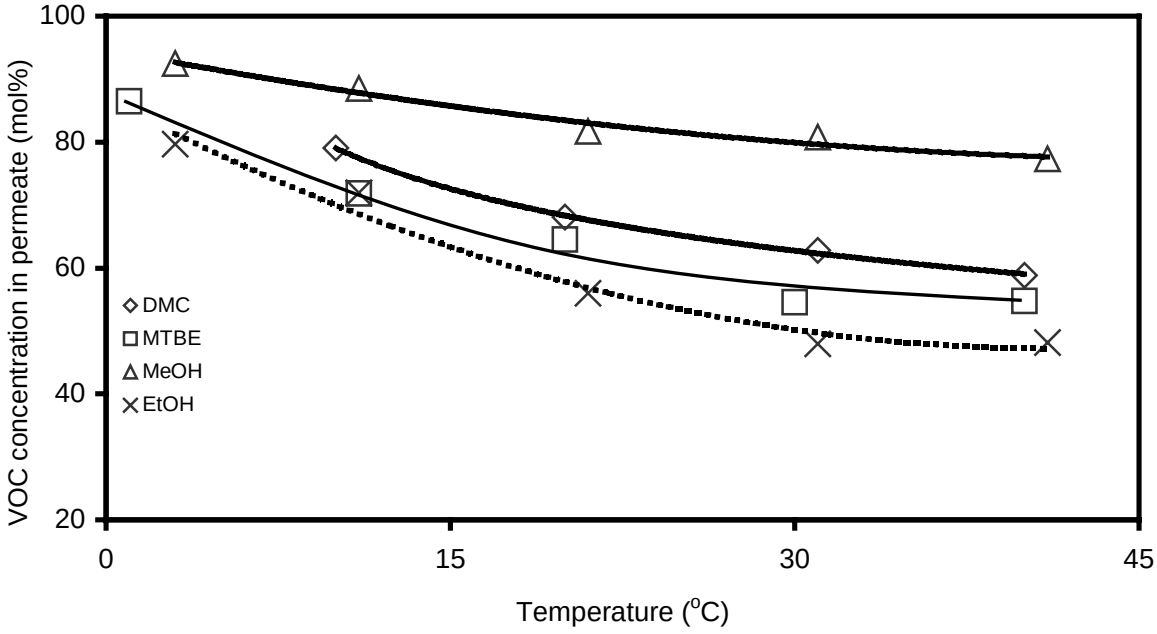

Figure 5.18 Effect of temperature on VOC concentration in permeate for permeation of binary DMC/N_2, MeOH/N_2, EtOH/N_2 and MTBE/N_2 mixtures

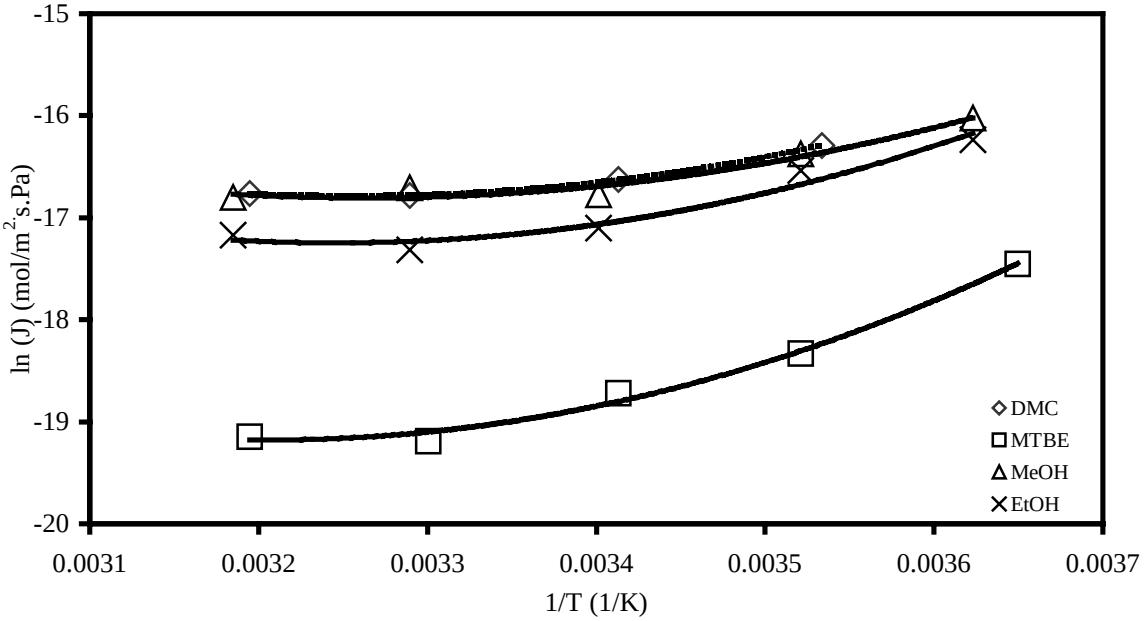

Figure 5.19 Effect of temperature on VOC permeance for permeation of binary DMC/N_2, MeOH/N_2, EtOH/N_2 and MTBE/N_2 mixtures

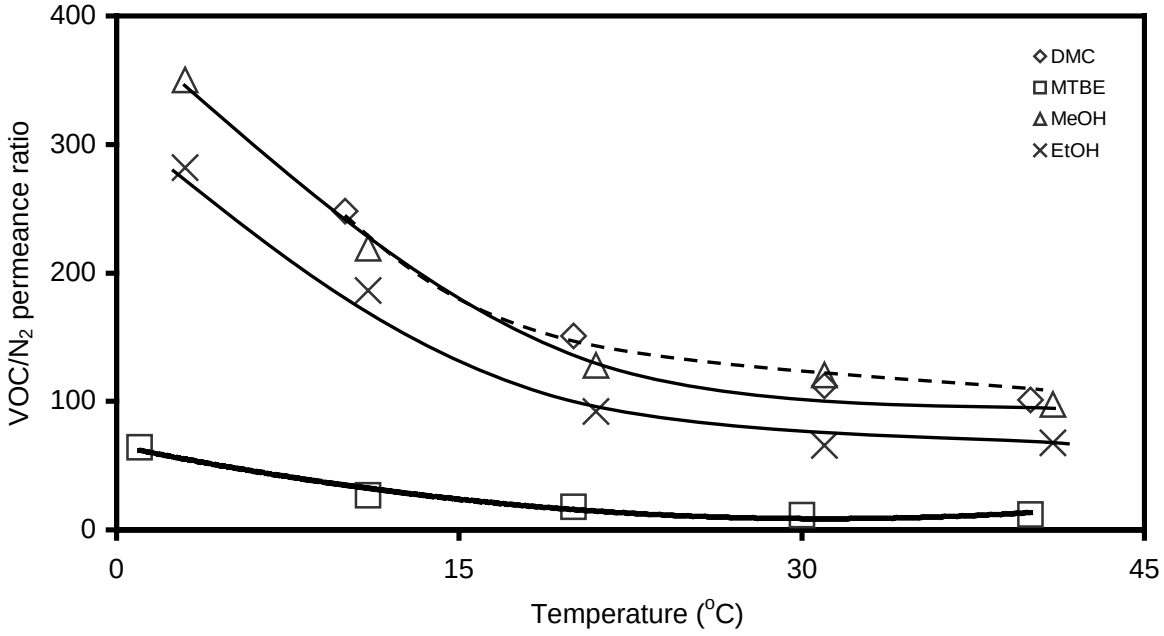

Figure 5.20 Effect of temperature on VOC/N_2 permeance ratio for permeation of binary DMC/N_2, MeOH/N_2, EtOH/N_2 and MTBE/N_2 mixtures

5.2.4 Gasoline recovery from nitrogen

Gasoline is a complicated mixture with a lot of components. A maximum of 44 peaks were obtained from samples of gasoline vapor in feed and permeate by a Varian CP 3800 GC in the experiment. Identification of each and every peak was not attempted in this work, and the fractional peak area was reported instead of the mole fractions due to technical difficulty in determining the actual concentration of each component in the mixture.

The separation experiments were carried out at 22 ^{o}C using the same equipmental setup. The feed gasoline concentration was varied from 22 to 41 wt%. Because of the different volatilities of the components in gasoline, the feed concentration tended to change with time. In order to obtain the membrane performance data at a given VOC concentration,

50 ml 'fresh' gasoline was added to the bubbling liquid reservoir every 20 minutes while keeping the total volume of gasoline constant (850 ml).

VOC and nitrogen concentrations in feed and permeate are summarized in Table 5.3. It is shown that the permeate was enriched with gasoline. Figure 5.21 shows the concentration of gasoline in feed and permeate (excluding N_2) at four different feed gasoline vapor concentrations. The enrichment factor of a component with short retention time (small peak numbers) is smaller than that of a component with a long retention time (large peak numbers). The raw GC analysis data and sample chromatographs are listed in Appendix A.

Table 5.3 Experimental data for gasoline/N_2 separation

Run number	Feed concentration (wt%)		Total permeate flux ($g/m^2.s$)	Permeate concentration (wt%)	
	nitrogen	gasoline		nitrogen	gasoline
#1	59.19	40.81	1.9×10^{-2}	8.45	91.55
#2	61.08	38.92	2.6×10^{-2}	6.28	93.72
#3	66.59	33.41	3.4×10^{-2}	4.87	95.13
#4	78.33	21.67	5.5×10^{-2}	29.52	70.48

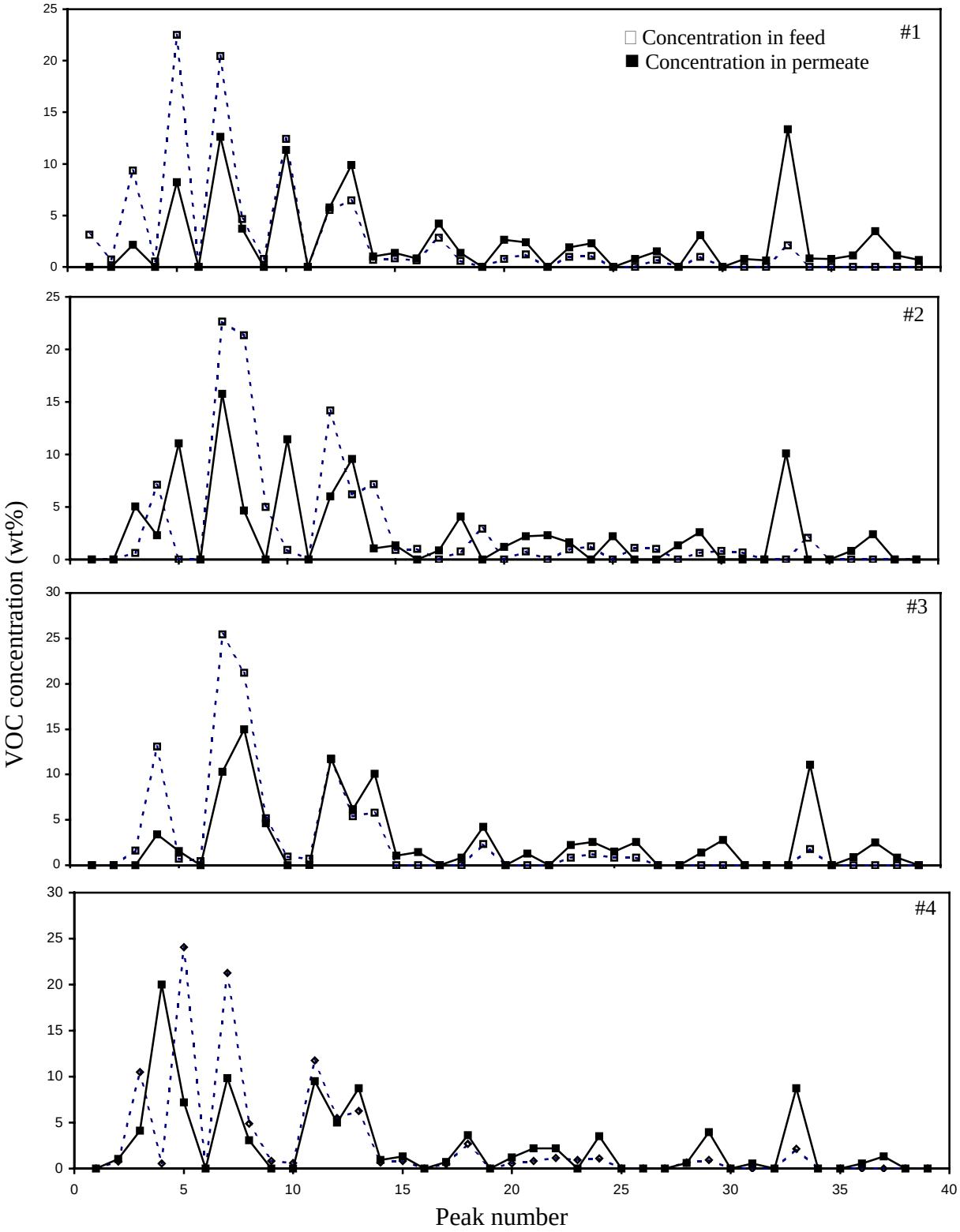

Figure 5.21 Relative concentration of VOCs in gasoline (excluding N_2) in feed and permeate.

5.2.5 Separation of gasoline with additives from nitrogen

Oxygenates are usually added in gasoline for better combustion efficiencies. As mentioned earlier, MeOH, EtOH, MTBE and DMC are the main oxygenates. It is thus of interest to test the membrane for separation of gasoline vapor from nitrogen in the presence of the gasoline additives. The experiments were carried out at the 22 ^{o}C and the experimental procedure was the same as that described previously except that additive was added to gasoline. Four runs were conducted; #1: gasoline with 5 wt% DMC, #2: gasoline with 5 wt% EtOH, #3: gasoline with 5 wt% MeOH, #4: gasoline with 5 wt% MTBE. GC was employed to determine the composition in feed and permeate.

The total VOC and nitrogen concentrations in feed and permeate are listed in Table 5.4. When the feed nitrogen concentration was around 65 wt% in all cases, and the nitrogen concentration in permeate was much lower, indicating the gasoline vapor was enriched substantially. The concentrations of various components in gasoline are summarized in Figure 5.22. Obviously all DMC, EtOH, MeOH and MTBE were enriched in the permeate side. It is interesting to find out that methanol showed the highest enrichment ratio. The order of the enrichment factors for the four additives is: MeOH (9.4) > DMC (6.5) > EtOH (5.5) > MTBE (2.9). This is in agreement with results obtained from binary VOC/N2 separation except for DMC which had the largest enrichment factor (i.e. DMC> MeOH> EtOH > MTBE). This is presumably due to the fact that gasoline is a complex mixture and there are some interactions between components. more studied are needed to clarify this. Nevertheless, it has been demonstrated that the membrane is suitable for recovering gasoline vapor from nitrogen stream.

Table 5.4 Experimental data for the separation of gasoline (with 5 wt% additive) from nitrogen

Run number	Feed concentration (wt%)		Total permeate flux ($g/m^2.s$)	Permeate concentration (wt%)	
	nitrogen	gasoline		nitrogen	gasoline
#1	64.64	35.36	3.52×10^{-2}	4.80	95.20
#2	64.96	35.04	2.47×10^{-2}	6.28	93.72
#3	64.96	35.04	2.04×10^{-2}	6.54	93.46
#4	66.44	33.56	3.13×10^{-2}	5.23	94.77

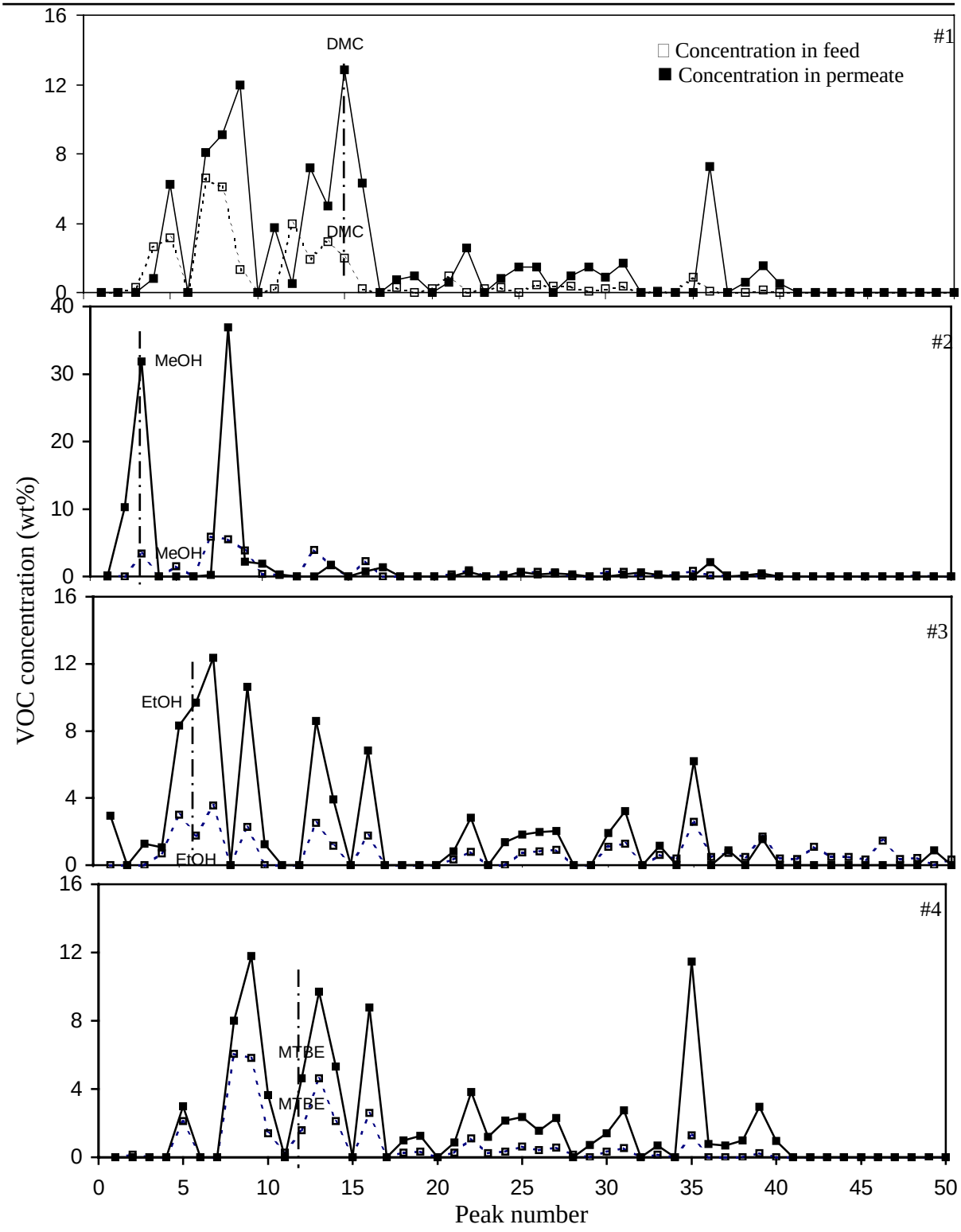

Figure 5.22 Relative concentration of VOCs in gasoline (with 5 wt% additive) (excluding N_2) in feed and permeate.

5.3 **Conclusions**

The following conclusions can be drawn from the above experimental results:

1) Composite hollow fiber PEBA/PVDF membrane was successfully developed for binary vapor separation from nitrogen.

2) Hexane, cyclohexane, heptane, DMC, EtOH, MeOH and MTBE could be effectively separated from nitrogen by the PEBA/PVDF composite hollow fiber membrane.

3) The VOC flux and VOC concentration in permeate increased with an increase in the feed VOC concentration.

4) An increase in operating temperature led to an increase in the nitrogen permeance, and a decrease in the VOC permeance. A low temperature was favorable for separating VOC from nitrogen

5) Gasoline vapors could be separated effectively by the PEBA/PVDF composite hollow fiber membrane.

Chapter 6 General conclusions

The separation of hexane, cyclohexane, heptane, DMC, MTBE, methanol, ethanol and gasoline from nitrogen by PEBA/PVDF composite hollow fiber membranes was studied. The following general conclusions can be drawn:

1) Composite hollow fiber PEBA/PVDF membranes were developed successfully. The microporous hollow fiber PVDF substrate was prepared by the phase inversion technique, and the composite PEBA/PVDF membrane were prepared by dip coating method.

2) The composite hollow fiber membranes were tested extensively for separation of gasoline vapors from nitrogen.

3) At a given relative pressure, the VOC permeability follows the following order: DMC > MeOH ≈ EtOH > heptane > cyclohexane ≈ hexane ≈ MTBE.

4) The permselectivity of the membrane increased with an increase in feed VOC concentration and/or a decrease in operating temperature.

5) The membrane was stable for the separations tested, at least during the ten-month period that the membrane was tested at varying operating conditions (e.g. temperature, composition and concentration).

Chapter 7 Recommendations

The followings are recommended for future investigation:

1) Reduce the thickness of the separation layer. As discussed in Chapter 2, the permeance is the permeability normalized by the membrane thickness. For a given permeability of the membrane material, reducing the thickness will increase the permeance, thereby increasing the permeation rate of the membrane. There might be two methods that can be used to achieve this goal: i) keeping the concentration of membrane coating solution around 0.5wt%; ii) reducing the coating time.

2) Optimize the microstructure of the substrate. The pore size should be large enough to minimize its mass transfer resistance, but not too large to ensure a good uniform coating of the PEBA selective layer and to retain sufficient mechanical stability of the membrane. Controlling the ratio of solution extrusion speed and wind-up speed is the best way to achieve uniform porous fibers.

3) Hybrid processes. By combining membranes with other VOC removal method (such as adsorption and condensation) for gasoline vapor recovery, the overall process might be more efficient than either process alone.

References

Aptel, P, N. Abidine, F. Ivaldi and J.P. Lafaille, Polysulfone hollow fibers-Effect of spinning conditions on ultrafiltration properties, *J. Membrane Sci.*, 22 (1985) 199.

Baker, R.W., N. Yoshioka, J. M. Mohr and A.J. Khan, Separation of organic vapors from air, *J. Membrane Sci.*, 31 (1987) 259-271.

Baker, R.W., Recent developments in membrane vapour separation systems, *Membrane Tech*., 9 (2002) 114.

Bartels, C. R., A surface science investigation of composite membrane, *J. Membrane Sci.*, 45 (1989) 225-246.

Behling, R.D. In *Proceeding of the Six Annual Membrane Technology Planning Conference, (Session V-4)*: Business Communications Co., Inc.: Norwalk, CT, 1986.

Behling, R.D., K. Ohlrogge, K.V. Peinemann and E. Kyburz, The Separation of Hydrocarbons from Waste Vapor Streams. *AIChE Symp. Ser*., 85 (1989) 68-78.

Bhaumik, D., S. Majumdar and K.K. Sirkar, Pilot-plant and laboratory studies on vapor permeation removal of VOCs from waste gas using silicone-coated hollow fibers, *J. Membrane Sci.*, 167 (2000) 107-122.

Billmeyer, F.W. JR., *Textbook of Polymer Science*, 3rd ed., John Wiley & Sons: New York, 1984, p. 520.

Blume, I., P.J.F. Schwering, M.H.V. Mulder and C.A. Smolders, Vapor sorption and permeation properties of poly(dimethylsiloxane) films, *J. Membrane Sci.*, 61 (1991) 85-98.

Bondar, V.I., B.D. Freeman and I. Pinnau, Gas sorption and characterization of poly(ether-b-amide) segmented block copolymers, *J. Poly. Sci.: Poly. Phy.*, 37 (1999) 2463-2475.

Bondar, V.I., B.D. Freeman and I. Pinnau, Gas transport properties of poly(ether-b-amide) segmented block copolymers, *J. Poly. Sci: Poly. Phy.*, 38 (2000) 2051-2062.

Cabasso, I., E. Klein and J.K. Smith, Polysulfone hollow fibers I. Spinning and properties, *J. Appl. Poly. Sci.*, 20 (1976) 2377-2394.

Cabasso, I., E. Klein and J.K. Smith, Polysulfone hollow fibers. II. Morphology, *J. Appl. Poly. Sci.*, 21 (1977a) 165-180.

Cabasso, I., E. Klein and J.K. Smith, Porosity and pore size determination in polysulfone hollow fibers, *J. Appl. Poly. Sci.*, 21 (1977b) 1883-1900.

Cen, Y. and R.N. Lichtenthaler, Vapor permeation, in *Membrane Separation Technology: Principles and Applications*, R.D. Noble and S.A. Stern (Eds.), Elsevier Science, 1995 P91.

Cen, Y., C. Staudt-Bickel and R.N. Lichtenthaler, Sorption properties of organic solvents in PEBA membranes, *J. Membrane Sci*., 206 (2002) 341-349.

Cha, J. S., V. Malik, D. Bhaumik, R. Li, and K.K. Sirkar, Removal of VOCs from waste gas streams by permeation in a hollow fiber permeator, *J. Membrane Sci*., 128 (1997) 195-211.

Chang, Y. -H., J. -H. Kim, and H. -W Rhe, Polysiloxaneimide membranes for removal of VOCs from water by pervaporation, *J. Appl. Poly. Sci*., 77 (2000) 2691-2702.

Cheng, L.P., Effect of temperature on the formation of microporous PVDF membranes by precipitation from 1-octanol/DMF/PVDF and water/DMF/PVDF systems, *Macromolecules*, 32 (1999) 6668-6674.

Christian, J.B., Estimate the effects of air emissions, with this process screening model, *Chem. Eng. Prog*., 91 (6) (1995) 59-62.

Chung, T.S., J. J. Qin, and J. Gu., Effect of shear rate within the spinneret on morphology, separation performance and mechanical properties of ultrafiltration polyethysulfone hollow fiber membranes, *Chem. Eng. Sci.*, 55 (2000) 1077-1091.

de Nevers, N., (Ed.), *Air Pollution Control Engineering*, McGraw-Hill, New York, 1995.

del Rio, O.L. and A.W. Neumann, Axisymmetric drop shape analysis: Computational methods for the measurement of interfacial properties from the shape and dimensions of pendant and sessile drops, *J. Colloid Interface Sci.*, 196 (1997) 136-147.

Deleens, G., A comprehensive review in: *Thermoplastic Elastomers*, N. R Legge, G. H. Schroeder and H. E. Schroeder (Eds.), Hansen Publisher: New York, 1987; pp215-230.

Deng, S., A. Tremblay and T. Matsuura, Preparation of hollow fibers for the removal of volatile organic compounds from air, *J. Appl. Poly. Sci.*, 69 (1998) 371-379.

Deng, S., S. Sourirajan, and T. Matsuura, Study of volatile hydrocarbon emission control by an aromatic polyetherimide membrane, *Ind. Eng. Chem. Res*., 34 (1995) 4494-4500.

Dennis, G. M. and G. O'Brien, Poly(ether block amide) resins: Bridging the gap between thermoplastics and rubbers, Presented at a meeting of Rubber Division, American Chemical Society, October 17-20, 2000.

Deshmukh, S.P. and K. Li, Effect of ethanol composition in water coagulation bath on morphology of PVDF hollow fiber membranes, *J. Membrane Sci.*, 150 (1998) 75-85.

Djebbar, M., Q. Nguyen, R. Clement, and Y. Germain, Pervaporation of aqueous ester solutions through hydrophobic poly(ether-block-amide) copolymer membranes, *J. Membrane Sci*., 146 (1998) 125-133.

Dohany, J.E. and L.E. Robb, Polyvinylidene flouride, in *Kirk-Othmer Encyclopedia of Chemical Technology*, 3rd ed., Wiley, New York, NY, 11 (1980) 64-74.

Favre, E., P. Schaetzel, Q.T. Nguygen, R. Clement and J. Neel, Sorption, diffusion and vapor permeation of various penetrants through dense polydimethylsiloxane membranes: a transport analysis, *J. Membrane Sci*., 92 (1994) 169-184.

Feng, X., S. Sourirajan, H. Tezel and T. Matsuura, Separation of organic vapor from air by aromatic polyimide membranes, *J. Appl. Poly. Sci*., 43 (1991) 1071-1079.

Feng, X., S. Sourirajan, F. Handan Tezel, T. Matsuura and B.A. Farnand, Separation of volatile organic compound/ nitrogen mixtures by polymeric membranes, *Ind. Eng. Chem. Res*., 32 (1993) 533-539.

Ferguson, J., G. Doulgeris and G.R. Mckay, Rheological and coagulation features in the wet spinning process, *J. Non-Newtonian Fluid Mechanics*, 6 (1980) 333-338.

Fischer, K., H. Sengder, R. Buchner and A. Schlesinger, *Progress and Trends in Rheology II*, 388 (1988)

Gales, L., A. Mendes and C. Costa, Removal of acetone, ethyl acetate and ethanol vapors from using a hollow fiber PDMS membrane module, *J. Membrane Sci*., 197 (2002) 211-222.

Garg, A., Specify better low-NO_x burners for furnaces, *Chem. Eng. Prog.*, 90(1) (1994) 46-54.

Gordeyer, S.A., G.B. Lees, I.R. Dunkin, and S.J. Shilton, Super-selective polysulfone hollow fiber membranes for gas separation; Rheological assessment of the spinning solution, *Polymer*, 42 (2001) 4347-4352.

Groβ, A. and A. Heintz, Diffusion coefficients of aromatics in nonporous PEBA membranes, *J. Membrane Sci*., 168 (2000) 233-242.

Guizard, C., B. Boutevin, F. Guida, A. Ratsimihety, P. Amblard, J.-C. Lasserre and S. Naiglin, VOC vapor transport properties of new membranes based on cross-linked fluorinated elastomers, *Sep. Pur. Technol*., 22 (2001) 23-30.

Gupta, V.K. and N. Verma, Removal of volatile organic compounds by cryogenic condensation followed by adsorption, *Chem. Eng. Sci*., 57 (14) (2002) 2679-2696.

Hagler, G.E., Qualitative prediction of effects of changes in spinning conditions on spun fiber orientation, *Poly. Eng. Sci*., 21 (1981) 121-123.

Heintz, A., H. Funke and R.N. Lichtenthaler, Sorption and diffusion in pervaporation membranes, in: R.Y.M. Huang (Ed.), *Pervaporation Membrane Separation Processes*, Elsevier, Amsterdam, 1991, Chap. 6, pp. 279-319.

Herck, R.M. and R.J. Farrauto, *Catalytic Air Pollution Control*, Van Nostrand Reinhold, New York, 1995.

Hickey, P. J., and C.H. Gooding. The economic optimization of spiral wound membrane modules for the pervaporation removal of VOCs from water, *J. Membrane Sci.*, 97 (1994) 53-70

Hines, A.L., T.K. Ghosh; S.K. Loyalka and R.C. Warder, Jr., *Indoor Air Quality & Control*, Prentice Hall, Englewood Cliffs, NJ, 1993.

Hitchens, L., L. M. Vane and F. Alvavez, VOC removal from water and surfactant solutions by pervaporation: a pilot study. *Sep. Pur. Technol.*, 24 (2001) 67-84.

Ho, W.S.W and K.K. Sirkar, *Membrane Handbook*, Van Nostrand Reinhold, New York, 1992.

Huang, R.Y.M. and X. Feng, Studies on solvent evaporation and polymer precipitation pertinent to the formation of asymmetric polyetherimide membranes, *J. Appl. Poly. Sci.*, 57 (1995) 613-621.

Hunter, P. and S. T. Oyama (Ed.), *Control of Volatile Organic Compound Emissions*, Wiley- Interscience, New York, 2000.

Kim, J. H., S. Y. Ha and Y. M. Lee, Gas permeation of poly(amide-6-b-ethylene oxide) copolymer, *J. Membrane Sci.*, 190 (2001) 179-193.

Kim, J.H., Y.-I. Park, J. Jegal and K.-H. Lee, The effects of spinning conditions on the structure formation and the dimension of the hollow-fiber membranes and their relationship with the permeate dry-wet spinning technology, *J. Appl. Poly. Sci.*, 57 (1995) 1637.

Kimmerle, K., C.M. Bell, W. Gudernatsch and H. Chmiel, Solvent recovery from air, *J. Membrane Sci.*, 36 (1988) 477-488.

Kong, J. and K. Li, Preparation of PVDF hollow-fiber membranes via immersion precipitation, *J. Appl. Poly. Sci*., 81 (2001) 1643-1653.

Koros, W.J. and G.K. Fleming, Membrane-based gas separation, *J. Membrane Sci.*, 83 (1993) 1-80.

Kroschwitz, J. I. and M. Howe-Grant, Poly(Vinylidene Fluoride), Fluorine Compounds, Organic (Polymers), in *Kirk-Othmer Encyclopedia of Chemical Technology*, A Wiley-Interscience Publication, John Wiley & Sons, New York, 1991, Vol. 11., pp 695.

Li, K., J.F. Kong, D. Wang and W.K. Teo, Tailor-made asymmetric PVDF hollow fiber for soluble gas removal, *AIChE J*., 45 (1999) 1211-1219.

Lonsdale, H. K., The evaluation of ultrathin synthetic membrane., *J. Membrane Sci*., 33 (1987) 121-136.

MacDonald, J.W., Packed Wet Scrubbers, in *Air Pollution Control and Design Handbook,* Part 2, P.N. Cheremisionoff and R.T. Young (Eds.), Marcel Dekker, New York, 1977, Ch. 26, p721.

Mishima, S. and T. Nakagawa, Plasma-grafting of fluoroalkyl methacrylate onto PDMS membranes and their VOC separation properties for pervaporation, *J. Appl. Poly. Sci.*, 73 (1999) 1835-1844.

Moretti, E. C. and N. Mukhopadhyay, VOC control: Current practices and future trends, *Chem. Eng. Prog*., 89 (7) (1993) 20-26.

Mulder, M., *Basic Principles of Membrane Technology*, Kluwer Academic Publishers, Boston, 1996.

Nakao, S., Review determination of pore size and pore size distribution, 3. Filtration membranes, *J. Membrane, Sci.*, 96 (1994) 131-165.

Noble, R.D. and S.A. Stern (Eds.), *Membrane Separations Technology Principles and Applications*, Elsevier, 1995.

Pandey, P. and R.S. Chauhan, Membrane for gas separation, *Prog. Poly. Sci*., 26 (2001) 853-893.

Paul, H., C. Philipsen, F.J. Gerner and H. Strathmann, Removal of organic vapors from air by selective membrane permeation, *J. Membrane Sci*., 36 (1988) 363-372.

Prokop, W.H., "Odors," in *Air Pollution Engineering Manual*, A. J. Buonicore and W.T. Davis (Eds.), Van Nostrand Reinhold, New York, 1992.

Qiu, M.M. and S.-T. Hwang, Continuous vapor-gas separation with a porous membrane permeation system, *J. Membrane. Sci*., 59 (1991) 53-72.

Rezac, M.E., T. John and P.H. Pfromm, Effect of copolymer composition on the solubility and diffusivity of water and methanol in a series of polyether amides, *J. Appl. Poly. Sci.* 65 (1997) 1983-1993.

Ross, R.D., Thermal Incineration, in *Air Pollution Control and Design Handbook,* Part 1, P.N. Cheremisinoff and R.A. Young (Eds.), Marcel Dekker, New York, 1977.

Ruddy, E. N. and A. C. Leigh, Select the best VOC control strategy, *Chem. Eng. Prog.*, 89 (7) (1993) 28-36.

Ruhl, M.J., Recover VOCs via adsorption on activated carbon, *Chem. Eng. Prog.*, 89(7) (1993) 37-41.

Sander, U. and H. Janssen, Industrial application of vapour permeation, *J. Membrane Sci.*, 61 (1991) 113-129.

Shao, P., R.Y.M.. Huang, X. Feng and W. Anderson, Gas-liquid displacement method for estimating membrane pore size distributions, *AIChE J.* in press, 2003.

Sharpe, I.D., A.F. Ismail and S.J. Shilton, A study of extrusion shear and forced convection residence time in the spinning of polysulfone hollow fiber membranes for gas separation, *Sep. Pur. Technol.*, 17 (1999) 101.

Shilton, S.J. and G.Bell, The deduction of fine structural details of gas separation hollow fiber membranes using resistance modeling of gas permeation, *Polymer,* 37 (1996) 485.

Simmons, V., J . Kaschemekat, M.L. Jacobs and D.D. Dortmundt, Membrane systems offer a new way to recover volatile organic air pollutants, *Chem. Eng.*, 101 (9) (1994) 93-95.

Steele, W.V., R.D. Chirico, S.E. Knipmeyer and A. Nguyen, Vapor pressure, heat capacity, and density along the saturation line measurements for dimethyl isophalate, dimethyl carbonate, 1,3,5-triethylbenzene, pentafluorophenol, 4-ter-butylcatechol, α-methylstyrene, and N, N'-bis (2-hydroxyethyl) ethylenediamine, *J. Chem. Eng. Data*, 42 (1997) 1008-1020.

Stenzel, M.H., Remove organics by activated carbon, *Chem. Eng. Prog.*, 89(4) (1993) 36.

Stern, A. (Ed.), *Air Pollution*, Vol. III, Academic Press, New York, 1968.

Tomaszewska, M., Preparation and properties of flat-sheet membranes from poly(vinylidene fluoride) for membrane distillation, *Desalination*, 104 (1996) 1-11.

Wang, D., K. Li and W.K. Teo, Porous PVDF asymmetric hollow fiber membranes prepared with the use of small molecular addictives, *J. Membrane Sci*., 178 (2000) 13-23.

Wang, D., K. Li and W.K. Teo, Preparation and characterization of polyvinylidene fluoride (PVDF) hollow fiber membranes, *J. Membrane Sci.*, 163 (1999) 211-220.

Wilks, B. and M. E. Rezac, Properties of rubbery polymers for the recovery of hydrogen sulfide from gasification gases, *J. Appl. Poly. Sci*., 85 (2002) 2436-2444.

Yaws, C.L., *Handbook of Vapor Pressure*, Gulf Publishing, Houston, 1994

Yeom, C.K. S.H. Lee and J.M. Lee, Study of transport of pure and mixed CO_2/N_2 gases through polymeric membranes, *J. Appl. Poly. Sci.*, 78 (2000) 179-189.

Yeom, C.K., S.H. Lee, H.Y. Song and J.M. Lee, Vapor permeation of a series of VOCs/N_2 mixtures through PDMS membrane, *J. Membrane Sci*., 198 (2002a) 129-143.

Yeom, C.K. S.H. Lee, H.Y. Song and J.M. Lee, A characterization of concentration polarization in a boundary layer in the permeation of VOCs/N_2 mixtures through PDMS membrane, *J. Membrane Sci.*, 205 (2002b) 155-174.

Yeow, M.L., R.W. Field, K. Li and W.K. Teo, Preparation of divinyl-PDMS/PVDF composite hollow fibre membranes for BTX removal, *J. Membrane Sci.*, 203 (2002) 137-143.

Young, T, L.P. Cheng, D.J. Lin, L.Fane and W.Y. Chuang, Mechanisms of PVDF membrane formation by immersion-precipitation in soft (1-octanol) and harsh (water) nonsolvents, *Polymer*, 40 (1999) 5315-5323.

Nomenclature

A	Membrane area
E_d	Diffusional activation energy
F	Flow rate
$Fext$	Force at take-up position
f_L	Ultimate orientation factor
G	Mass flow rate
ΔH_s	Heat of sorption
J	Permeance
l	Pore length
L	Spin draw ratio
M	Molecular weight
P	Permeability
p	Pressure
p^0	Saturated vapor pressure
Q	Flux
r	Pore radius
R	Gas constant
T	Temperature
t	Time
V	Volumetric permeation rate

V_0 Extrusion velocity

V_L Take-up velocity

X Mole fraction of component in feed

Y Mole fraction of component in permeate

Greek letters

θ Contact angle

ρ Density

ε Effective porosity

λ Mean free path

β Permeance ratio

τ Relaxation time

α Separation factor

γ Surface tension

η Viscosity

η^* Extrusion viscosity

$\dot{\gamma}$ Shear rate

Superscriptions:

f Feed

p Permeate

Subscriptions:

i, j	Components *i* and *j*
kun	Knudsen flow
v	Organic vapor
vis	Viscous flow
N	Nitrogen
t	Total

Appendices

Appendix A Experimental data

A1. Phase separation data for PVDF/solvent/water systems-cloud points

Without LiCl at 25 ^{o}C			Without LiCl at 40 ^{o}C			With LiCl at 40 ^{o}C		
PVDF (wt%)	DMAc (wt%)	Water (wt%)	PVDF (wt%)	DMAc (wt%)	Water (wt%)	PVDF (wt%)	DMAc (wt%)	Water (wt%)
4.32	82.00	13.68	2.53	81.83	15.64	0.90	84.60	14.50
8.86	79.72	11.42	4.26	80.97	14.77	1.73	85.00	13.17
13.59	77.00	9.41	8.80	79.23	11.97	2.75	84.26	12.99
18.51	74.06	7.43	13.46	76.26	10.28	3.70	84.26	12.04
20.50	72.68	6.82	18.34	73.36	8.30	4.65	83.62	11.73
			20.30	71.95	7.75	9.47	80.53	10.00
						14.48	77.21	8.31
						17.60	75.29	7.11
						19.68	73.79	6.53

Table A.2 LiCl additive leaching rate during polymer precipitation at 25 ^{o}C at different membrane thicknesses (dry)

Thickness	0.02 mm	Thickness	0.08 mm	Thickness	0.19 mm		
Time (min)	C_t/C_∞ (%)	Time (min)	C_t/C_∞ (%)	Time (min)	C_t/C_∞ (%)	Time (min)	C_t/C_∞ (%)
0.00	0.00	0.00	0.00	0.00	0.00	6.25	98.13
0.25	51.59	0.08	4.90	0.17	18.32	6.50	98.18
0.42	97.13	0.25	39.31	0.25	28.02	6.67	98.29
1.00	98.09	0.33	57.24	0.33	35.24	7.00	98.44
1.33	98.09	0.50	74.95	0.42	40.74	7.33	98.55
1.50	98.73	0.67	85.46	0.58	51.53	7.67	98.65
1.83	99.04	0.75	88.19	0.67	58.43	8.00	98.81
2.17	99.36	0.92	93.23	0.83	67.57	8.50	99.01
2.33	99.68	1.00	94.24	1.00	74.36	9.00	99.17
2.50	99.68	1.17	96.69	1.17	82.20	9.50	99.12
2.83	100.00	1.33	97.70	1.33	87.55	10.00	99.43
3.17	100.00	1.50	97.91	1.50	90.30	10.50	99.53
3.50	100.00	1.67	97.91	1.67	91.33	11.00	99.58
3.83	100.00	2.33	98.20	1.83	91.90	11.50	99.64
4.17	100.00	2.50	98.34	2.00	92.37	12.00	99.79
5.00	100.00	2.67	98.56	2.17	92.89	12.50	99.79
		2.83	98.78	2.33	93.25	13.00	99.84
		3.00	99.06	2.50	93.57	14.00	100.00
		3.17	99.14	2.67	94.08	15.00	100.00
		3.33	99.28	2.83	94.50		
		3.50	99.35	3.00	95.23		
		3.67	99.50	3.17	95.49		
		3.83	99.50	3.33	95.64		
		4.00	99.50	3.50	96.00		
		4.17	99.64	3.67	96.11		
		4.33	99.64	3.83	96.21		
		4.50	99.71	4.00	96.47		
		4.67	99.78	4.17	96.73		
		4.83	99.78	4.33	96.89		
		5.00	99.78	4.50	97.04		
		5.17	99.93	4.67	97.15		
		5.33	99.86	4.83	97.30		
		5.50	99.93	5.08	97.51		
		5.83	100.14	5.33	97.66		
		6.17	100.00	5.50	97.82		
		7.00	99.71	5.67	97.82		
		7.50	100.00	6.00	97.98		

Table A.3 DMAc leaching rate during polymer precipitation at 25 ^{o}C at different membrane thicknesses (dry)

#1 Thickness 0.11 mm		#2 Thickness 0.21 mm		#3 Thickness 0.11 mm		#4 Thickness 0.63 mm	
Time (min)	C_t/C_∞ (%)	Time (min)	C_t/C_∞ (%)	Time (min)	C_t/C_∞ (%)	Time (min)	C_t/C_∞ (%)
0	0	0	0	0	0	0	0
0.50	76.50	1.00	24.90	0.50	71.98	0.50	21.56
1.00	80.30	1.50	27.65	1.00	86.38	1.00	36.35
1.50	91.13	2.00	44.82	1.50	88.09	1.50	43.86
2.00	90.65	2.17	55.91	2.00	90.42	2.00	50.68
2.50	90.68	2.50	71.00	2.50	91.92	2.50	55.72
3.00	87.10	3.00	80.06	3.00	95.25	3.00	58.80
3.50	94.20	3.50	80.48	3.50	94.79	3.50	64.27
4.00	86.08	4.00	82.95	4.00	94.71	4.00	66.77
5.00	90.20	4.50	83.59	4.50	97.32	4.50	73.17
6.00	89.60	5.00	97.12	5.00	93.76	5.00	77.15
7.00	85.55	6.00	99.33	6.00	95.52	6.00	86.44
8.00	86.88	7.00	97.62	7.00	96.48	7.00	89.25
9.00	78.60	8.00	99.42	8.00	94.57	8.00	92.79
11.00	82.40	9.00	98.94	10.00	95.12	9.00	97.05
13.00	87.13	10.00	98.54	12.00	95.46	10.00	97.83
15.00	94.55	12.00	99.25	14.00	100.00	12.00	99.45
17.00	90.25	15.00	99.06	17.00	99.28	16.00	99.66
19.00	92.35	18.00	99.93	21.00	98.92	19.00	100.00
22.50	97.38	22.00	100.00	25.00	94.69	23.00	99.39
26.50	100.00	28.50	98.20	30.50	99.72	27.00	98.46
		34.50	98.81	37.00	97.36	31.00	97.82
		48.00	97.93				

#1, #2: PVDF/DMAc/LiCl = 20/75/5

#3, #4: PVDF/DMAc = 26/74

Table A.4 Gas permeation data for hollow fibers prepared at different take-up speeds

Fiber #1		Fiber #2		Fiber #3		Fiber #4	
p (psig)	N_2 Flux×10^6 (mol/m^2.s)	p (psig)	N_2 Flux×10^6 (mol/m^2.s)	p (psig)	N_2 Flux×10^6 (mol/m^2.s)	p (psig)	N_2 Flux×10^6 (mol/m^2.s)
14.5	4.1	11.0	5.8	14.5	7.2	11.0	6.1
24.0	4.4	21.5	6.5	25.0	8.0	20.5	6.6
32.5	4.8	27.5	7.5	34.5	8.3	28.0	6.8
42.5	4.8	33.0	7.1	42.0	8.6	39.0	7.2
50.5	4.9	40.0	7.3	49.0	9.0	49.0	7.5
55.0	5.1	44.0	7.7	55.5	9.3	58.0	7.9
60.5	5.2	57.0	8.0	61.5	9.7	68.0	8.2
66.5	5.3	73.5	8.9	71.5	1.0	78.0	8.5
81.5	5.3	91.0	8.4	80.5	1.1	97.0	9.0
92.5	5.6	110	9.1	88.5	1.1		
				96.5	1.1		
				111.5	1.2		

Take-up speed

#1: 8.3 m/min

#2: 9.7 m/min

#3: 11.1 m/min

#4: 12.5 m/min

Table A. 5 Gas permeation data for hollow fibers prepared at different extrusion rates

Fiber #5		Fiber #6		Fiber #7		Fiber #8	
p (psig)	N_2 Flux $\times 10^6$ (mol/m^2.s)	p (psig)	N_2 Flux$\times 10^6$ (mol/m^2.s)	p (psig)	N_2 Flux$\times 10^6$ (mol/m^2.s)	p (psig)	N_2 Flux $\times 10^6$ (mol/m^2.s)
14.5	1.5	16.75	1.8	20.0	2.1	14.0	1.7
27.0	1.7	27.0	1.8	26.0	2.2	20.5	1.8
33.5	1.7	33.5	1.9	36.5	2.3	27.0	1.9
40.0	1.8	39.5	1.9	42.0	2.3	36.0	1.9
44.5	1.8	44.5	2.0	48.0	2.4	42.0	1.9
51.5	1.8	52.0	2.0	55.0	2.5	46.5	2.0
61.5	1.8	59.0	2.0	60.0	2.9	53.5	2.1
74.0	1.8	69.0	2.3	75.0	2.6	61.5	2.2
				93.0	2.8	73.0	2.4
				104.0	2.8	84.5	2.3
				112.0	2.8	99.0	2.4

Fiber #9	
p (psig)	N_2 Flux $\times 10^6$ (mol/m^2.s)
20.0	2.8
29.0	2.9
35.5	3.0
42.0	3.1
50.0	3.2
56.0	3.2
64.0	3.5
73.5	3.4

Extrusion rate

#5: 2.9 ml/min

#6: 3.2 ml/min

#7: 4.0 ml/min

#8: 4.3 ml/min

#9: 5.7 ml/min

A.6 Gas permeation data for hollow fibers prepared at different inner coagulant speeds

Fiber #10		Fiber #11		Fiber #12		Fiber #13	
p (psig)	N_2 Flux $\times 10^6$ (mol/m^2.s)	p (psig)	N_2Flux $\times 10^6$ (mol/m^2.s)	p (psig)	N_2Flux $\times 10^6$ (mol/m^2.s)	p (psig)	N_2Flux $\times 10^7$ (mol/m^2.s)
11.0	2	10.5	1.6	17.5	1.4	17.5	8.7
17.0	2.2	16.5	1.7	30.5	1.6	29.5	9.3
23.5	2.2	26.5	1.9	39.0	1.7	37.0	9.5
29.5	2.2	33.5	1.9	48.0	1.8	43.0	9.8
38.5	2.3	42.5	2.0	57.0	1.8	52.0	10.0
45.0	2.3	51.0	2.1	65.5	1.8	59.0	10.0
52.0	2.3	61.5	2.1	76.5	2.0	68.5	11.0
57.5	2.3	70.5	2.2	91.0	2.0	79.0	11.0
69.0	2.5	84.0	2.3	113.0	2.2	93.5	12.0
		98.5	2.4			112.0	12.0
		111.5	2.5				

Fiber #14		Fiber #15	
p (psig)	N_2 Flux $\times 10^6$ (mol/m^2.s)	p (psig)	N_2 Flux $\times 10^6$ (mol/m^2.s)
7.0	1.7	10.0	2.3
12.5	1.9	14.5	2.4
18.5	2.0	20.0	2.4
23.0	2.0	25.0	2.6
28.5	2.0	30.5	2.6
33.5	2.1	36.0	2.6
39.5	2.1	42.0	2.7
45.5	2.2		
50.0	2.3		
56.0	2.3		
62.0	2.3		

Inner coagulant speed:

#10: 9.8 m/min; #11: 14.7 m/min; #12: 19.7 m/min

#13: 23.6 m/min; #14: 29.5 m/min; #15: 34.5 m/min

Table A. 7 Liquid-gas displacement data for determining pore size distribution of PVDF hollow fiber membranes

Fiber #2		Fiber #16		Fiber #13	
p (psig)	N_2 flux (mol/m^2.s.Pa)	p (psig)	N_2 flux (mol/m^2.s.Pa)	p (psig)	N_2 flux (mol/m^2.s. Pa)
38.5	3.69×10^{-10}	56	1.56×10^{-9}	71	4.63×10^{-10}
40	4.21×10^{-10}	58	2.07×10^{-9}	72.5	9.24×10^{-10}
41.5	4.84×10^{-10}	60	2.30×10^{-9}	74	9.43×10^{-10}
43	5.97×10^{-10}	62	2.42×10^{-9}	75.5	1.02×10^{-9}
45	7.37×10^{-10}	64	2.54×10^{-9}	77	1.16×10^{-9}
47	1.26×10^{-9}	65.5	2.73×10^{-9}	78.5	1.32×10^{-9}
48.5	1.40×10^{-9}	67	3.01×10^{-9}	81	1.42×10^{-9}
50	1.67×10^{-9}	69	3.55×10^{-9}	83	1.55×10^{-9}
52.5	2.04×10^{-9}	70.5	3.59×10^{-9}	85.5	1.80×10^{-9}
53.5	2.14×10^{-9}	72	3.79×10^{-9}	90	2.57×10^{-9}
55.5	2.40×10^{-9}	74	3.93×10^{-9}	92	3.59×10^{-9}
58	3.03×10^{-9}	76	4.18×10^{-9}	93.5	6.20×10^{-9}
60	3.36×10^{-9}	78	4.60×10^{-9}	95.5	7.23×10^{-9}
62.5	4.13×10^{-9}	80	5.76×10^{-9}		
64.5	4.71×10^{-9}	82	9.59×10^{-9}		
66.5	5.33×10^{-9}	84	1.04×10^{-9}		
68	6.41×10^{-9}	86	1.10×10^{-9}		
70.5	7.40×10^{-9}	88	1.21×10^{-9}		
72.5	9.04×10^{-9}	90	1.75×10^{-8}		
75	2.42×10^{-8}	91.5	2.88×10^{-8}		
76.5	2.65×10^{-8}	93	3.54×10^{-7}		
79	2.71×10^{-8}	95	3.57×10^{-7}		
		97	3.59×10^{-7}		
		99	3.65×10^{-7}		
		105	4.52×10^{-7}		

Table A.8 Permeation data for binary VOC/N_2 separation at different feed VOC concentrations

Feed Flow rate (mol/s)		Permeate Flux (mol/m^2.s)	
Nitrogen×10^4	Hexane×10^5	Nitrogen×10^8	Hexane×10^4
3.91	3.82	6.67	1.09
3.76	6.61	6.23	2.44
6.98	5.61	6.78	0.70
7.19	4.56	6.89	0.49
4.61	6.72	6.39	1.84
4.21	6.67	6.32	2.05
6.22	7.29	6.56	1.13
4.49	5.80	6.49	1.40
Nitrogen×10^4	Heptane×10^5	Nitrogen×10^8	Heptane×10^4
5.36	1.43	7.14	1.08
8.17	2.06	7.15	0.91
10.1	2.73	7.13	1.13
9.52	2.66	7.13	1.11
3.18	1.61	6.96	2.86
3.23	1.48	7.00	2.65
4.12	1.89	7.00	2.71
4.62	2.07	7.01	2.13
4.10	1.28	7.10	1.15
4.05	1.26	7.10	1.39
4.97	1.26	7.14	1.00
18.2	3.46	7.19	0.59
5.39	1.62	7.11	1.13
5.30	2.05	7.05	1.99
Nitrogen×10^4	cyclohexane×10^5	Nitrogen×10^8	cyclohexane×10^4
5.72	4.42	6.80	0.95
5.76	4.38	6.81	1.06
5.78	4.15	6.84	0.83
7.56	3.53	7.00	0.44
8.52	5.06	6.92	0.61
5.74	3.51	6.87	0.72
5.42	3.63	6.83	0.98
2.94	2.15	6.59	2.98
1.87	2.03	6.66	2.51
2.61	2.01	6.75	1.70
3.99	3.98	6.70	1.66

Table A.8 Permeation data for binary VOC/N_2 separation at different feed VOC concentrations

Feed Flow rate (mol/s)		Permeate Flux (mol/m^2.s)	
Nitrogen×10^4	DMC×10^5	Nitrogen×10^8	DMC×10^4
11.1	2.93	7.14	3.41
8.58	2.60	7.11	4.21
5.86	2.73	6.98	9.79
6.52	2.87	7.00	9.38
7.18	3.90	6.93	12.3
8.53	4.08	6.98	9.88
8.58	2.70	7.10	4.40
6.72	2.18	7.09	5.01
8.91	3.70	7.03	6.74
13.3	3.15	7.16	3.13
6.38	2.52	7.04	6.04
Nitrogen ×10^4	MTBE ×10^4	Nitrogen ×10^8	MTBE ×10^4
7.58	1.27	6.27	1.58
6.14	1.15	6.17	2.45
5.53	1.47	5.78	4.03
5.39	1.82	5.47	4.69
5.76	1.19	6.07	2.64
10	0.77	6.80	0.64
9.15	0.46	6.98	0.45
7.30	0.70	6.69	1.10
Nitrogen ×10^4	MeOH ×10^5	Nitrogen ×10^8	MeOH ×10^4
7.52	5.58	6.81	5.10
7.49	10.1	6.44	12.6
7.39	7.67	6.63	8.01
5.28	5.69	6.60	10
4.62	7.05	6.33	14.7
7.16	6.53	6.71	5.92
4.15	3.71	6.71	6.08
Nitrogen ×10^4	EtOH ×10^5	Nitrogen ×10^8	EtOH ×10^4
10.4	3.29	7.10	2.21
6.83	2.71	7.05	2.55
8.22	1.36	7.21	0.66
3.61	1.79	6.97	4.77
9.20	0.96	7.25	0.48

Table A.9 Binary VOC/N_2 separation data of PEBA/PVDF composite membrane at different temperatures

Feed Concentration	Temp (^oC)	Permeate flux (mol/m^2.s)	
		Hexane $\times 10^5$	Nitrogen $\times 10^8$
	3	13.3	5.35
Hexane: 5.27 mol%	11.5	8.97	6.04
	21	6.63	6.87
	31	6.73	7.78
	40	6.54	8.83
		Heptane $\times 10^5$	Nitrogen $\times 10^8$
	1	6.88	5.61
	11	4.17	6.25
Heptane: 11.08 mol%	20	3.30	7.06
	30	2.95	8.09
	40.5	3.18	9.08
		Cyclohexane $\times 10^5$	Nitrogen $\times 10^8$
	10.5	7.98	6.07
Cyclohexane: 3.5 mol%	21	3.82	6.99
	31	3.91	7.94
	40	3.97	8.98

Table A.9 Binary VOC/N_2 separation data of PEBA/PVDF composite membrane at different temperatures

Feed concentration	Temp (^oC)	Permeate flux (mol/m^2.s)	
		DMC $\times 10^5$	Nitrogen $\times 10^8$
DMC: 1.50 mol%	10	12.7	5.97
	20	8.44	7.04
	31	7.67	8.09
	40	7.37	9.16
		MTBE $\times 10^5$	Nitrogen $\times 10^8$
MTBE :10.00 mol%	1	23.9	6.67
	11	9.59	6.69
	20	6.82	6.66
	30	4.48	6.62
	40	4.53	6.65
		MeOH $\times 10^4$	Nitrogen $\times 10^8$
MeOH: 3.47 mol%	3	3.79	5.44
	11	2.64	6.10
	21	1.75	6.99
	31	1.88	7.93
	41	1.71	8.93
		EtOH $\times 10^5$	Nitrogen $\times 10^8$
EtOH: 1.34 mol%	3	12.2	5.55
	11	9.01	6.23
	21	5.10	7.14
	31	4.20	8.09
	41	4.77	9.11

Table A.10 GC analysis data for gasoline permeation at different feed VOC concentrations

Peak number	#1		#2		#3		#4	
	Feed (wt%)	Permeate (wt%)	Feed (wt%)	Permeate (wt%)	Feed (wt%)	Permeate (wt%)	Feed (wt%)	Permeate (wt%)
1	3.14	-	-	-	-	-	-	-
2	0.72	-	-	-	-	-	0.755	1.07
3	9.35	2.15	0.61	5.04	1.62	-	10.516	4.1
4	0.56	-	7.1	2.32	13.09	3.4	0.55	20
5	22.5	8.24	-	11.06	0.7	1.56	24.08	7.22
6	-	-	-	-	0.47	-	-	-
7	20.43	12.64	22.64	15.77	25.44	10.27	21.25	9.85
8	4.67	3.71	21.36	4.65	21.18	14.96	4.89	3.05
9	0.8	-	4.99	-	5.18	4.63	0.82	-
10	12.45	11.33	0.89	11.43	0.96	-	0.61	-
11	-	-	-	-	0.71	-	11.78	9.5
12	5.51	5.75	14.16	6	11.69	11.74	5.5	5.01
13	6.48	9.89	6.21	9.58	5.39	6.19	6.25	8.74
14	0.67	1.05	7.16	1.04	5.77	10.06	0.68	0.96
15	0.82	1.38	0.9	1.34	-	1.05	0.81	1.32
16	0.63	0.84	1.03	-	-	1.43	-	-
17	2.84	4.22	-	0.86	-	-	0.5	0.74
18	0.58	1.36	0.78	4.07	-	0.86	2.67	3.65
19	-	-	2.92	-	2.32	4.25	-	-
20	0.79	2.64	-	1.21	-	-	0.56	1.22
21	1.22	2.4	0.75	2.2	-	1.27	0.81	2.19
22	-	-	-	2.32	-	-	1.18	2.18
23	0.98	1.89	0.97	1.62	0.82	2.24	0.93	-
24	1.07	2.3	1.26	-	1.25	2.54	1.08	3.53
25	-	-	-	2.23	0.82	1.48	-	-
26	-	0.77	1.09	-	0.83	2.55	-	-
27	0.67	1.5	1.02	-	-	-	-	-
28	-	-	-	1.37	-	-	0.68	0.59
29	0.97	3.1	0.63	2.6	-	1.41	0.96	3.93
30	-	-	0.8	-	-	2.78	-	-
31	-	0.76	0.65	-	-	-	-	0.54
32	-	0.66	-	-	-	-	-	-
33	2.11	13.34	-	10.09	-	-	2.13	8.75
34	-	0.85	2.09	-	1.77	11.1	-	-
35	-	0.79	-	-	-	-	-	-
36	-	1.12	-	0.8	-	0.88	-	0.55
37	-	3.47	-	2.38	-	2.51	-	1.3
38	-	1.14	-	-	-	0.83	-	-
39	-	0.67	-	-	-	-	-	-

Table A.11 GC analysis data for the separation of gasoline (with 5 wt% DMC) from nitrogen

Peak number	Feed		Permeate	
	Conc. (wt%)	Flow rate (g/s)	Conc. (wt%)	Flow rate (g/s)
N_2	63.61	1.22×10^{-2}	4.8	2.89×10^{-6}
1	-	-	-	-
2	-	-	-	-
3	0.3	2.08×10^{-5}	-	-
4	2.63	1.84×10^{-4}	0.78	4.72×10^{-7}
5	3.13	2.19×10^{-4}	6.22	3.75×10^{-6}
6	-	-	-	-
7	6.62	4.63×10^{-4}	8.07	4.86×10^{-6}
8	6.08	4.26×10^{-4}	9.07	5.46×10^{-6}
9	1.34	9.41×10^{-4}	11.98	7.21×10^{-6}
10	-	-	-	-
11	0.25	1.73×10^{-5}	3.76	2.26×10^{-6}
12	3.99	2.79×10^{-5}	0.51	3.09×10^{-7}
13	1.91	1.33×10^{-4}	7.21	4.34×10^{-6}
14	2.9	2.03×10^{-4}	4.97	2.99×10^{-6}
15 (DMC)	1.98	1.38×10^{-4}	12.87	7.75×10^{-6}
16	0.2	1.43×10^{-5}	6.34	3.81×10^{-6}
17	-	-	-	-
18	0.29	2.00×10^{-5}	0.75	4.49×10^{-7}
19	-	-	0.92	5.56×10^{-7}
20	0.2	1.38×10^{-5}	-	-
21	0.94	6.55×10^{-5}	0.58	3.48×10^{-7}
22	-	-	2.59	1.56×10^{-7}
23	0.21	1.48×10^{-5}	-	-
24	0.27	1.90×10^{-5}	0.8	4.83×10^{-7}
25	-	-	1.47	8.82×10^{-7}
26	0.46	3.21×10^{-5}	1.45	8.71×10^{-7}
27	0.4	2.77×10^{-5}	-	-
28	0.37	2.59×10^{-5}	0.94	5.67×10^{-7}
29	0.11	7.91×10^{-6}	1.44	8.65×10^{-7}
30	0.25	1.78×10^{-5}	0.85	5.11×10^{-7}
31	0.38	2.67×10^{-5}	1.69	1.02×10^{-6}
32	-	-	-	-
33	0.1	6.67×10^{-6}	-	-
34	-	-	-	-
35	0.88	6.18×10^{-5}	-	-

Table A. 11 (Cont'd)

36	0.07	5.19×10^{-6}	7.26	4.37×10^{-6}
37	-	-	-	-
38	-	-	0.59	3.54×10^{-7}
39	0.15	1.04×10^{-5}	1.56	9.38×10^{-7}
40	-	-	0.53	3.20×10^{-7}
41	-	-	-	-
42	-	-	-	-
43	-	-	-	-
44	-	-	-	-
45	-	-	-	-
46	-	-	-	-
47	-	-	-	-
48	-	-	-	-
49	-	-	-	-
50	-	-	-	-

Table A.12 GC analysis data for the separation of gasoline (with 5wt% EtOH) from nitrogen

Peak number	Feed		Permeate	
	Conc. (wt%)	Flow rate (g/s)	Conc. (wt%)	Flow rate (g/s)
N_2	64.96	1.85×10^{-4}	6.54	2.89×10^{-6}
1	-	-	2.95	1.31×10^{-6}
2	-	-	-	-
3	-	-	1.27	5.61×10^{-7}
4	0.68	6.85×10^{-5}	1.07	4.72×10^{-7}
5	3.01	3.01×10^{-4}	8.31	3.67×10^{-6}
6 (EtOH)	1.77	1.77×10^{-4}	9.69	4.28×10^{-6}
7	3.54	3.54×10^{-4}	12.37	5.47×10^{-6}
8	-	-	-	-
9	2.28	2.28×10^{-4}	10.63	4.70×10^{-6}
10	-	-	1.23	5.44×10^{-7}
11	-	-	-	-
12	-	-	-	-
13	2.53	2.53×10^{-4}	8.60	3.80×10^{-6}
14	1.16	1.16×10^{-4}	3.91	1.73×10^{-6}
15	-	-	-	-

Table A. 12 (Cont'd)

16	1.76	1.76×10^{-4}	6.83	3.02×10^{-6}
17	-	-	-	-
18	-	-	-	-
19	-	-	-	-
20	-	-	-	-
21	0.33	3.26E-05	0.82	3.61×10^{-7}
22	0.78	7.8×10^{-5}	2.83	1.25×10^{-6}
23	-	-	-	-
24	-	-	1.36	6.00×10^{-7}
25	0.77	7.72×10^{-5}	1.82	8.06×10^{-7}
26	0.81	8.13×10^{-5}	1.99	8.78×10^{-7}
27	0.92	9.20×10^{-5}	2.02	8.94×10^{-7}
28	-	-	-	-
29	-	-	-	-
30	1.10	1.10×10^{-4}	1.90	8.39×10^{-7}
31	1.27	1.27×10^{-4}	3.22	1.42×10^{-6}
32	-	-	-	-
33	0.59	5.94×10^{-5}	1.14	5.06×10^{-7}
34	0.40	3.96×10^{-5}	-	-
35	2.57	2.57×10^{-4}	6.20	2.74×10^{-6}
36	0.48	4.79×10^{-5}	-	-
37	0.73	7.26×10^{-5}	0.87	3.83×10^{-7}
38	0.49	4.91×10^{-5}	-	-
39	1.70	1.70×10^{-5}	1.56	6.89×10^{-7}
40	0.39	3.88×10^{-5}	-	-
41	0.38	3.75×10^{-5}	-	-
42	1.09	1.09×10^{-5}	-	-
43	0.49	4.87×10^{-5}	-	-
44	0.48	4.83×10^{-5}	-	-
45	0.32	3.22×10^{-5}	-	-
46	1.47	1.47×10^{-4}	-	-
47	0.36	3.59×10^{-5}	-	-
48	0.42	4.17×10^{-5}	-	-
49	-	-	0.87	3.83×10^{-7}
50	0.33	3.26×10^{-5}	-	-

Table A.13 GC analysis data for the separation of gasoline (with 5 wt% MeOH) from nitrogen

Peak number	Feed		Permeate	
	Conc. (wt%)	Flow rate (g/s)	Conc. (wt%)	Flow rate (g/s)
N_2	64.96	1.67×10^{-2}	6.28	2.89×10^{-6}
1	0.11	2.79×10^{-5}	-	-
2	-	-	10.28	4.73×10^{-6}
3 (MeOH)	3.38	8.19×10^{-4}	31.87	1.47×10^{-5}
4	-	-	-	-
5	1.49	3.62×10^{-4}	-	-
6	-	-	-	-
7	5.91	1.43×10^{-3}	0.21	9.87×10^{-8}
8	5.47	1.33×10^{-3}	36.87	1.70×10^{-5}
9	3.86	9.37×10^{-4}	2.16	9.92×10^{-7}
10	0.36	8.63×10^{-5}	1.90	$8.72\times10^{-7}7$
11	0.22	5.31×10^{-5}	0.30	1.40×10^{-7}
12	-	-	-	-
13	3.92	9.51×10^{-4}	-	-
14	1.68	4.07×10^{-4}	1.73	7.95×10^{-7}
15	-	-	0.00	-
16	2.24	5.42×10^{-4}	0.77	3.53×10^{-7}
17	-	-	1.33	6.13×10^{-7}
18	-	-	-	-
19	-	-	-	-
20	-	-	-	-
21	0.32	7.73×10^{-5}	-	-
22	0.89	2.16×10^{-4}	0.65	3.01×10^{-7}
23	0.00	-	-	-
24	0.21	5.13×10^{-5}	-	-
25	0.56	1.36×10^{-4}	0.64	2.96×10^{-7}
26	0.68	1.65×10^{-4}	0.29	1.35×10^{-7}
27	0.61	1.48×10^{-4}	0.46	2.13×10^{-7}
28	-	-	0.32	1.45×10^{-7}
29	-	-	-	-
30	0.68	1.65×10^{-4}	-	-
31	0.65	1.58×10^{-4}	0.33	1.51×10^{-7}
32	-	-	0.58	2.65×10^{-7}
33	-	7.01×10^{-5}	0.23	1.0×10^{-7}
34	0.13	3.24×10^{-5}	-	-
35	0.84	2.04×10^{-5}	-	-

Table A. 13 (Cont'd)

36	0.12	2.88×10^{-5}	2.15	9.87×10^{-7}
37	0.11	2.79×10^{-5}	-	-
38	0.00	-	0.17	7.79×10^{-8}
39	0.16	3.96×10^{-5}	0.49	2.23×10^{-7}
40	-	-	-	-
41	-	-	-	-
42	-	-	-	-
43	-	-	-	-
44	-	-	-	-
45	-	-	-	-
46	-	-	-	-
47	-	-	-	-
48	0.14	3.33×10^{-5}	-	-
49	-	-	-	-
50	-	-	-	-

Table A.14 GC analysis data for the separation of gasoline (with 5 wt% MTBE) from nitrogen

Peak number	Feed		Permeate	
	Conc. (wt%)	Flow rate (g/s)	Conc. (wt%)	Flow rate (g/s)
N_2	66.44	2.57×10^{-4}	5.23	2.89×10^{-6}
1	-	-	-	-
2	0.16	6.09×10^{-5}	-	-
3	-	-	-	-
4	-	-	-	-
5	2.11	8.16×10^{-4}	2.98	1.65×10^{-6}
6	-	-	-	-
7	-	-	-	-
8	6.06	2.35×10^{-3}	8.00	4.42×10^{-6}
9	5.83	2.26×10^{-3}	11.78	$6.51E\times10^{-6}$
10	1.40	5.42×10^{-4}	3.65	2.02×10^{-6}
11	0.26	1.00×10^{-4}	-	-
12 (MTBE)	1.58	6.11×10^{-3}	4.62	2.56×10^{-6}
13	4.62	1.79×10^{-3}	9.70	5.36×10^{-6}
14	2.11	8.16×10^{-4}	5.31	2.94×10^{-6}
15	-	-	-	-

Table A. 14 (Cont'd)

16	2.60	1.01×10^{-3}	8.79	4.86×10^{-6}
17	-	-	-	-
18	0.27	1.04×10^{-4}	0.99	5.46×10^{-7}
19	0.33	1.29×10^{-4}	1.26	6.99×10^{-7}
20	-	-	-	-
21	0.28	1.07×10^{-5}	0.86	4.75×10^{-7}
22	1.11	4.29×10^{-5}	3.81	2.11×10^{-6}
23	0.24	9.47×10^{-5}	1.20	6.66×10^{-7}
24	0.32	1.26×10^{-5}	2.16	1.20×10^{-6}
25	0.61	2.38×10^{-5}	2.37	1.31×10^{-6}
26	0.43	1.65×10^{-5}	1.56	8.63×10^{-7}
27	0.58	2.25×10^{-5}	2.30	1.27×10^{-6}
28	0.15	5.90×10^{-5}	-	-
29	-	-	0.72	3.99×10^{-7}
30	0.34	1.33×10^{-4}	1.41	7.81×10^{-7}
31	0.53	2.04×10^{-4}	2.76	1.52×10^{-6}
32	-	-	-	-
33	0.14	5.41×10^{-5}	0.68	3.77×10^{-7}
34	-	-	-	-
35	1.28	4.95×10^{-4}	11.46	6.33×10^{-6}
36	-	-	0.78	4.31×10^{-7}
37	-	-	0.68	3.77×10^{-7}
38	-	-	0.99	5.46×10^{-7}
39	0.24	9.20×10^{-5}	2.94	1.63×10^{-6}
40	-	-	0.95	5.24×10^{-7}
41	-	-	-	-
42	-	-	-	-
43	-	-	-	-
44	-	-	-	-
45	-	-	-	-
46	-	-	-	-
47	-	-	-	-
48	-	-	-	-
49	-	-	-	-
50	-	-	-	-

-: The mount was too small to be detected

Appendix B Sample calculations

1 Nitrogen permeance (J)

$$J = \frac{F}{A\Delta p}$$

$$J = \frac{2.02 ml/s}{22.4 \times 1000 \times 225.5 mm^2 \times 10^{-6} \times 11 psi \times 6893.98}$$

$$J = 5.27 \times 10^{-6} mol/m^2.s.Pa$$

2. Pore radius of the PVDF hollow fiber membranes

$$r = \frac{2\gamma \cos\theta}{\Delta p}$$

$$r = \frac{2 \times 23.5 dyn/cm \times \cos 0^o}{2 psi} = \frac{2 \times 23.5 \times 0.001 N/m}{1251257.37 Pa} = 3.76 \times 10^{-8} m$$

3. VOC permeance (J)

$$Q_{vi} = \frac{G_{pi}}{M_i t A}$$

$$Q_{vi} = \frac{0.287 g}{60 g/mol \times 71 \min \times 17.7 cm^2} = 7.49 \times 10^{-7} mol/m^2.s$$

$$J_i = \frac{Q_{vi}^p}{p^f X_i}$$

$$J_i = \frac{7.49 \times 10^{-7}}{(1.01 \times 10^5 Pa \times 3.03\% - 0 \times 91.33\%)} = 1.38 \times 10^{-7} mol/m^2.s.Pa$$

4. Permeance ratio (β)

$$\beta = \frac{J_{vi}}{J_N}$$

$$\beta = \frac{1.38 \times 10^{-7}\, mol/m^2.s.Pa}{4.14 \times 10^{-10}\, mol/m^2.s.Pa} = 333.33$$

Appendix C Sample gas chromatograms

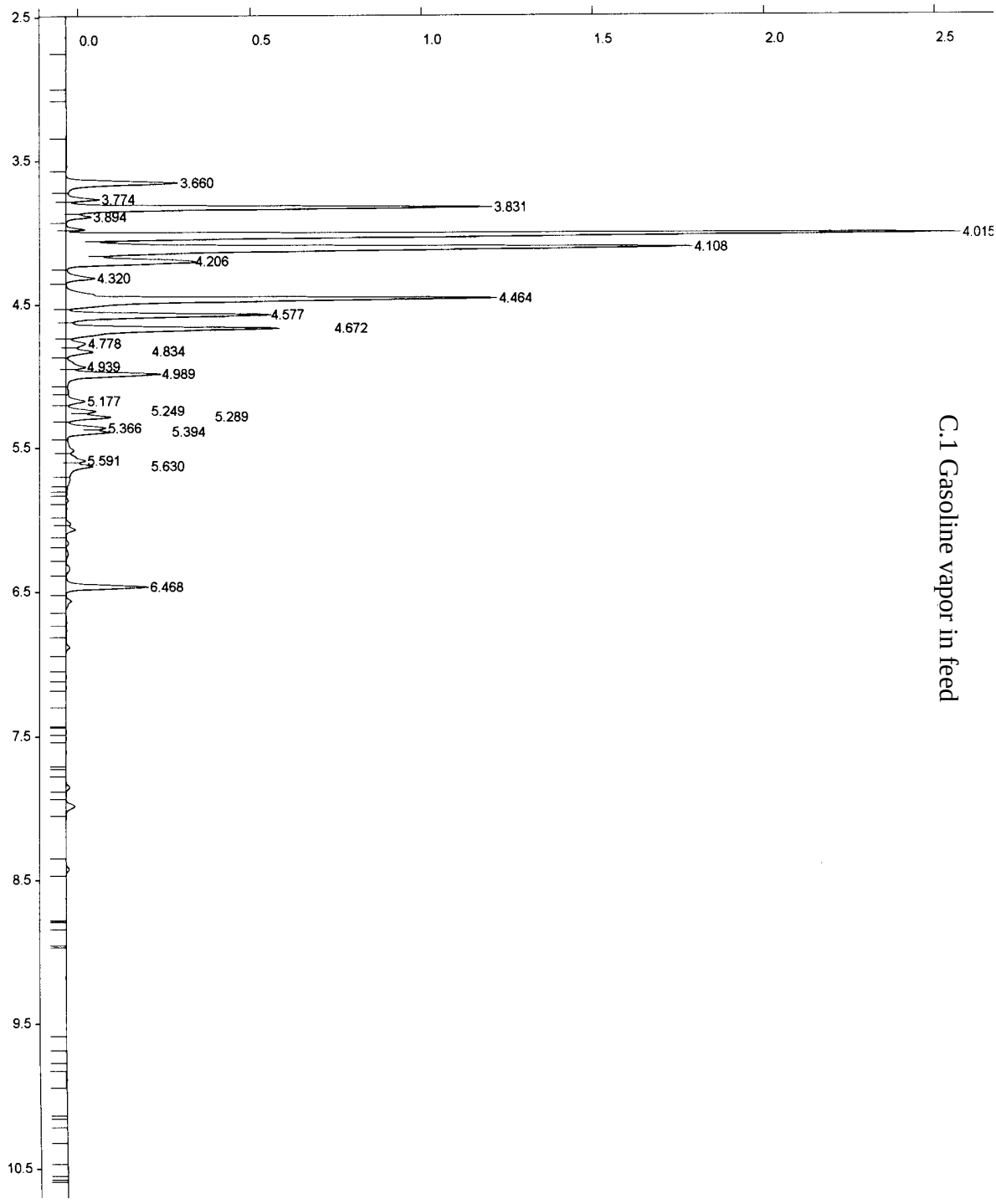

C.1 Gasoline vapor in feed

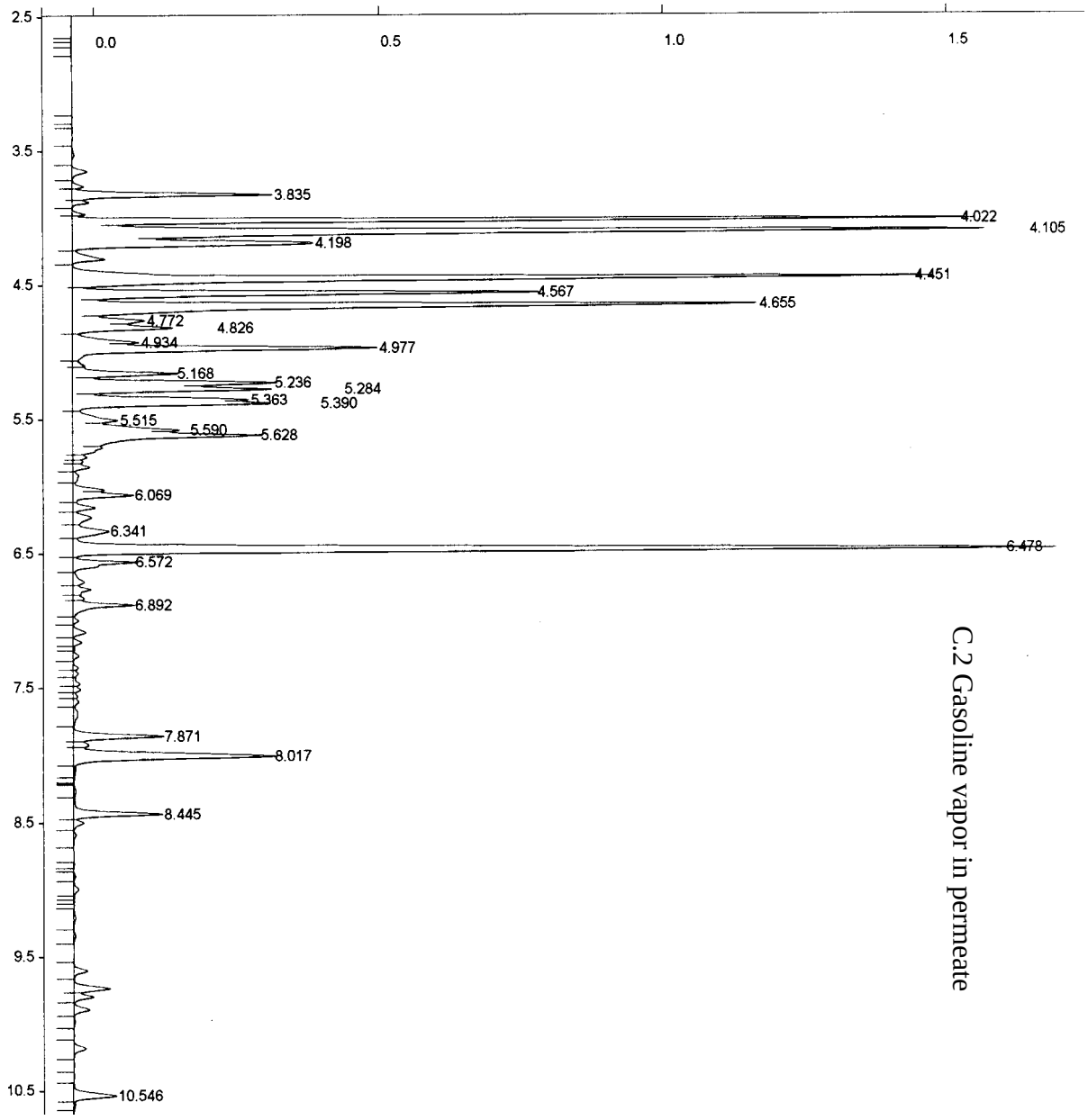

C.2 Gasoline vapor in permeate